PHYS 6751 Laboratory: *Determination of a Neutron Long-Counter Efficiency*

Lab overview:

- *Objective:* Determine the neutron-detection efficiency of a neutron long-counter using a neutron-emitting calibration source ^{252}Cf, correcting for decays from the ^{250}Cf impurity , and comparing to Monte Carlo calculation results
- *Gain familiarity with:* Neutron detection, neutron-sensitive proportional counters, fission neutron sources
- *Report style:* Nuclear Instruments and Methods in Physics Research A (NIMA)

Brief description:

High-efficiency detection of ~MeV-scale neutrons is of critical importance for a variety of topics in low-energy nuclear physics, such as homeland security, nuclear energy, and nuclear astrophysics. The neutron long-counter is an important tool that was developed for such a purpose, employing a moderating material to slow neutrons and gas-filled proportional counters to capture thermalized neutrons. This device provides neutron detection efficiencies of tens of percent for neutron energies typically produced by fissile materials and nuclear reactions performed at energies of astrophysical interest, as well as in the β-delayed neutron emission of exotic nuclides. Notably, the cost of such high detection efficiency is a loss of most of the information regarding the neutron's initial energy or incident angle, as well as a significant room background.

In this experiment, we will determine the neutron detection efficiency of the FIGARO long-counter for several different positions of a ^{252}Cf source on FIGARO's surface. Signals from the 18 boron-trifluoride proportional counters embedded within the polyethylene moderator will be processed to indicate neutron detections, which will be used to determine an overall neutron rate. The neutron-detection rate will be compared to the neutron emission rate from the ^{252}Cf source, where the ^{250}Cf contamination must also be taken into account, in order to determine a neutron detection efficiency. Detection efficiency results will be compared to Monte Carlo calculations which have already been performed.

Expectations for Run-plan:

The run-plan should consist of time-saving calculations and an order of operations. For instance,

- How does the ^{250}Cf impurity affect our expected neutron rate given an initial source activity and purity?
- What does a boron-trifluoride (BF_3) neutron spectrum look like (and why)?
- Where does the neutron background come from and what is its anticipated rate?

- What is the experiment order-of-operations? (e.g. What bias do we apply? How long to take a background measurement? How many positions will source-runs be possible?
- How will the data analysis be performed? (e.g. neutron-signal extraction, background subtraction)
- How can we determine the neutron–detection efficiency?
- ...of course, other preparatory notes are welcome, so long as they're useful!

NOTE: The above examples are suggestions. Please do not feel obligated to have all of them done prior to the lab start. You will be working in a group, so with any luck your partners will have prepared for some different portions of the lab.

Expectations for Lab Report:

The lab report should be a publication-quality paper typeset in the style of Nuclear Instruments and Methods in Physics Research Section A. As such, it should include a brief motivation for our measurement, a technical description of the set-up, and a thorough description of the experimental methods, along with benchmarking against simulations.

The reports will be written individually, but your group members should appear as co-authors on the paper. As such, you are free to share calculations and plots. In fact, sharing in this sense is expected, as this is how real experiments work. However, all writing must be your own.

NOTE: It is quite possible that the lab contains more work than you could possibly get done during the experiment time allotted. This is OK, as I don't expect you to necessarily complete every single task. However, a reasonable amount of work must be completed and that work must be thoroughly described in an articulate way.

WARNINGS:

- Be careful with the bias voltage
  - Don't electrocute yourself
  - Don't exceed the maximum bias voltage for the detector
- Be careful when around the ^{252}Cf-source
  - Only handle with gloves
  - Never touch the surface of the ^{252}Cf-source to any other surface
  - Report any incidents (e.g. dropped the source) immediately to Zach Meisel or Tom Massey or Carl Brune
- If you aren't sure, ask!

Appendices

1. General info on fast neutron detection
2. Paper on modern neutron long-counter
3. Paper on first neutron long-counter
4. Paper on FIGARO neutron long-counter
5. Info on our BF3 tubes
6. MCNP simulation results for FIGARO
7. Notes on our ^{252}Cf neutron source properties
8. Paper on neutron emission properties of ^{252}Cf
9. Paper on characterizing ^{250}Cf contamination

Radiation Detection and Measurement

Third Edition

Glenn F. Knoll

Professor of Nuclear Engineering and Radiological Sciences
University of Michigan
Ann Arbor, Michigan

John Wiley & Sons, Inc.
New York/Chichester/Weinheim/Brisbane/Toronto/Singapore

The thermal neutron cross section for this reaction is 5330 barns, significantly higher than that for the boron reaction, and its value also falls off with a $1/v$ energy dependence (see Fig. 14.1). Although ^{3}He is commercially available, its relatively high cost is a factor in some applications.

D. The Gadolinium Neutron Capture Reaction

The cross section for thermal neutron capture of 255,000 barns in ^{157}Gd is among the highest nuclear cross sections found in any material. The isotope is 15.7% abundant in natural gadolinium, and neutron absorption results in an assortment of prompt reaction products that include gamma rays and conversion electrons. Because they are directly ionizing, it is the fast electrons that are the useful product in the application of this reaction for neutron detection and imaging. The most significant of these is a 72 keV conversion electron that is emitted in 39% of the capture reactions. Its range in typical Gd-containing layers is about 20 μm, so deposits of roughly this thickness can be employed as converters of incident neutrons into fast electrons that can be recorded in an adjacent detector. The conversion efficiency can be as high as 30% in such a layer, much larger than the 1% and 3–4% more typical of ^{6}Li- and ^{10}B-containing foils, respectively.[8] This reaction is frequently applied in neutron imaging, where the conversion electron serves to record the position of interaction of the neutron in an adjacent photographic film or other position-sensitive detector.

Liquid scintillators can also contain gadolinium in solution, typically at about 0.5% concentration, to make them highly sensitive to neutrons. Because the reaction products are fast electrons and gamma rays, gamma-ray backgrounds are more of a problem than for other conversion reactions in which heavily charged particles are produced and pulse shape discrimination techniques can be employed.

E. Neutron-Induced Fission Reactions

The fission cross sections of ^{233}U, ^{235}U, and ^{239}Pu are relatively large at low neutron energies and thus these materials can be used as the basis of slow neutron detectors. One characteristic of the fission reaction is its extremely large Q-value (approximately 200 MeV) compared with the reactions discussed previously. As a result, detectors based on the fission reaction can often give output pulses that are orders of magnitude larger than those induced from competing reactions or incident gamma rays, and very clean discrimination can be accomplished. Figure 14.2 shows a plot of fission cross sections of a variety of fissile nuclides, including some that are of primary use as fast neutron detectors. Almost all fissile nuclides are naturally alpha radioactive and consequently any detector that incorporates these materials will also show a spontaneous output signal due to decay alpha particles. The energy of the alpha particles, however, is always many times less than the energy given off in a fission reaction, and again these events can usually be discriminated easily on a pulse amplitude basis.

II. DETECTORS BASED ON THE BORON REACTION

A widely used detector for slow neutrons is the BF_3 proportional tube. In this device, boron trifluoride serves both as the target for slow neutron conversion into secondary particles as well as a proportional gas. A number of other boron-containing gases have been evaluated, but BF_3 is the near-universal choice because of its superior properties as a proportional gas, as well as its high concentration of boron. In nearly all commercial detectors, the gas is highly enriched in ^{10}B, resulting in an efficiency some five times greater than if the gas contained naturally occurring boron. Because the performance of BF_3 as a proportional gas is poor when operated at higher pressures, its absolute pressure in typical tubes is limited to about 0.5–1.0 atm.

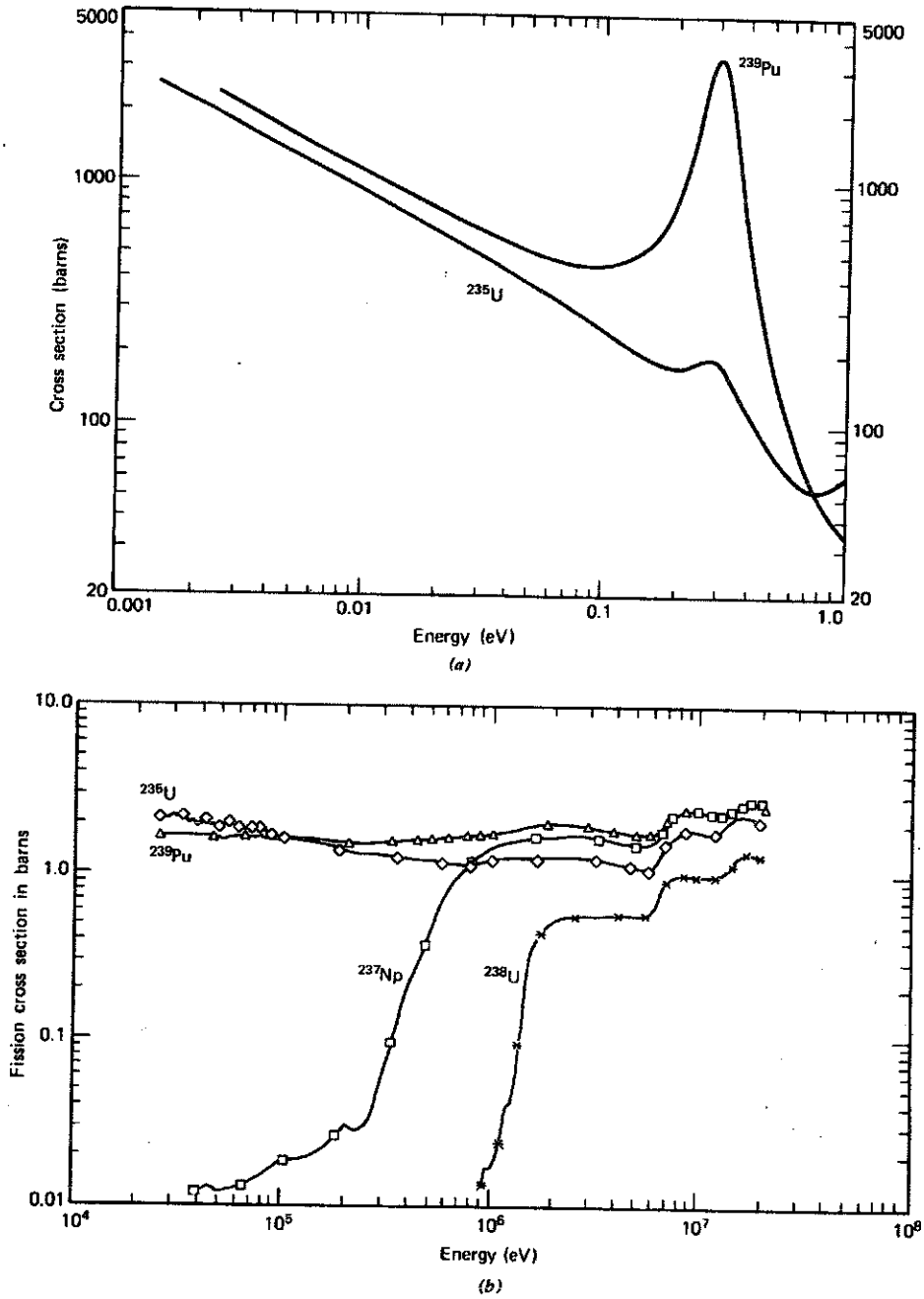

Figure 14.2 Fission cross sections of some common target nuclides used in fission chambers. (*a*) Slow neutron region where the cross sections shown are relatively large. (*b*) Fast neutron region. Chambers with ^{237}Np or ^{238}U are used as *threshold detectors* sensitive only to fast neutrons.

A. BF_3 Tube Pulse Height Spectra—The Wall Effect

Figure 14.3*a* shows the ideal pulse height spectrum expected from a BF_3 tube of very large dimensions. For a large tube, nearly all the reactions occur sufficiently far from the walls of the detector to deposit the full energy of the products within the proportional gas. In that event, all the energy of the reaction is deposited in the detector and the only variation is a result of the branching of the reaction between the excited state and ground state of the ^7Li product nucleus. The branching ratio for thermal neutrons is such that about 6% of the reactions lead to the ground state and 94% to the first excited state. Therefore, the areas under the peaks shown in Fig. 14.3*a* should be in the ratio 94:6 as illustrated.

Once the size of the tube is no longer large compared with the range of the alpha particle and recoil lithium nucleus produced in the reaction, some events no longer deposit the full reaction energy in the gas. If either particle strikes the chamber wall, a smaller pulse is produced. The cumulative effect of this type of process is known as the *wall effect* in gas counters. Because the range of the alpha particle produced in the reaction is on the order of 1 cm for typical BF_3 gas pressures, almost all practical tubes are small enough in diameter so that the wall effect is significant.

Figure 14.3*b* shows the differential pulse height spectrum expected from a tube in which the wall effect is important. The primary change from the spectrum shown in Fig. 14.3*a* is the addition of a continuum to the left of the peaks corresponding to partial energy deposition in the gas of the tube. The two steps or discontinuities in the continuum are an interesting feature of the spectrum and can be explained through the following argument.

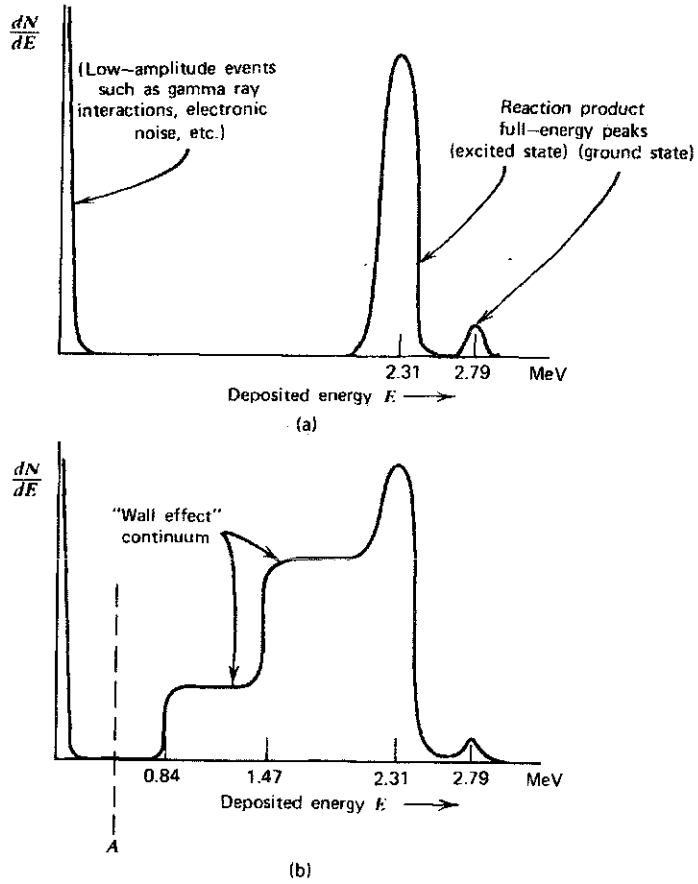

Figure 14.3 Expected pulse height spectra from BF_3 tubes. (*a*) Spectrum from a large tube in which all reaction products are fully absorbed. (*b*) Additional continuum due to the wall effect.

Because the incoming neutron carries no appreciable momentum, the two reaction products must be oppositely directed. If the alpha particle strikes the wall, the ^{7}Li recoil is therefore directed away from the wall and is very likely to deposit its full energy within the gas. Conversely, if the ^{7}Li recoil strikes a wall, the entire energy of the alpha particle from that same reaction is usually fully absorbed.

Thus, we expect to see wall losses for only one reaction product at a time. There are two possibilities: (1) the alpha particle hits a wall after depositing some fraction of its energy in the fill gas, whereas the ^{7}Li recoil is fully absorbed in the gas, or (2) the ^{7}Li recoil hits a wall after depositing part of its energy and the alpha particle is fully absorbed. Under case 1 above, the reaction could occur at a distance from the wall that might be anywhere between zero and the full alpha particle range. The amount of energy deposited in the gas can correspondingly vary from $(E_{Li} + 0)$ to $(E_{Li} + E_\alpha)$, as illustrated below.

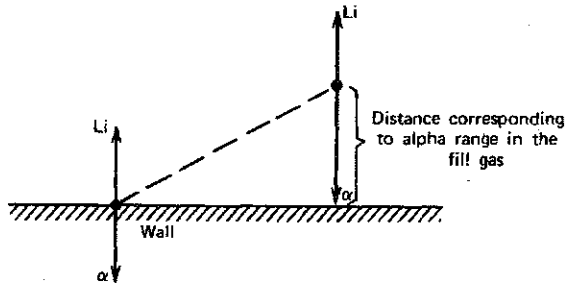

Because all locations of the reaction are more or less equally probable, the distribution of deposited energy will be approximately uniform between these two extremes.

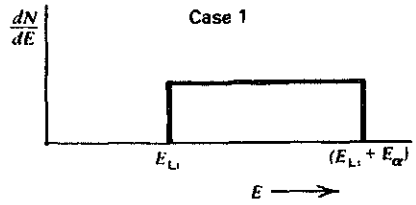

Parallel arguments can be made for case 2 to show that the energy deposited in the gas will vary from $(E_\alpha + 0)$ to $(E_\alpha + E_{Li})$.

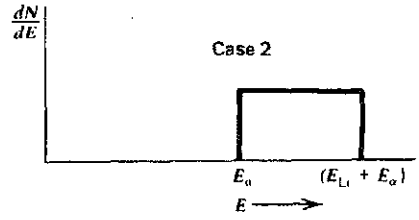

The combined energy deposition distribution of all events in which either reaction product strikes a wall will simply be the sum of the two cases.

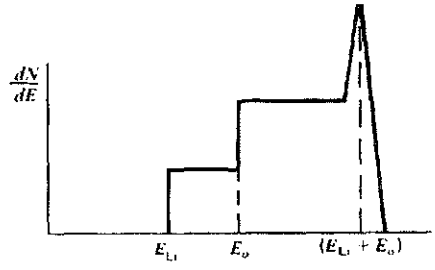

In addition to the wall effect events, the sketch above also shows the location of the full-energy peak that results from all those reactions from which both products are fully absorbed in the gas. The wall effect continuum extends from E_{Li}(0.84 MeV) up to the full-energy peak at $(E_{Li} + E_\alpha)$ (2.31 MeV). We have considered only those reactions leading to the ^{7}Li excited state because the wall effect continuum associated with the much less probable ground state is normally so small as to be submerged by the remainder of the spectrum.

The BF_3 tube is an example of a detector from which the differential pulse height spectrum tells us nothing about the energy spectrum of the incident radiation but is a function only of the size and geometry of the detector itself. In routine applications, there is consequently no motivation to record the pulse height spectrum from a BF_3 tube other than in an indirect manner. Instead, we are likely to seek a stable operating point or a counting plateau for which small drifts in operating parameters do not significantly affect the neutron sensitivity of the counter. That objective would be met by setting a fixed discriminator level at the point labeled *A* in Fig. 14.3*b*, which is below the minimum possible pulse amplitude from a neutron-induced reaction. From the arguments given in Chapter 4, we would expect a counting plateau to appear as the high voltage to the tube is varied, changing the internal gain of the proportional gas multiplication process. The flattest portion of that plateau should occur when the effective discrimination point is at the minimum in the differential pulse height spectrum, or point *A*. Under these conditions, all the neutrons will be counted, whereas low-amplitude events will be rejected. If the wall effect is eliminated or greatly suppressed by making the tube very large, a pulse height spectrum similar to that shown in Fig. 14.3*a* results. The counting plateau will then extend over a much greater range of applied voltage and thereby extend the useful operating range over which all neutron interactions are counted. A rather complete sample of spectra from a variety of BF_3 tubes is presented by Anderson and Malmskog.[9] A theoretical model has been developed by Cervellati and Kazimierski for the expected pulse height distribution from a BF_3 tube and is compared with experimentally measured distributions.[10]

B. BF_3 Tube Construction

The neutron detection efficiency can be increased and the wall effect suppressed by making the tube larger in dimension. Similar improvements can be achieved by raising the pressure of the BF_3 fill gas. Fowler[11] has reported the successful construction and operation of BF_3 tubes with diameter up to 15 cm and 180 cm long. Filling pressure ranged from 100 to 600 torr (approximately 13–80 kPa). Pressures in the range 200–300 torr (approximately 27–40 kPa) gave the best resolution in this work, whereas the full-energy peaks in the spectrum broadened considerably at higher pressure due to recombination and negative ion formation. In many counting situations, the poorer resolution is of no real consequence, and tubes with the higher gas pressure would be quite acceptable as long as a distinct counting plateau is maintained. Small-diameter tubes filled to several atmospheres pressure are commercially available, although pressures in the range 500–600 torr (approximately 67–80 kPa) are much more common.

In common with most proportional counters, BF_3 tubes are universally constructed using cylindrical outer cathodes and small-diameter central wire anodes. Aluminum is often the material of choice for the cathodes because of its low neutron interaction cross section. For low background applications, other materials such as stainless steel are preferred because aluminum normally shows a small amount of low-level alpha activity. With typical anode diameters of 0.1 mm or less, operating voltages tend to be about 2000–3000 V. Larger-diameter anode wires and/or higher fill gas pressures require higher applied voltages. Typical gas multiplication at operating voltage is on the order of 100–500.

BF_3 tubes of typical construction are normally limited to operating temperatures up to about 100°C, but tubes of special design can extend the operating range to as high as 150°C. However, the pulse amplitude decreases and the pulse height resolution decreases

sharply[12] when operated well above room temperature. These changes may be related to the possible desorption of impurities from the counter wall or other components at elevated temperatures.

Because of the relatively high operating voltages, BF_3 tubes share some temperamental qualities with other proportional counters. Spurious pulses of about the same size as signal pulses can sometimes arise from fluctuations in leakage currents through insulators, especially under conditions of high humidity. Spurious counts can also arise in applications in which the counter is subject to vibration or shock.[13] These effects are attributed to detector microphonics and the influence of small particles of lint or dirt within the counter.

In common with other proportional counters, BF_3 tubes show significant effects of aging. In some cases[14] significant degradation in the performance is observed after operation of 10^{10}–10^{11} registered counts. This degradation is likely related to the contamination of the anode wire and cathode wall by molecular disassociation products produced in the avalanches. The same study indicates that ^3He tubes described later in this chapter are more resistant to these effects.

C. Gamma-Ray Discrimination

A very important consideration in many applications of BF_3 tubes is their ability to discriminate against gamma rays, which often are found together with the neutron flux to be measured. Gamma rays interact primarily in the wall of the counter and create secondary electrons that may produce ionization in the gas. Because the stopping power for electrons in gases is quite low, a typical electron will deposit only a small fraction of its initial energy within the gas before reaching the opposite wall of the counter. Thus, we should expect that most gamma-ray interactions will result in low-amplitude pulses that will lie in the tail to the left of point *A* in Fig. 14.3*b*. Simple amplitude discrimination can then easily eliminate these gamma rays without sacrificing neutron detection efficiency.

If the gamma-ray flux is sufficiently high, however, several complications can reduce the effectiveness of this amplitude discrimination. At high rates, pulse pile-up can result in apparent peak amplitudes for gamma rays which are considerably larger than any individual pulse. Brown[15] discusses the compromise that must then be struck in choosing the pulse-shaping time constant in the detector electronics. Short time constants are desirable to reduce the gamma-ray pile-up but may lead to reduction in the neutron-induced pulse amplitude due to incomplete charge integration. At very high gamma rates, there is evidence that chemical changes occur in the BF_3 gas caused by molecular disassociation, leading to degraded pulse height spectra from neutron-induced events.[16] If this degradation is sufficiently severe, it may no longer be possible to separate gamma- and neutron-induced events.[17] In extreme cases, the radiation-induced chemical changes can result in permanent damage to the tube. Verghese et al.[18] report successful discrimination against gamma rays at exposure rates as high as 12 R/h using a conventional BF_3 tube. Developmental tubes that employ activated charcoal within the tube to act as an absorbing agent for contaminants have been reported.[19] These tubes exhibit good operating characteristics in gamma-ray fluxes up to 1000 R/h.

D. Detection Efficiency of a BF_3 Tube

The detection efficiency for neutrons incident along the axis of a BF_3 tube is given approximately by

$$\epsilon(E) = 1 - \exp\left[-\Sigma_a(E)L\right] \tag{14.4}$$

where $\Sigma_a(E)$ = macroscopic absorption cross section of ^{10}B at neutron energy E

L = active length of the tube

Using Eq. (14.4), we find that the calculated efficiency for a 30-cm long BF_3 tube (96% enriched in ^{10}B) filled to 600 torr (80 kPa) is 91.5% at thermal neutron energies (0.025 eV) but drops to 3.8% at 100 eV. Thus, a BF_3 tube exposed to neutrons with mixed energies will respond principally to the slow neutron component. Equation (14.4) slightly overestimates the neutron counting efficiency because there usually are regions near the end of the tube in which charge collection is inefficient, resulting in reduced neutron response. The influence of these *dead spaces* is most severe for detectors whose length is small and has been the subject of experimental investigations that lead to a more precise prediction of detector efficiency.[20] *End window* designs are common in which the dead space and structural materials at one end of the tube are minimized.

Most practical BF_3 counters are filled with pure boron trifluoride enriched to about 96% in ^{10}B. However, because BF_3 is not ideal as a proportional counter gas, counters are sometimes manufactured using BF_3 with an admixture of a more suitable gas such as argon. This dilution causes a decrease in detection efficiency, but the pulse height spectrum from the tube generally shows sharper peaks and consequently a more stable counting plateau than tubes filled with pure BF_3.

E. Boron-Lined Proportional Counters

An alternate approach is to introduce the boron in the form of a solid coating on the interior walls of an otherwise conventional proportional tube. This configuration has the advantage that a more suitable proportional gas than BF_3 can now be used. Some applications, particularly those in which fast timing is important, are better served by introducing one of the common proportional gases discussed in Chapter 6. Also, the chemical degradation problems in BF_3 when exposed to high gamma ray fluxes can be greatly reduced by using alternative fill gases.

Because the maximum range of the alpha particles from the boron reaction is on the order of 1 mg/cm^2, the efficiency of boron-lined counters will improve only as the coating thickness is increased to about this value. Making the deposit any thicker will simply create layers in the coating that are too far from the filling gas to permit any reaction products to reach the gas, and the efficiency will actually begin to decrease slightly because of the added attenuation of the incident neutrons. Efforts have been made to increase the surface area available for coating by introducing boron-coated plates or baffles within cylindrical tubes, but these configurations have not achieved widespread popularity.

The pulse height spectrum to be expected from a boron-lined proportional chamber with a thick boron layer is sketched in Fig. 14.4. Because the interactions are now taking place in the wall of the chamber and the reaction products are oppositely directed, only one reaction product can be expected per interaction. If the alpha particle is directed toward the interior of the tube, the maximum energy it can deposit is its initial kinetic energy of 1.47 MeV. The actual alpha particle energy deposited in the gas will vary from this value down to zero as the possible location of the neutron interaction varies from the surface of the boron coating through those locations that are more than an alpha range away from the counter gas. Because all these locations are almost equally probable, the expected energy deposition distribution for alpha particles will be approximately rectangular in shape with a maximum at 1.47 MeV. This distribution is sketched in Fig. 14.4*a* as a dashed rectangle. A parallel argument can be made for the lithium recoil nucleus, with its maximum possible

Chapter 15

Fast Neutron Detection and Spectroscopy

In Chapter 14 on slow neutron detection, a number of neutron-induced reactions were discussed which can serve as the basis for the conversion of neutrons to directly detectable charged particles. In principle, all these reactions could be applied to detect fast neutrons as well. As shown in the cross-section plot of Fig. 14.1, however, the probability that a neutron will interact by one of these reactions decreases rapidly with increasing neutron energy. As a result, conventional BF_3 tubes have an extremely low detection efficiency for fast neutrons and consequently are almost never used for this purpose. For reasons to be discussed later in this chapter, the ^3He proportional counter is useful both for thermal neutron detection and for fast neutron spectroscopy. As a rule, however, fast neutron devices must employ a modified or completely different detection scheme to yield an instrument with acceptable detection efficiency.

The most important additional conversion process useful for fast neutrons is elastic neutron scattering. In this interaction an incident neutron transfers a portion of its kinetic energy to the scattering nucleus, giving rise to a *recoil nucleus*. The energy that can be transferred from a slow neutron is therefore very small, and the resulting recoil nuclei are too low in energy to generate a usable detector signal. Once the neutron energy reaches the keV range, however, recoil nuclei can be detected directly and assume a large importance for fast neutron detection. By far the most popular target nucleus is hydrogen. The cross section for neutron elastic scattering from hydrogen is quite large and its energy dependence is accurately known. More important, however, is the fact that an incident neutron can transfer up to its entire energy in a single collision with a hydrogen nucleus, whereas only a small fraction can be transferred in collisions with heavy nuclei. Therefore, the resulting *recoil protons* are relatively easy to detect and serve as the basis for a wide variety of fast neutron detectors.

An important distinction in the application of fast neutron detectors is whether an attempt is made to measure the energy of the incoming neutron. For all the slow neutron detection methods discussed in Chapter 14, the information on initial neutron kinetic energy is hopelessly lost in the conversion process, because the neutron energy is extremely small compared with the energy liberated in the conversion reaction itself (the Q-value). Once the incoming neutron energy is no longer negligible compared with the reaction Q-value (that means at least 10–100 keV for most of the reactions discussed in Chapter 14), the energy of the reaction products begins to change appreciably with changes in the neutron energy. An accurate measurement of the reaction product energies can then, in principle, be used to deduce the incoming neutron energy by simply subtracting the reaction Q-value. In elastic scattering the reaction Q-value is zero, so that neutron energies can begin to be measured

by this technique at the point at which the resulting recoils have measurable kinetic energy. The collection of instruments and techniques applied to the measurement of fast neutron energy is conventionally included in the category of *fast neutron spectroscopy.*

In some instances, however, the purpose of the measurement is simply to record the presence of fast neutrons without a corresponding measurement of their energy. Such fast neutron counters can employ any of the methods discussed to convert neutrons to charged particles, and then simply record all pulses from the detector. Fast neutron counters of this type will have a severe variation in efficiency with neutron energy, but if the incident neutron energy is not likely to change greatly between measurements, they can provide useful information on the relative intensity of a fast neutron flux. Other applications in which the fast neutron spectrum may change considerably between measurements benefit from counters tailored to the application. We begin our discussion of fast neutron devices with counters of this type.

I. COUNTERS BASED ON NEUTRON MODERATION

A. General Considerations

The inherently low detection efficiency for fast neutrons of any slow neutron detector can be somewhat improved by surrounding the detector with a few centimeters of hydrogen-containing moderating material. The incident fast neutron can then lose a fraction of its initial kinetic energy in the moderator before reaching the detector as a lower-energy neutron, for which the detector efficiency is generally higher. By making the moderator thickness greater, the number of collisions in the moderator will tend to increase, leading to a lower value of the most probable energy when the neutron reaches the detector. One would therefore expect the detection efficiency to increase with moderator thickness if that were the only factor under consideration. A second factor, however, tends to decrease the efficiency with increasing moderator thickness: The probability that an incident fast neutron ever reaches the detector will inevitably decrease as the moderator is made thicker. Several effects are at work here, as illustrated in Fig. 15.1. As the detector becomes a smaller and smaller fraction of the total volume of the system, there will be a lower probability that a typical neutron path will intersect the detector before escaping from the surface of the moderator. Furthermore, a neutron may be absorbed within the moderator before it has a chance of reaching the detector. The absorption probability will increase rapidly with increasing moderator thickness because absorption cross sections generally are larger at lower neutron energies.

As a result of all these factors, the efficiency of a moderated slow neutron detector when used with a monoenergetic fast neutron source will show a maximum at a specific moderator thickness. Assuming that the moderator is the usual choice of a hydrogenous material such as polyethylene or paraffin, we find that the optimum thickness will range from a few centimeters for keV neutrons up to several tens of centimeters for neutrons in the MeV energy range.

If the thickness of the moderator is fixed at a fairly large value, the overall counting efficiency of the system versus incident neutron energy will also tend to show a maximum. Low-energy neutrons will not penetrate far enough into the moderator before they are likely to be captured in the moderator itself, whereas high-energy neutrons will not be adequately moderated for efficient detection. By careful choice of the diameter and composition of the moderator–detector system, its overall efficiency versus energy curve can often be shaped and tailored to suit a specific application.

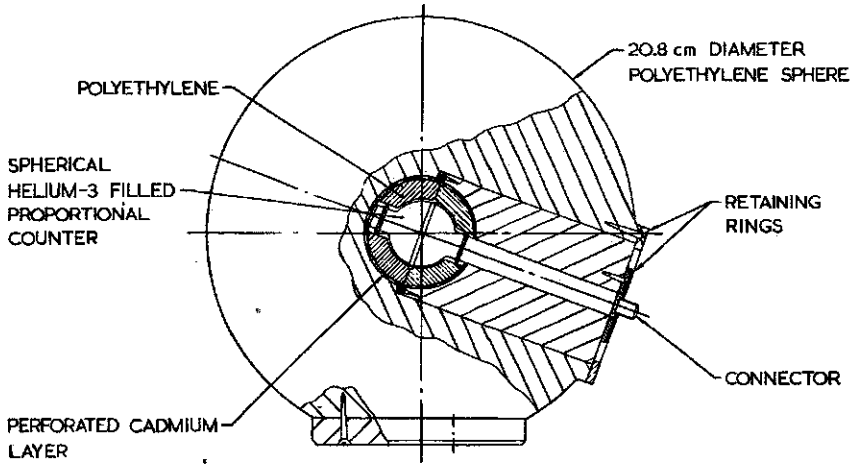

Figure 15.5 A spherical neutron dosimeter based on a ^{3}He neutron detector. (From Leake.[14])

minimize the response of the detector to gamma rays, and Leake reports application of the dosimeter in gamma-ray fields as high as 20 R/h. Used with a simple 20.8-cm diameter polyethylene moderator, the energy response of the system to thermal and epithermal neutrons is higher than ideal. Therefore, a spherical cadmium absorber, perforated with holes, is placed around the ^{3}He detector to shape the response curve. Although the instrument still overresponds to neutrons in the keV energy range (by a factor of 4.9 at 10 keV), the response to broad neutron spectra typical of shielded fission sources does not deviate by more than ±40% for a very wide range of experimental and calculated spectra.[15,16] The response at high neutron energies drops off somewhat; the instrument underestimates the dose from 14 MeV neutrons shielded by concrete by about a factor of 2 (Ref. 15).

There have been continuing efforts to develop new designs of spherical or cylindrical neutron dosimeters[17–20] whose sensitivity more closely matches the dose per neutron curve over a wide energy range. Some of the challenge comes about because of evolving standards for quality factors (see Chapter 2) that are necessary inputs in calculating the desired curve shape. The incorporation of lead or other high-Z elements as heterogeneous components[21,22] increases the relative response to high-energy neutrons, where the response of a pure moderator tends to fall off. Secondary neutrons produced in (n,2n) and other multiplying reactions in these heavy elements at high energies can extend the useful sensitivity to several hundred MeV.

C. The Long Counter

A detector whose counting efficiency does not depend on the neutron energy can be a very useful device in many areas of neutron physics. For an ideal detector of this type, a graph of the detection efficiency versus neutron energy is a horizontal line, which has led to the name *flat response* detectors. Although no real detector exists with a perfectly flat response over the entire range of possible neutron energies, several designs have evolved that come close to this ideal.

Over the years, the most popular flat response neutron detector has been the *long counter.* Like the spherical neutron dosimeter, it is based on the principle of placing a slow neutron detector at the center of a moderating medium. For the long counter, however, the slow neutron detector is a BF_3 tube, and the system is designed to respond properly to neutrons only when they are incident from a specific direction.

The combination of a BF_3 tube and cylindrical moderator was first suggested as a flat response neutron detector by Hanson and McKibben.[23] A later design by McTaggart[24] is shown in Fig. 15.6*a* and has achieved fairly widespread acceptance as the standard long counter. The counter is designed to be sensitive only to neutrons incident on the right-hand face of the counter within the boron oxide shell. Those incident from other directions tend to be moderated by the outer annulus of paraffin and are subsequently captured in the boron layer without giving rise to a count. Neutrons incident on the front face parallel to the cylindrical axis will penetrate some distance before undergoing moderation. The

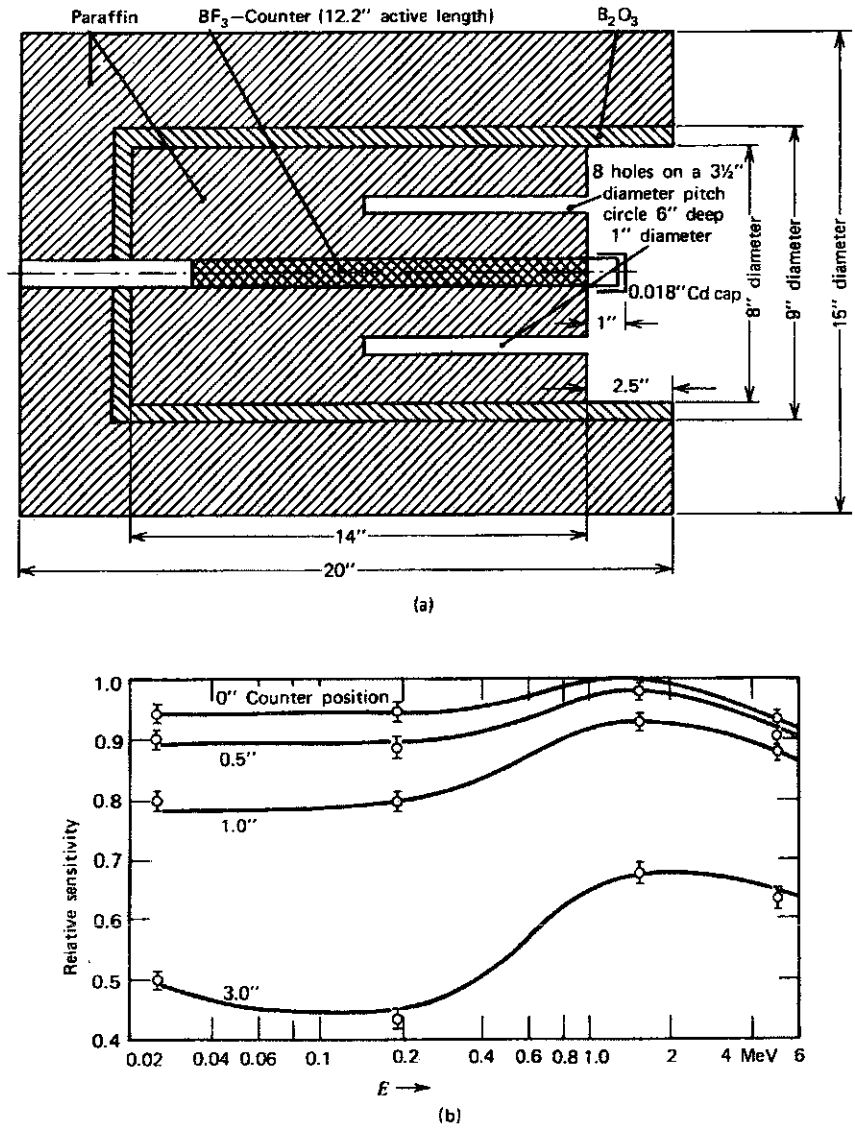

Figure 15.6 (*a*) Cross-section of the long counter developed by McTaggart. (*b*) Relative sensitivity of McTaggart long counter versus neutron energy. The parameter varied for the different curves is the distance the end of the BF_3 tube is shifted in from the front of the moderator face. The flattest response occurs when the tube is flush with the front face. (From K. H. Beckurts and K. Wirtz, *Neutron Physics*. Copyright 1964 by Springer-Verlag, Inc. Used with permission.)

average distance of penetration will increase as the neutron energy increases. If the BF_3 tube and cylindrical moderator are sufficiently long, then a typical cross section through the cylinder at the point of moderation will not be different for various energy neutrons. Therefore, the probability that the moderated neutron will find its way to the BF_3 tube and produce a count should not depend strongly on neutron energy. It is this property that leads to the flat energy response of the detector. The holes provided in the front surface prevent a fall-off in the efficiency at neutron energies below 1 MeV by allowing lower-energy neutrons to penetrate farther into the moderator, away from the front surface from which they might otherwise escape. Figure 15.6*b* shows a plot of the efficiency of a McTaggart long counter versus neutron energy for various axial positions of the BF_3 tube. With the BF_3 tube flush with the front surface, the efficiency does not change by more than 10% over the neutron energy range shown. A long counter of similar design by DePangher and Nichols[25] has also achieved some recognition as a standard in health physics measurements, and documentation of its flat response between about 2 keV and 6 MeV is given in Refs. 26–28.

Long counters derive many of their operational characteristics from the BF_3 tube on which their design is based. Sensitivity to relatively high levels of gamma rays can be eliminated by simple amplitude discrimination, while continuing to count all the neutron interactions in the tube. The long counter normally displays good long-term stability and traditionally has achieved widespread application as a neutron flux monitor in a wide variety of neutron physics experiments.

A modified long counter with some improved characteristics has been developed by East and Walton[29] and is shown in Fig. 15.7. It substitutes ^3He detectors for the BF_3 tube used in McTaggart design and provides five separate detectors near the center of the cylindrical moderator. By using high-pressure ^3He tubes, the multiple detector arrangement leads to a rather high overall neutron detection efficiency of 11.5%, compared with a standard long counter efficiency of about 0.25%. The 12 holes that penetrate the inner polyethylene cylinder are covered on the front face by a 19-mm thick ring of polyethylene to provide a geometry of moderation that best favors an overall flat response. The measured efficiency of this detector is plotted in Fig. 15.8 for a number of neutron sources with broad energy distributions. While the measured efficiency is essentially constant for these sources, greater fluctuation has been observed[30] for more nearly monoenergetic neutrons. These variations can arise because of narrow resonances in the cross sections of some of the constituent materials.

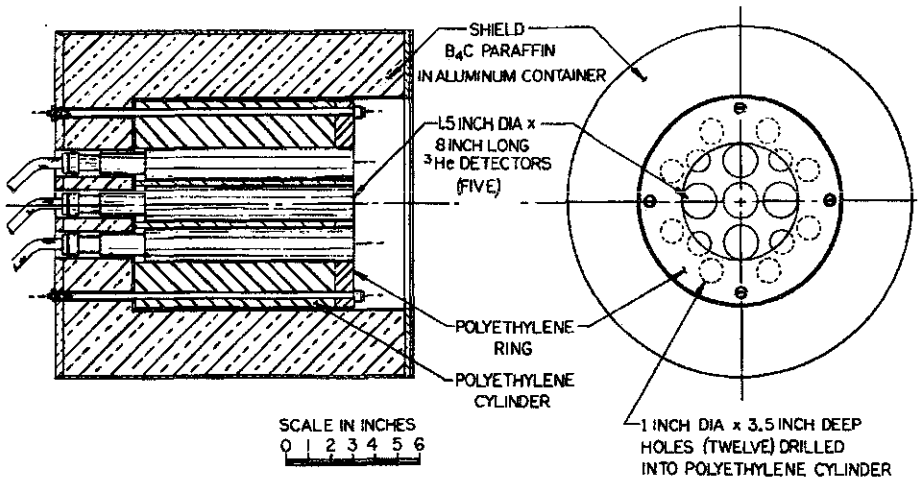

Figure 15.7 A high-efficiency long counter utilizing multiple ^3He tubes. (From East and Walton.[29])

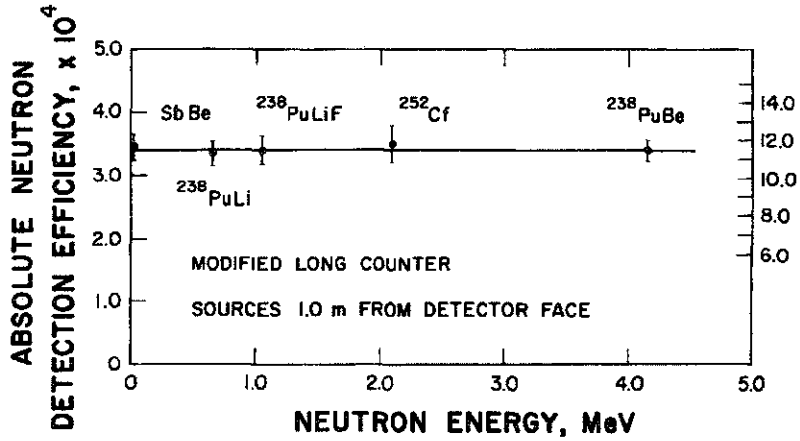

Figure 15.8 Efficiency of the long counter shown in Fig. 15.7 versus the average energy of some neutron sources. The efficiency figures are for a point source located 1 m from the detector face. (From East and Walton. [29])

D. Other Detectors Based on Moderation

A number of detection systems have evolved that consist of a spherical assembly into which the neutron source is inserted. This approach can obviously be used for small portable neutron sources and can also be adapted for a highly collimated parallel beam of neutrons by providing a small-diameter entrance channel through which the beam can pass to reach the center of the assembly. A typical design consists of placing multiple ^{3}He or BF_3 counters in a hydrogenous moderator,[31–36] and in some sense is a spherical version of the long counter. Overall counting efficiencies on the order of 1% can be achieved with a response that is flat to within ±1% over a neutron energy range from 30 keV to 5 MeV.[31]

Other flat response detectors that also rely on neutron moderation have been developed. The *grey neutron detector* of Poenitz[37,38] uses a NaI(Tl) scintillator to detect the 2.2 MeV capture gamma rays produced when neutrons are thermalized in a hydrogenous sphere. To provide a faster response, the *black neutron detector* was also introduced,[39,40] which is based on the light produced in a hydrogenous spherical scintillator as the neutron is moderated. Both types of detectors can provide a very flat efficiency curve over several decades of neutron energy.

II. DETECTORS BASED ON FAST NEUTRON-INDUCED REACTIONS

The detectors described in the previous section rely on the slowing down of a fast neutron in a moderating material before its detection as a thermal neutron. The moderating process eliminates all information on the original energy of the fast neutron and normally cannot be used if an attempt is made to extract energy information. Furthermore, the detection process is relatively slow. In most designs, the neutron must undergo multiple collisions with moderator nuclei followed by diffusion as a thermal neutron (that may take tens or hundreds of microseconds) before the detection signal is generated. As a result, such detectors cannot provide a fast detection signal required in many neutron detection applications.

Both these limitations may be overcome if the fast neutron can be made to induce directly a suitable nuclear reaction without the moderation step. The reaction products will then have a total kinetic energy given by the sum of the incoming neutron kinetic energy and the Q-value of the reaction. Provided the neutron energy is not a hopelessly small fraction of the Q-value, a measurement of the reaction product energies will give the neutron energy by simple subtraction of the Q-value. Additionally, the detection process can potentially be fast because the incoming fast neutron will typically spend no more than a few

15.11 Show that the angle (in the laboratory frame) between a recoil proton and the corresponding scattered neutron is always 90°.

15.12 Using the parameters listed in Table 6.1, estimate the maximum pulse amplitude expected if a methane-filled proportional counter with the following properties is irradiated by 1-MeV neutrons: gas pressure, 0.75 atm; applied voltage, 2000 V; anode radius, 0.005 cm; cathode radius, 2 cm; tube capacitance, 60 pF.

15.13 A silicon detector is irradiated by 1 MeV neutrons. Find the minimum and maximum energies expected for the silicon recoil nuclei produced in elastic scattering of the incident neutrons.

15.14 What basic physical difference leads to the observation that the recoil energy distribution from 5 MeV neutron scattering from hydrogen is uniform or rectangular shaped, while it is highly nonuniform for scattering from helium?

15.15 What factor limits increasing the detection efficiency of a proton recoil telescope by simply increasing the thickness of the hydrogenous radiator?

15.16 A capture-gated neutron spectrometer is based on the use of a plastic scintillator that is loaded with natural boron to 5% by weight (see properties of BC-454 in Table 8.1). Assume that an incident neutron is fully moderated at a position near the center of the scintillator, and begins to diffuse as a thermal (0.025 eV) neutron. Calculate the expected mean time from the start of the diffusion process to the time the thermal neutron triggers a capture reaction in ^{10}B. Offer a justification for why this value is likely to be smaller than the observed pulse pair separation times for capture-gated spectrometers with this composition.

REFERENCES

1. R. L. Bramblett, R. I. Ewing, and T. W. Bonner, *Nucl. Instrum. Meth.* **9**, 1 (1960).
2. T. L. Johnson, Y. Lee, K. A. Lowry, and S. C. Gorbics, *Proceedings of the American Nuclear Society Topical Meeting on Theory and Practices in Radiation Protection and Shielding*, April 1987.
3. G. J. H. Jacobs and R. L. P. van den Bosch, *Nucl. Instrum. Meth.* **175**, 483 (1980).
4. L. W. Brackenbush and R. I. Scherpelz, PNL-SA-11645, CONF-840202-13 (1983).
5. W. H. Miller and R. M. Brugger, *Nucl. Instrum. Meth.* **A236**, 333 (1985).
6. D. W. O. Rogers, *Health Phys.* **37**, 735 (1979).
7. N. E. Hertel and J. W. Davidson, *Nucl. Instrum. Meth.* **A238**, 509 (1985).
8. V. Mares, G. Schraube, and H. Schraube, *Nucl. Instrum. Meth.* **A307**, 398 (1991).
9. A. Aroua et al., *Nucl. Instrum. Meth.* **A321**, 298, 305, and 312 (1992).
10. V. Mares and H. Schraube, *Nucl. Instrum. Meth.* **A337**, 461 (1994).
11. V. Mares and H. Schraube, *Nucl. Instrum. Meth.* **A366**, 203 (1995).
12. D. E. Hankins, LA-2717 (1962).
13. D. E. Hankins and R. A. Pederson, LAMS-2977 (1964).
14. J. W. Leake, *Nucl. Instrum. Meth.* **63**, 329 (1968).
15. K. G. Harrison, *Nucl. Instrum. Meth.* **166**, 197 (1979).
16. J. W. Leake, *Nucl. Instrum. Meth.* **178**, 287 (1980).
17. C. Birattari et al., *Nucl. Instrum. Meth.* **A297**, 250 (1990).
18. C. Birattari et al., *Nucl. Instrum. Meth.* **A324**, 232 (1993).
19. M. Tan, C. M. Chen, Y. Q. Wen, and Z. Wang, *Nucl. Instrum. Meth.* **A339**, 573 (1994).
20. A. Klett and B. Burgkhardt, *IEEE Trans. Nucl. Sci.* **44**(3), 757 (1997).
21. C. Birattari et al., *Rad. Prot. Dosim.* **44**(1/4), 193 (1992).
22. H. H. Hsu, K. R. Alvar, and D. G. Vasilik, *IEEE Trans. Nucl. Sci.* **41**(4), 938 (1994).
23. A. O. Hanson and M. L. McKibben, *Phys. Rev.* **72**, 673 (1947).
24. M. H. McTaggart, AWRE NR/A1/59 (1958).
25. J. De Pangher and L. L. Nichols, BNWL-260 (1966).
26. J. B. Hunt and J. C. Robertson, *Proceedings of the First Symposium on Neutron Dosimetry in Biology and Medicine*, EUR 4896 d-f-e, 935 (1972).
27. D. R. Slaughter and D. W. Rueppel, *Nucl. Instrum. Meth.* **145**, 315 (1977).
28. J. B. Hunt and R. A. Mercer, *Nucl. Instrum. Meth.* **156**, 451 (1978).
29. L. V. East and R. B. Walton, *Nucl. Instrum. Meth.* **72**, 161 (1969).
30. A. E. Evans, *Nucl. Instrum. Meth.* **199**, 643 (1982).
31. R. F. Barrett, J. R. Birkelund, and H. H. Thies, *Nucl. Instrum. Meth.* **68**, 277 (1969).
32. B. K. Kamboj, M. G. Shahani, U. V. Phadnis, and D. Sharma, *Nucl. Instrum. Meth.* **148**, 57 (1978).
33. E. Hochhäuser and E. Schönfeld, *Nucl. Instrum. Meth.* **80**, 347 (1970).
34. K. K. Sekharan, H. Laumer, B. D. Kern, and F. Gabbard, *Nucl. Instrum. Meth.* **133**, 253 (1976).
35. E. A. Sokol et al., *Nucl. Instrum. Meth.* **219**, 336 (1984).
36. R. E. Mayer et al., *Nucl. Instrum. Meth.* **A324**, 501 (1993).
37. W. P. Poenitz, *Nucl. Instrum. Meth.* **58**, 39 (1968).
38. W. P. Poenitz, *Nucl. Instrum. Meth.* **72**, 120 (1969).
39. W. P. Poenitz, ANL-7915 (1972).
40. D. J. DeSimone et al., *Nucl. Instrum. Meth.* **A388**, 443 (1997).
41. J. R. P. Eaton and J. Walker, *Proc. Phys. Soc. (London)* **83**, 301 (1964).
42. D. R. Johnson, J. H. Thorngate, and P. T. Perdue, *Nucl. Instrum. Meth.* **75**, 61 (1969).
43. R. B. Murray, *Nucl. Instrum. Meth.* **2**, 237 (1958).
44. A. R. Spowart, *Nucl. Instrum. Meth.* **75**, 35 (1969).
45. A. R. Spowart, *Nucl. Instrum. Meth.* **82**, 1 (1970).
46. J. M. Neill, D. Huffman, C. A. Preskitt, and J. C. Young, *Nucl. Instrum. Meth.* **82**, 162 (1970).
47. W. R. McMurray, N. J. Pattenden, and G. S. Valail, *Nucl. Instrum. Meth.* **114**, 429 (1974).

48. A. R. Spowart, *Nucl. Instrum. Meth.* **135**, 441 (1976).
49. A. R. Spowart, *Nucl. Instrum. Meth.* **140**, 19 (1977).
50. E. J. Fairley and A. R. Spowart, *Nucl. Instrum. Meth.* **150**, 159 (1978).
51. S. Yamaguchi, *Nucl. Instrum. Meth.* **A274**, 573 (1989).
52. G. L. Jensen and J. B. Czirr, *Nucl. Instrum. Meth.* **205**, 461 (1983).
53. K. H. Abel et al., *Nucl. Instrum. Meth.* **A353**, 114 (1994).
54. G. B. Spector, T. McCollum, and A. R. Spowart, *Nucl. Instrum. Meth.* **A329**, 223 (1993).
55. G. Zanella et al., *Nucl. Instrum. Meth.* **A359**, 547 (1995).
56. C. Maroni, F. Russo, and E. Verondini, *Nucl. Instrum. Meth.* **74**, 256 (1969).
57. I. C. Rickard, *Nucl. Instrum. Meth.* **113**, 169 (1973).
58. M. G. Silk, *Nucl. Instrum. Meth.* **66**, 93 (1968).
59. G. B. Bishop, *Nucl. Instrum. Meth.* **62**, 247 (1968).
60. R. A. Wolfe and W. F. Stubbins, *Nucl. Instrum. Meth.* **60**, 246 (1968).
61. H. Bluhm and D. Stegemann, *Nucl. Instrum. Meth.* **70**, 141 (1969).
62. G. Koutzoukos and C. B. Besant, *J. Br. Nucl. Energy Soc.* **14**, 83 (1975).
63. P. J. Clements, *Nucl. Instrum. Meth.* **127**, 61 (1975).
64. T. Pinelli et al., *Nucl. Instrum. Meth.* **150**, 497 (1978).
65. A. Sayres and M. Coppola, *Rev. Sci. Instrum.* **35**, 431 (1964).
66. J. L. Friedes and R. E. Chrien, *Rev. Sci. Instrum.* **35**, 469 (1964).
67. T. Fuse, T. Miura, A. Yamaji, and T. Yoshimura, *Nucl. Instrum. Meth.* **74**, 322 (1969).
68. S. Nishino, T. Nakamura, and T. Hyodo, *Mem. Fac. Eng. (Kyoto Univ.)* **35**(3), 309 (1973).
69. E. Dietze et al., *Nucl. Instrum. Meth.* **A332**, 521 (1993).
70. N. Takeda and K. Kudo, *IEEE Trans. Nucl. Sci.* **41**(4), 880 (1994).
71. S. Izumi and Y. Murata, *Nucl. Instrum. Meth.* **94**, 141 (1971).
72. J. M. Cuttler, S. Greenberger, and S. Shalev, *Nucl. Instrum. Meth.* **75**, 309 (1969).
73. H. Takahashi et al., *Nucl. Instrum. Meth.* **A353**, 164 (1994).
74. H. Franz et al., *Nucl. Instrum. Meth.* **144**, 253 (1977).
75. J. G. Owen, D. R. Weaver, and J. Walker, *Nucl. Instrum. Meth.* **188**, 579 (1981).
76. W. A. Fisher, S. H. Chen, D. Gwinn, and R. R. Parker, *Nucl. Instrum. Meth.* **219**, 179 (1984).
77. A. E. Evans, *IEEE Trans. Nucl. Sci.* **NS-32**(1), 54 (1985).
78. K.-H. Beimer, G. Nyman, and O. Tengblad, *Nucl. Instrum. Meth.* **A245**, 402 (1986).
79. H. Ohm, K.-L. Kratz, and S. G. Prussin, *Nucl. Instrum. Meth.* **A256**, 76 (1987).
80. F. Hoenen and W. Bieger, *Nucl. Instrum. Meth.* **A259**, 529 (1987).
81. M. J. Loughlin, J. M. Adams, and G. Sadler, *Nucl. Instrum. Meth.* **A294**, 606 (1990).
82. T. Iguchi, N. Nakayamada, H. Takahashi, and M. Nakazawa, *Nucl. Instrum. Meth.* **A353**, 152 (1994).
83. S. Shalev and J. Cuttler, *Nucl. Sci. Eng.* **51**, 52 (1973).
84. A. E. Evans, Jr., "Development of a High-Pressure ^{3}He Neutron Scintillator Spectrometer," Los Alamos National Laboratory Program Technical Note, LA-Q2TN-82-109, Apr. 29, 1982.
85. M. S. Derzon, D. R. Slaughter, S. G. Prussin, *IEEE Trans. Nucl. Sci.* **NS-33**(1), 247 (1986).
86. H. Bluhm, *Nucl. Instrum. Meth.* **115**, 325 (1974).
87. M. G. Silk, "The Determination of the Fast Neutron Spectrum in Thermal Reactors Using ^{6}Li and ^{3}He Semiconductor Spectrometers," AERE-R-5183 (1966).
88. T. R. Jeter and M. C. Kennison, *IEEE Trans. Nucl. Sci.* **NS-14**(1), 422 (1967).
89. J. B. Marion and F. C. Young, *Nuclear Reaction Analysis*, North-Holland, Amsterdam, 1968.
90. J. A. Harvey and N. W. Hill, *Nucl. Instrum. Meth.* **162**, 507 (1979).
91. A. A. Naqvi et al., *Nucl. Instrum. Meth.* **A325**, 574 (1993).
92. A. Aksoy et al., *Nucl. Instrum. Meth.* **A337**, 486 (1994).
93. S. Mouatassim et al., *Nucl. Instrum. Meth.* **A359**, 530 (1995).
94. A. A. Naqvi, M. M. Nagadi, S. Shaheen, and A. Bari, *Nucl. Instrum. Meth.* **A356**, 330 (1995).
95. N. Colonna and G. Tagliente, *Nucl. Instrum. Meth.* **A416**, 109 (1998).
96. F. Arneodo et al., *Nucl. Instrum. Meth.* **A418**, 285 (1998).
97. J. H. Lee and C. S. Lee, *Nucl. Instrum. Meth.* **A402**, 147 (1998).
98. F. D. Brooks et al., *Nucl. Instrum. Meth.* **A410**, 319 (1998).
99. J. Devos et al., *Nucl. Instrum. Meth.* **135**, 395 (1976).
100. R. H. Johnson et al., *Nucl. Instrum. Meth.* **145**, 337 (1977).
101. D. Slaughter and R. Strout II, *Nucl. Instrum. Meth.* **198**, 349 (1982).
102. R. Ofek, A. Tsechanski, A. E. Profio, and G. Shani, *Nucl. Instrum. Meth.* **A278**, 513 (1989).
103. P. R. P. Coelho, A. A. Da Silva, and J. R. Maiorino, *Nucl. Instrum. Meth.* **A280**, 270 (1989).
104. M. J. Coolbaugh, R. E. Faw, and W. Meyer, "Fast Neutron Spectroscopy in Aqueous Media Using an NE213 Proton Recoil Spectrometer System," COO-2049-7 (1971).
105. M. E. Toms, *Nucl. Instrum. Meth.* **92**, 61 (1971).
106. P. Marinkovic, S. Avdic, M. Pesic, and N. Zavaljevski, *Nucl. Instrum. Meth.* **A321**, 333 (1992).
107. N. Sasamoto and S. Tanaka, *Nucl. Instrum. Meth.* **148**, 395 (1978).
108. M. Bormann, R. Kühl, K. Schäfer, and U. Seebeck, *Nucl. Instrum. Meth.* **88**, 245 (1970).
109. D. Hermsdorf, K. Pasieka, and D. Seeliger, *Nucl. Instrum. Meth.* **107**, 259 (1973).
110. J. L. Fowler et al., *Nucl. Instrum. Meth.* **175**, 449 (1980).
111. M. Drosg, D. M. Drake, and P. Lisowski, *Nucl. Instrum. Meth.* **176**, 477 (1980).
112. J. Cub et al., *Nucl. Instrum. Meth.* **A274**, 217 (1989).
113. K. Gul, A. A. Naqvi, and H. A. Al-Juwair, *Nucl. Instrum. Meth.* **A278**, 470 (1989).
114. T. Akimoto et al., *IEEE Trans. Nucl. Sci.* **38**(5), 1040 (1991).
115. S. Meigo, *Nucl. Instrum. Meth.* **A401**, 365 (1997).
116. M. A. Al-Ohali et al., *Nucl. Instrum. Meth.* **A396**, 388 (1997).
117. R. Cherubini et al., *Nucl. Instrum. Meth.* **A281**, 349 (1989).
118. G. Dietze and H. Klein, *Nucl. Instrum. Meth.* **193**, 549 (1982).
119. A. V. Hristova, E. I. Vapirev, L. T. Tsankov, and V. Jordanov, *Appl. Radiat. Isot.* **41**(9), 887 (1990).
120. R. E. Howe, *Nucl. Instrum. Meth.* **190**, 309 (1981).
121. A. G. Da Silva et al., *Nucl. Instrum. Meth.* **A264**, 381 (1988).
122. M. Moszynski et al., *Nucl. Instrum. Meth.* **A317**, 262 (1992).
123. M. Moszynski et al., *Nucl. Instrum. Meth.* **A350**, 226 (1994).
124. N. A. Lurie, L. Harris, Jr., and J. C. Young, *Nucl. Instrum. Meth.* **129**, 543 (1975).
125. C. Chen, J. A. Lockwood, and L. Hsieh, *Nucl. Instrum. Meth.* **138**, 363 (1976).
126. D. T. Ingersoll and B. W. Wehring, *Nucl. Instrum. Meth.* **147**, 551 (1977).
127. L. Büermann et al., *Nucl. Instrum. Meth.* **A332**, 483 (1993).
128. T. Novotny, L. Büermann, S. Guldbakke, and H. Klein, *Nucl. Instrum. Meth.* **A400**, 356 (1997).
129. P. L. Reeder et al., *Nucl. Instrum. Meth.* **A422**, 84 (1999).

130. V. V. Verbinski and R. Giovannini, *Nucl. Instrum. Meth.* **114**, 205 (1974).
131. P. K. Ray and E. S. Kenney, *Nucl. Instrum. Meth.* **144**, 579 (1977).
132. E. F. Bennett, *Nucl. Sci. Eng.* **27**, 16 (1967).
133. P. W. Benjamin, C. D. Kemshall, and J. Redfearn, *Nucl. Instrum. Meth.* **59**, 77 (1968).
134. E. Korthaus, EURFNR-1197; KFK-1994 (1974).
135. W. H. Miller, *Nucl. Instrum. Meth.* **A279**, 546 (1989).
136. K. Weise, M. Weyrauch, and K. Knauf, *Nucl. Instrum. Meth.* **A309**, 287 (1991).
137. E. F. Bennett and T. J. Yule, ANL-7763 (1971).
138. E. F. Bennett and T. J. Yule, *Nucl. Instrum. Meth.* **98**, 393 (1972).
139. N. L. Snidow and H. D. Warren, *Nucl. Instrum. Meth.* **51**, 109 (1967).
140. R. Gold and E. F. Bennett, *Nucl. Instrum. Meth.* **63**, 285 (1968).
141. D. W. Vehar and F. M. Clikeman, *Nucl. Instrum. Meth.* **190**, 351 (1981).
142. S. A. Heiberg, *Nucl. Instrum. Meth.* **63**, 71 (1968).
143. M. Weyrauch, A. Casnati, P. Schillebeeckx, and M. Clapham, *Nucl. Instrum. Meth.* **A403**, 442 (1998).
144. H. F. Atwater, *Nucl. Instrum. Meth.* **100**, 453 (1972).
145. I. R. Brearley, A. Bore, N. Evans, and M. C. Scott, *Nucl. Instrum. Meth.* **192**, 439 (1982).
146. H. Werle, G. Fieg, H. Seufert, and D. Stegemann, *Nucl. Instrum. Meth.* **72**, 111 (1969).
147. T. B. Ryves, *Nucl. Instrum. Meth.* **135**, 455 (1976).
148. M. Cambiaghi, F. Fossati, and T. Pinelli, *Nucl. Instrum. Meth.* **82**, 106 (1970).
149. H. Gotoh and H. Yagi, *Nucl. Instrum. Meth.* **97**, 419 (1971).
150. H. Gotoh and H. Yagi, *Nucl. Instrum. Meth.* **101**, 395 (1972).
151. D. Sloan and J. C. Robertson, *Nucl. Instrum. Meth.* **198**. 365 (1982).
152. B. R. L. Siebert, H. J. Brede, and H. Lesiecki, *Nucl. Instrum. Meth.* **A235**, 542 (1985).
153. K. N. Geller, D. Eccleshall, and T. T. Bardin, *Nucl. Instrum. Meth.* **69**, 141 (1969).
154. J. H. Osborne et al., *Nucl. Instrum. Meth.* **A345**, 308 (1994).
155. H. Borst, *Nucl. Instrum. Meth.* **169**, 69 (1980).
156. C. Mori et al., *Nucl. Instrum. Meth.* **A422**, 75 (1999).
157. W. C. Feldman, G. F. Auchampaugh, and R. C. Byrd, *Nucl. Instrum. Meth.* **A306**, 350 (1991).
158. E. A. Kamykowski, *Nucl. Instrum. Meth.* **A317**, 559 (1992).
159. T. Aoyama et al., *Nucl. Instrum. Meth.* **A333**, 492 (1993).
160. J. B. Czirr and G. L. Jensen, *Nucl. Instrum. Meth.* **A349**. 532 (1994).

Nuclear Instruments and Methods in Physics Research A 618 (2010) 275–283

Contents lists available at ScienceDirect

Nuclear Instruments and Methods in Physics Research A

journal homepage: www.elsevier.com/locate/nima

The neutron long counter NERO for studies of β–delayed neutron emission in the r-process

J. Pereira [a,b,*], P. Hosmer [a,b,c,1], G. Lorusso [a,b,c], P. Santi [a,b,2], A. Couture [d,e,f], J. Daly [d,e,f], M. Del Santo [a,b], T. Elliot [a,b,c], J. Görres [d,e,f], C. Herlitzius [b,g], K.-L. Kratz [h,i], L.O. Lamm [d,e,f], H.Y. Lee [d,e,f], F. Montes [a,b], M. Ouellette [a,b,c], E. Pellegrini [a,b,c], P. Reeder [j], H. Schatz [a,b,c], F. Schertz [g,i], L. Schnorrenberger [a,b,k], K. Smith [a,b,c], E. Stech [d,e,f], E. Strandberg [d,e,f], C. Ugalde [d,e,f], M. Wiescher [d,e,f], A. Wöhr [d,e,f]

[a] National Superconducting Cyclotron Laboratory, Michigan State University, East Lansing, Michigan, USA
[b] Joint Institute for Nuclear Astrophysics, Michigan State University, East Lansing, Michigan, USA
[c] Department of Physics and Astronomy, Michigan State University, East Lansing, Michigan, USA
[d] Institute of Structure and Nuclear Astrophysics, University of Notre Dame, South Bend, Indiana, USA
[e] Department of Physics and Astronomy, University of Notre Dame, South Bend, Indiana, USA
[f] Joint Institute for Nuclear Astrophysics, University of Notre Dame, South Bend, Indiana, USA
[g] Institute für Kernchemie, Universität Mainz, Germany
[h] Max-Plank-Insitut für Chemie, Universität Mainz, Germany
[i] Virtuelles Institut für Struktur der Kerne and Nuklearer Astrophysik, Mainz, Germany
[j] Pacific Northwest National Laboratory, Richland, Washington, USA
[k] Institute für Kernphysik, TU Darmstadt, Germany

ARTICLE INFO

Article history:
Received 8 October 2009
Received in revised form
8 February 2010
Accepted 24 February 2010
Available online 4 March 2010

Keywords:
Large neutron counter
β–delayed neutron emission
Astrophysical r-process
Neutron detection efficiency
Neutron background

ABSTRACT

The neutron long counter NERO was built at the National Superconducting Cyclotron Laboratory (NSCL), Michigan State University, for measuring β–delayed neutron-emission probabilities. The detector was designed to work in conjunction with a β–delay implantation station, so that β decays and β–delayed neutrons emitted from implanted nuclei can be measured simultaneously. The high efficiency of about 40%, for the range of energies of interest, along with the small background, are crucial for measuring β–delayed neutron emission branchings for neutron-rich r-process nuclei produced as low intensity fragmentation beams in in-flight separator facilities.

Published by Elsevier B.V.

1. Introduction

The emission of β–delayed neutrons by neutron-rich nuclei significantly influences [1] the nucleosynthesis of heavy elements in the rapid (r-) neutron-capture process [2,3]. This decay mechanism competes with the β decay of r-process nuclei towards the valley of stability and serves as an additional source of neutrons in late stages of the r-process [4]. Measurements of β–delayed neutron emission probabilities (P_n) are needed for reliable r-process model calculations, and to test the astrophysical assumptions in various r-process models by comparing their final abundance predictions with observations.

From a nuclear-structure point of view, the P_n value provides model constraints at low beam intensities where γ–spectroscopy is difficult. The P_n value probes β–delay strength at excitation energies slightly above the neutron threshold. It therefore provides nuclear structure information complementary to β–delay, which often favors low energy β–delay strength owing to the larger phase space (see for example Refs. [5,6]).

The experimental determination of P_n requires the measurement of β–delayed neutrons in coincidence with the β particles emitted from the nucleus of interest. This is particularly challenging for nuclei near or at the r-process path due to their very low production rates and the relatively short half-lives—of the order of 10–100 ms. Experiments performed at ISOL-type facilities have successfully

* Corresponding author at: National Superconducting Cyclotron Laboratory, Michigan State University, East Lansing, Michigan, USA. Tel.: +1 517 908 7428; fax: +1 517 353 5967.
E-mail address: pereira@nscl.msu.edu (J. Pereira).
[1] Present address: Navy Nuclear Power School, Goose Creek, South Carolina, USA.
[2] Present address: Los Alamos National Laboratory, MS E540, Los Alamos, New Mexico, USA.

0168-9002/$ - see front matter Published by Elsevier B.V.
doi:10.1016/j.nima.2010.02.262

exploited the use of neutron long counters (NLC) [7] to measure P_n values of neutron-rich nuclei (see, for instance, the compilations of Refs. [8,9]). NLCs generally consist of a series of gas proportional counters embedded into a moderator block used to thermalize the neutrons prior to their detection. Performance requirements include a high detection efficiency for neutron energies ranging from a few keV to ≈ 1 MeV. Because the detector does not measure the energy of individual neutrons, variations of the efficiency as a function of energy have to be minimized as much as possible as they otherwise can translate into uncertainties in the measured P_n. Our goal was to keep detector induced systematic uncertainties well below the 10% level. Measurements at that level of accuracy are a dramatic improvement over theoretical predictions, and ensure that other uncertainties dominate astrophysical and nuclear structure models. With systematic errors at that level, statistical errors will tend to dominate in practice, as the most interesting isotopes will typically be produced at rather low rates.

We report here the development of NERO, a new NLC at National Superconducting Cyclotron Laboratory (NSCL) suitable for use with fast radioactive beams produced by in-flight fission and fragmentation. This technique provides exotic beams without some of the limitations induced by chemistry-based target-extraction techniques. The short time required to transport, separate, and identify the produced fragments, typically less than few hundred ns, makes it possible to study the very short-lived nuclei in the r-process. The fragments of interest are implanted in an active catcher that is part of the NSCL Beta Counting System (BCS) [37]. Implantation of a fragment and emitted β particles are detected event-by-event. The correlation of decays with a previously implanted nucleus requires large area highly pixelated catchers, typically double-sided silicon strip detectors (DSSDs). The challenge in the design of NERO was to include a large cylindrical cavity capable of accommodating such a system, while still fulfilling the performance requirements for the detection efficiency. The final design was inspired by existing NLC detectors such as the Mainz Neutron Detector [10].

2. Technical aspects

2.1. Design

The detector system consists of a 60 × 60 × 80 cm^3 polyethylene matrix (density 0.93(1) g/cm^3) with its long symmetry axis aligned with the beam. Along the beam axis, the matrix has a cylindrical cavity with a diameter of 22.8 cm to accommodate the BCS (see Fig. 1, left).

NERO includes three different types of cylindrical proportional counters manufactured by Reuter-Stokes: filled with ^{3}He (models RS-P4-0814-207 and RS-P4-0810-104), and filled with BF_3 (model RS-P1-1620-205) (see Table 1 for details). Sixty of these detectors are arranged in three concentric rings around the central symmetry axis, allowing for a nearly 4π solid angle coverage around the implantation detector (see Fig. 1, right). The optimum detector configuration was found using the MCNP code [11] to calculate the neutron-detection efficiency for different geometries, moderating materials, and number and arrangement of various types of proportional counters. Interactions of neutrons with the different detector materials were calculated, using the ENDF/B-VI [12] cross-sections in the energy range 10^{-5} eV to 20 MeV. The influence of different environments such as laboratory floor and wall configurations were investigated but were found to be negligible. According to these calculations, most of the neutrons emitted from the center of NERO are detected in the innermost ring. Therefore, 16 of the more compact and efficient ^{3}He gas-filled proportional counters are mounted in the innermost ring at a radius of 13.6 cm. For the middle and outer rings at radii of 19.2 and 24.8 cm we use 20 and 24 BF_3 proportional counters, respectively. The BF_3 counters are longer allowing one to cover more solid angle, and their efficiency just compensates the decreasing efficiency of the inner ring with increasing neutron energy.

To facilitate transportation and assembly, the polyethylene block is divided into an upper and lower half, and each half is subdivided into six equal parts along the longest symmetry axis. The 12 pieces are held together with eight stainless steel bolts.

2.2. Electronics

The NERO readout channels are grouped into four quadrants with 15 channels each (four ^{3}He counters and 11 BF_3 counters). Fig. 2 shows a schematic diagram of the NERO electronics for one quadrant. The proportional counters detect the charged particles produced in the exothermic neutron-capture reaction ^{3}He(n,p) or ^{10}B(n,α), respectively. Their signals feed 16-channel preamplifiers built at NSCL using Cremat CR-101D miniature charge-sensitive preamp chips. The pre-amplified signals are sent into four 16-channel shaper and discriminator modules, designed at Washington University, St. Louis, and manufactured by Pico Systems [13]. These modules integrate independent shaping and discriminating circuits sharing the same input. Shaping times and pole-zero cancelation are adjusted for each channel by properly selecting the capacitances. The gain and threshold levels of the shaper/discriminator are adjusted via computer control over the CAMAC bus.

The logic signals from the discriminator are recorded in scalers and in a 64-channel multi-hit (VME) TDC that is common for all quadrants. The TDC was programmed to work in start-gate mode, in which a gate signal, generated by a β decay detected in the BCS, enables the module to accept multiple stop signals in each

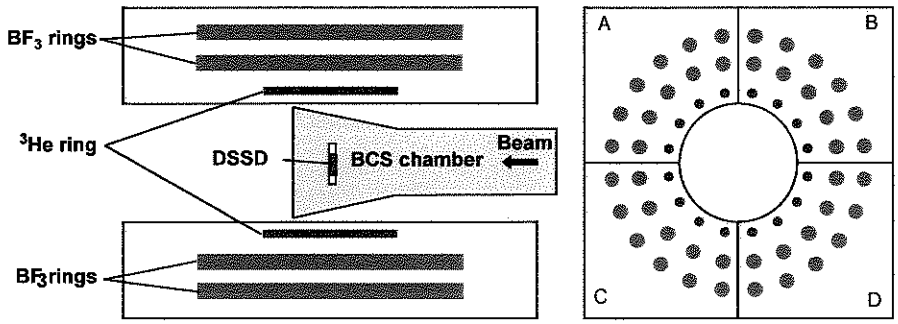

Fig. 1. Schematic drawings of the NERO detector. Left: side view showing the BCS chamber located inside of NERO with the DSSD at the central position. Right: backside showing the cylindrical cavity to house the BCS and the three concentric rings of gas-filled proportional counters. The labels A, B, C and D designate the four quadrants.

Table 1
Technical specifications of the NERO gas-filled proportional counters.

Detector	Active length (cm)	Radius (cm)	Nominal pressure (atm)	Gas composition	High voltage (+V)
^{3}He (a)	25.0(2)	1.3(2)	10.2	100% ^{3}He	1350
^{3}He (b)	35.6(2)	1.3(2)	4.0	100% ^{3}He	1100
BF_3	50.8(1)	2.5(2)	1.2	>96% ^{10}B	600

(a) and (b) refer to the ^{3}He detector models RS-P4-0810-104 and RS-P4-0814-207, respectively.

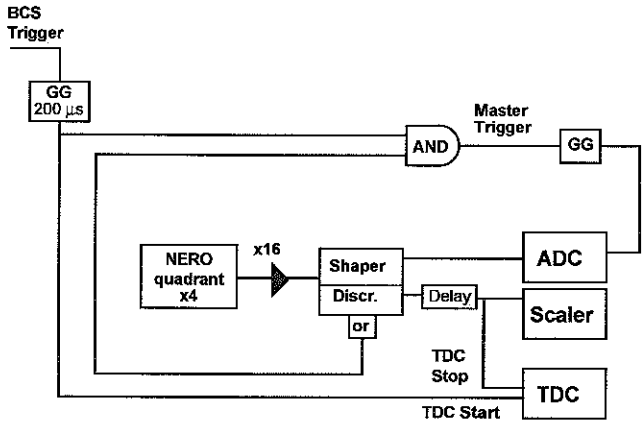

Fig. 2. NERO electronic diagram (see text for details). For clarity only one NERO quadrant is shown (GG stands for Gate Generator).

channel from any of the 60 gas counters. The duration of this gate ($\tau = 200\,\mu s$) was chosen to account for the time needed to moderate and detect the neutrons (see Section 3.1). The P_n value of a given nucleus is extracted from the number of stops-signals registered in the TDC (i.e., neutrons correlated with β decays) relative to the number of β decays detected in the BCS.

The shaper outputs are connected to 32-channel (VME) ADC cards. The pulse height spectra recorded by the ADCs are used to set the thresholds and gains of the shaper/discriminator units, and to monitor any background or gain variation during the course of an experiment. Fig. 3 shows typical ADC spectra for ^{3}He and BF_3 gas counters recorded under different conditions. The spectra show the typical wall-effect: The location of the peak at high amplitudes marks the Q value of the neutron-capture reaction, i.e., ^{3}He(n,p)t and ^{10}B(n,α)^{7}Li for the ^{3}He and BF_3 gas counters, respectively; the plateau or low energy tail at low amplitudes arises from events where reaction products hit the detector wall preventing the complete deposition of their energy in the counter gas. Thresholds are set below these low amplitude events and just above the tail of the prominent low energy peak generated by electronic noise and background γ radiation. Note that unlike the TDC, the ADCs only register one neutron per BCS trigger.

3. Detector performance

3.1. Moderation time

In order to determine the optimal duration of the TDC gate τ, we measured the time needed by the neutrons to slow down in the polyethylene moderator before their detection (τ_n). A ^{252}Cf source was located at the center of NERO facing a NaI scintillator at a distance of 5 cm. Neutrons and γ rays were emitted in coincidence from the fragments produced in the spontaneous fission of ^{252}Cf. The scintillator was used to detect the γ rays, which provided the external trigger of the NERO electronics (replacing the BCS trigger shown in Fig. 2). The time difference between the detection of a γ ray and the subsequent moderated neutrons recorded in the multi-hit TDC provided τ_n. The distribution of τ_n is shown in Fig. 4 (left) for the innermost, intermediate, and outer rings of proportional counters, as well as for the whole detector.

The largest differences between the three rings are found at the shortest times, when most of the neutrons emitted from the center of NERO reach the innermost ring. At late times, the neutrons are more uniformly distributed over the whole moderator, and the three rings have similar detection rates. For each ring, the excellent agreement of the measured, background-subtracted moderation-time distributions with MCNP simulations is shown in Fig. 4. Between 50 and 300 μs the time distributions can be approximated with exponential functions. The corresponding measured and calculated moderation time scales are 43 and 41 μs for the first ring, 51 and 52 μs for the second ring, and 55 and 59 μs for the third ring, respectively.

From Fig. 4, we find that 94.3(1)% of the neutrons are detected within $\tau_n \leq 200\,\mu s$. The energies E_n of the neutrons emitted in the spontaneous fission of ^{252}Cf are typically described by a Maxwell–Boltzmann distribution function with an effective temperature of $kT = 1.42$ MeV [14], an average neutron energy of 2.1 MeV and a smooth tail at higher energies that extends up to 9 MeV. These are higher energies than typically expected for β–delayed neutrons (see discussion at the end of Section 3.2.4). Since the moderation time increases with neutron energy, we expect that more than 94.3(1)% of β–delayed neutrons are detected within 200 μs. We therefore chose a TDC gate of $\tau = 200\,\mu s$.

3.2. Efficiency

In order to characterize the NERO efficiency and its energy dependence, different types of measurements were performed using a ^{252}Cf neutron source of known activity and neutrons produced in resonant and non-resonant reactions at the Institute for Structure and Nuclear Astrophysics (ISNAP) at the University of Notre Dame. The results obtained from these reactions were used to constrain the energy dependence of the NERO efficiency.

3.2.1. Measurement of NERO efficiency with a ^{252}Cf neutron source

Before and after the calibration measurements performed at the University of Notre Dame, the NERO efficiency was measured with a 1.251(5) μCi ^{252}Cf calibration source with an active diameter of 5 mm (neutron branching 11.6% and half-life 2.689 years). Additional contributions to the total neutron rate from contaminants were estimated. Besides ^{252}Cf, there are small impurities of $^{249-251}$Cf and ^{254}Cf. ^{249}Cf and ^{251}Cf have a negligibly small spontaneous fission branch, whereas the present amount of ^{254}Cf was very small due to its short half-life. Consequently, only the ^{250}Cf and ^{252}Cf isotopes had to be considered. At the time of the measurement, 3.6% of the total activity of the source was due to ^{250}Cf, whose contribution to the neutron activity was negligible due to its very low neutron branching of 0.296%. The alpha decay of ^{252}Cf produces ^{248}Cm, which undergoes spontaneous fission accompanied with neutron emission, with a branching ratio of

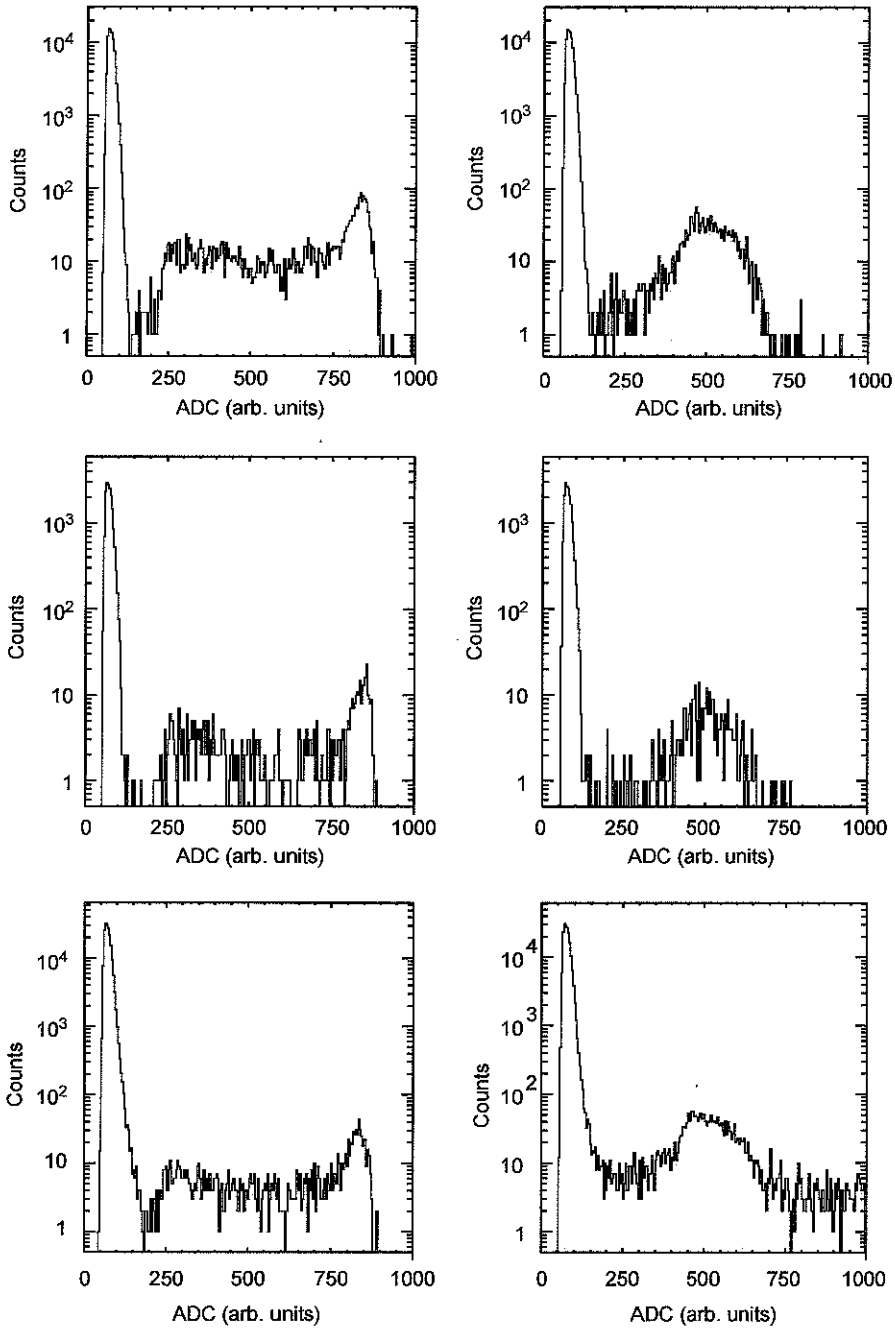

Fig. 3. NERO ADC spectra for one of the ^{3}He (left panels) and BF_3 (right panel) gas counters. The top panels were recorded during 5 min, using a ^{252}Cf neutron source at the center of NERO. The middle panels correspond to a 1-h measurement with nuclei produced in the reaction ^{136}Xe (150 MeV/u)+Be that were implanted in the BCS and included β delayed neutron emitters. The data displayed in the bottom panels were recorded during a 12-h background measurement without beam on target using NERO as trigger.

8.39%. The very long half-life of this radioisotope (3.48×10^5 years) made its contribution to the total neutron rate negligible.

The number of detected neutrons was recorded with scalers and the multi-hit TDC described in Section 2.2. We verified that data processing dead time is negligible up to 50 kHz, well above the activity of the source, using a random pulser. Similarly, the 2 μs dead-time in the proportional counters was negligible. Taking the ratio of the number of neutrons recorded with NERO to the number of neutrons emitted by the source, calculated from the known source activity and neutron branching, we obtained a neutron detection efficiency of 31.7(2)%. This value also serves as a reference point to verify the NERO efficiency before, during, and after experiments.

3.2.2. *Measurement of NERO efficiency with resonant reactions*

The two resonant reactions used to study the NERO efficiency were ^{13}C(α, n)^{16}O [15–17] and ^{11}B(α, n)^{14}N [18,19]. The ISNAP KN Van de Graff accelerated a beam of α particles impinging onto ^{13}C and ^{11}B targets of 14(2) and 12^{+4}_{-2} μg/cm^2 thickness, respectively, located at the center of the NERO symmetry axis. The rate of incident α particles (I_α) was monitored with an

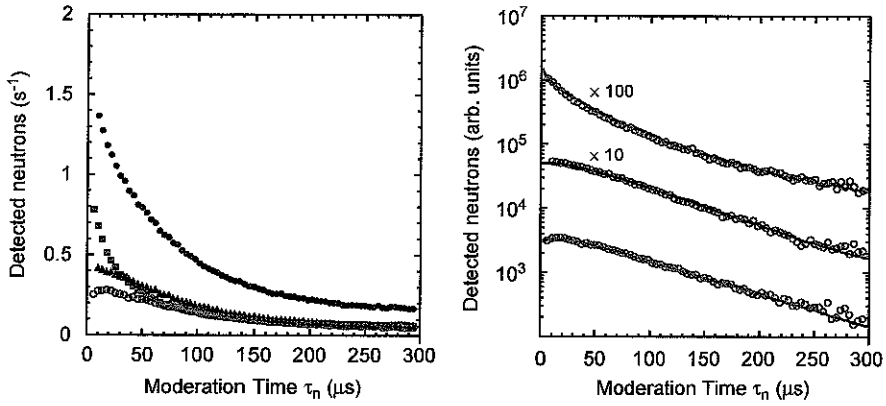

Fig. 4. (Color online). Left: measured background-subtracted moderation time distributions for a ^{252}Cf source for the innermost ring (squares), the intermediate ring (triangles), the outer ring (empty circles) and for the entire detector (solid circles). Right: moderation-time distribution for each ring (empty circles), compared with results obtained with MCNP (solid lines). For easy comparison, the measured and calculated distributions for the first and second rings are scaled by 100 and 10, respectively. Note that the error bars of the experimental data are smaller than the symbol sizes.

isolated electron-suppressed plate behind the target. A total of two resonances for the reaction ^{13}C(α, n)^{16}O, and one for the reaction ^{11}B(α, n)^{14}N were used (see Table 2). Each resonance was completely mapped around its peak energy E_R by detecting the number of neutrons as a function of α–beam energy E_α. A linear background function was fit underneath the resonance curve and used to subtract non-resonant contributions and background neutrons. The efficiency of NERO was determined as the ratio of the number of detected neutrons to the number of neutrons N_n produced in the resonant reaction. Since the resonances considered here fulfill $\Gamma_R \ll \Delta E = E_i - E_f$ and $\Gamma_R \ll E_R$ (see Table 3), one can use the thick-target narrow-resonance approximation and calculate N_n (see for example Ref. [20]) using

$$N_n = \frac{I_\alpha t \pi^2 \hbar^2 (\omega\gamma)_R N_A \rho}{\mu A E_R} \left(\frac{dE}{dz}\right)^{-1}, \quad (1)$$

where (dE/dz) is the stopping power of the α particle in the target material, calculated with the SRIM-2000 code [21] in the center-of-mass frame; t is the duration of the measurement; A is the mole mass of the target; ρ is the target mass density; μ is the reduced mass of the system and $(\omega\gamma)_R$ is the resonance strength. The resonance parameters used in the calculations were taken from Refs. [15–19]. They are summarized in Table 2.

The results of the efficiency measurements are shown in Table 4 for the three selected resonances, along with their corresponding evaluated average neutron energies in the laboratory frame $\langle E_n \rangle$. The calculation of this latter quantity is described in Section 3.2.4.

3.2.3. Measurement of NERO efficiency with non-resonant reactions

Additional measurements of the NERO efficiency were performed at ISNAP using neutrons produced in the ^{51}V(p,n)^{51}Cr reaction [22] at three different energies. This reaction has been used in the past for neutron detector calibrations [16,18]. Here, a proton beam was accelerated at the KN accelerator and impinged onto a ^{51}V target mounted in the center of NERO. Three incident proton energies of 1.8, 2.14 and 2.27 MeV were chosen from regions of the excitation function with no individual resonances, using three targets with a thickness of 32 μg/cm^2.

To determine the number of ^{51}V(p,n)^{51}Cr reactions that have occurred during a measurement one can take advantage of the fact that for every ^{51}V(p,n)^{51}Cr reaction, a radioactive ^{51}Cr is created with a half-life of 27.7025(24) days. The electron-capture decay of ^{51}Cr is followed by the emission of several X-rays [23] and a 320.0824(4) keV γ ray [24] with a branching ratio of 9.91(1)% [23]. The number of neutrons N_n produced in the reaction can then be simply determined from the activity of the target after irradiation. The number of 320.1 keV γ rays emitted was measured offline in a lead-shielded setup, where the irradiated target was mounted in a plastic holder facing a HPGe γ detector. Decay losses during the irradiation, transport, and offline counting were negligible. The HPGe efficiency at 320.1 keV was found to be 0.76(4)% using a ^{133}Ba calibration source, and by interpolating the efficiencies measured for the two γ rays emitted at 302 and 356 keV. The deduced NERO neutron efficiencies are listed in Table 4 for the three different proton energies. The systematic error is dominated by the 5% uncertainty in the activity of the γ–ray calibration source.

Table 2
Properties of the three selected resonances: resonance energy in the laboratory frame E_α, resonance width Γ_R, strength $(\omega\gamma)_R$, excitation energy E_x, and spin and parity J^π.

Reaction	E_α (MeV)	Γ_R (keV)	$(\omega\gamma)_R$ (eV)	E_x (keV)	J^π
^{13}C(α, n)^{16}O	1.053	1.5(2)	11.9(6)	7165	5/2$^-$
^{13}C(α, n)^{16}O	1.585	≤ 1	10.8(5)	7576(2)	7/2$^-$
^{11}B(α, n)^{14}N	0.606	2.5(5)× 10^{-3}	0.175(10)	11436	7/2$^-$

Table 3
Validation of the thick-target, narrow-resonance approximation. dρ is the target thickness and ΔE is the energy loss in the target at the resonance energy.

Reaction	E_α (MeV)	$d\rho$ (mg/cm^2)	ΔE (keV)	Γ_R (keV)	E_R (keV)
^{13}C(α, n)^{16}O	1.053	0.014	18	1.5(2)	806
^{13}C(α, n)^{16}O	1.585	0.014	16	≤1	1217
^{11}B(α, n)^{14}N	0.606	0.012	18	2.5(5)× 10^{-3}	445

3.2.4. Results and discussion

In order to evaluate the energy-dependence of the efficiency, the energy spectrum of the emitted neutrons needs to be known for each reaction used. These neutrons are, for our purposes, essentially mono-energetic in the center-of-mass frame. The center-of-mass energies $\hat{E}_n$ can be calculated from the known reaction Q-values. However, the corresponding laboratory frame neutron energy E_n depends on the center-of-mass polar angle $\hat{\theta}$ of the emitted neutron with respect to the beam axis. This leads to a

Table 4
Laboratory frame projectile energy E_{proj}, average neutron energy $\langle E_n \rangle$, and width of the neutron energy distribution ΔE_n with corresponding measured neutron detection efficiency ε_n.

Reaction	E_{proj} (MeV)	$\langle E_n \rangle$ (MeV)	ΔE_n (MeV)	ε_n (%)	ε_n isotr. (%)	ε_n MCNP (%)	ε_n MCNP scaled (%)
^{11}B(α, n)	0.606	0.56	0.12	33(2)	38(2)	42	37
^{13}C(α, n)	1.053	2.8	0.31	24(1)	30(1)	29	26
^{13}C(α, n)	1.585	3.2	0.41	27(1)	33(1)	29	24
^{51}V(p,n)	1.80	0.23	0.014	39(2)	36(2)	44	39
^{51}V(p,n)	2.14	0.55	0.024	34(2)	32(2)	42	37
^{51}V(p,n)	2.27	0.68	0.028	34(2)	34(2)	41	36

The last three columns list efficiencies for isotropic sources emitting neutrons at the energy $\langle E_n \rangle$. ε_n "isotr" is derived from the experimental value ε_n using corrections calculated with MCNP, ε_n "MCNP" is the calculated efficiency, and ε_n "MCNP scaled" is the calculated efficiency scaled to obtain a best fit to the experimental data.

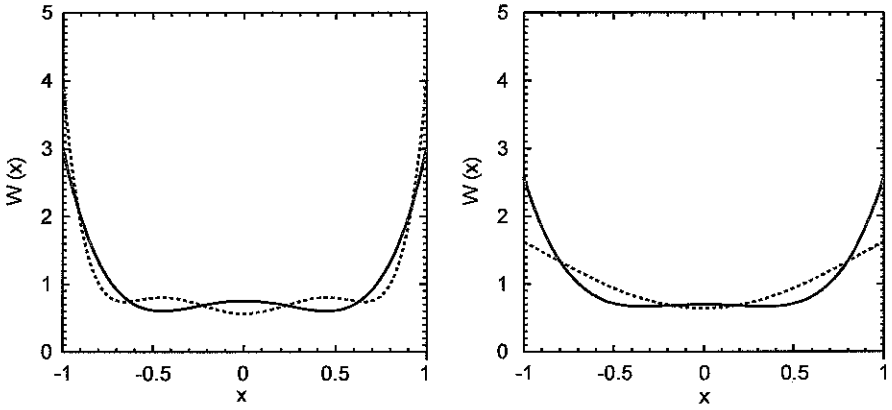

Fig. 5. Left: angular correlation $W(x)$ calculated in the center-of-mass frame for the 7.165 MeV, $5/2^-$ (solid line) and 7.576 MeV, $7/2^-$ (dashed line) resonances in the reaction ^{13}C(α, n)^{16}O. Right: angular correlation $W(x)$ calculated in the center-of-mass frame for J_f=$1/2^+$ (solid line) and J_f=$3/2^+$ (dashed line) of the 11.436 MeV, $7/2^-$ resonance in the resonant reaction ^{11}B(α, n)^{14}N, being J_f the final spin of the reaction.

broadening of the neutron energy distribution, with an average neutron energy $\langle E_n \rangle$ of

$$\langle E_n \rangle = \int_{-1}^{+1} E_n(x) W(x)\, dx, \tag{2}$$

where $x = \cos\hat{\theta}$. The angular-correlation functions $W(x)$ for each of the three resonances used here were calculated as described in Ref. [25] and are shown in Fig. 5. In the case of the ^{11}B(α, n)^{14}N reaction, the coupling of the neutron spin with the ground-state of ^{14}N leads to two possible values of the final spin. Variations of the results obtained using the two possible $W(x)$ functions were included in the final uncertainty. For ^{51}V(p,n)^{51}Cr we have chosen energies where the excitation function shows nonresonant behavior. This justifies the assumption of isotropic neutron emission in the center-of-mass frame, or, equivalently, $W(x) = 1/2$.

The average neutron energies calculated in the laboratory frame $\langle E_n \rangle$ together with the width of the energy distribution ΔE_n are shown in Table 4 for each reaction, along with the corresponding measured efficiencies ε_n. In the case of ^{51}V(p,n)^{51}Cr ΔE_n also includes a small contribution from the energy loss and straggling in the target. In order to determine the efficiencies for neutrons emitted isotropically with a given energy from the DSSD catcher in the BCS, our measured ε_n need to be corrected for the angular distribution and energy range of the neutrons (see e.g. Ref. [26] for the reaction ^{13}C(α, n)^{16}O). This was done using MCNP simulations: First, the NERO efficiencies were calculated with MCNP at the energies $\langle E_n \rangle$ of Table 4, assuming an isotropic mono-energetic neutron source located in the center of the detector. A second calculation was then performed, using the calculated laboratory frame angular and energy distributions of the neutrons. The MCNP-calculated anisotropic-to-isotropic efficiency ratios were then used as a correction factor to translate the measured efficiencies into efficiencies for isotropic emission at a single energy $\langle E_n \rangle$. In Table 4, we show the measured efficiencies for the different reactions (ε_n) and the corresponding corrected values (ε_n isotr.). The strongest correction of about 15% arises mainly from the angular correlation $W(x)$ in the resonant reactions. The isotropic efficiencies are shown in Fig. 6 for the whole detector (left), and for each ring separately (right).

The experimentally determined efficiencies covered a range of energies from about 0.2 to 3 MeV. In order to extrapolate the results to lower energies, we combined the experimental values (ε_n isotr.) with a MCNP calculation of the efficiency as a function of energy (see dotted line in Fig. 6, left). Despite a global absolute overestimation of about 5%, the calculated $\varepsilon_n(E_n)$ function follows very well the energy dependence obtained from the measured data.

As shown in Fig. 6 (right), the efficiencies calculated independently for each ring follow reasonably well the energy trends of the experimental data. For all the reactions investigated, MCNP reproduces the efficiency of the innermost ring, which is the most efficient of the three. The agreement is somewhat worse for the other rings at the lowest energies. In particular, the calculations overestimate the efficiency of the middle ring by about 3% at energies below 700 keV. We investigated the possibility that this discrepancy could be related to the type of detectors used. Several test measurements of the efficiency were performed with a ^{252}Cf source, using one single ^{3}He proportional counter placed in the first, second and third ring, using the ^{252}Cf source. A comparison of the calculated efficiencies with the values measured under these conditions was consistent with the results shown in Fig. 6 (right). The overall 5% absolute overestimation of the efficiency by the calculations could not be attributed to the uncertainty in the polyethylene density. First of all, variations of the density

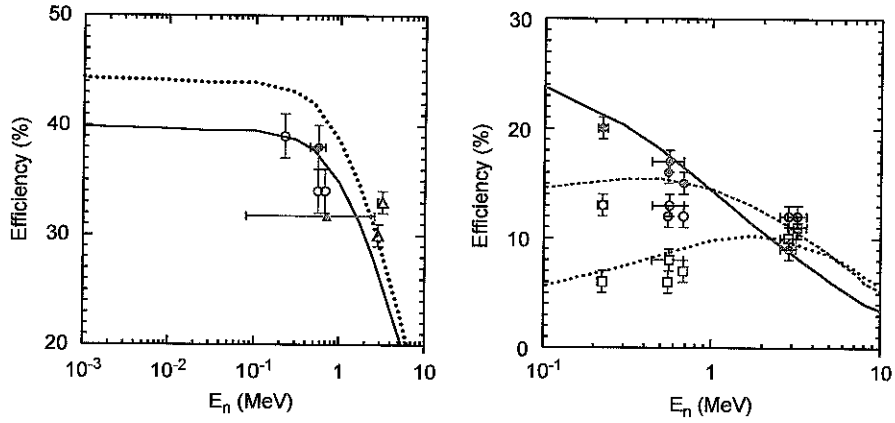

Fig. 6. (Color online). Left: MCNP-calculated total efficiency as a function of the neutron energy E_n scaled to the experimental data (solid line) and unscaled (dotted line), compared with measurements for the reactions ^{11}B(α, n) (solid circle), ^{13}C(α, n) (empty triangles), ^{51}V(p,n) (empty circles), and with the ^{252}Cf neutron source (solid triangle.). The energy width of the ^{252}Cf measurement was calculated according to the shortest-interval criterion defined by W. Brüchle for asymmetric distributions [27]. Right: MCNP-calculated efficiencies as a function of neutron energy E_n for the innermost ring (solid line), intermediate ring (dashed line) and outer ring (dotted line), compared to the measured values for the first (solid circles), second (empty circles) and third (empty squares) rings. Note the different scales of the two figures.

modified the calculated efficiencies for the second and third ring in the opposite direction of the first ring. Secondly, when the variations in density were limited to the uncertainties provided by the supplier, no differences in the calculated results were observed.

The good agreement of MCNP with experimental data observed in Fig. 6 (right) for the first NERO ring with a thinner moderator layer, and the small discrepancies found for the second and third rings with thicker moderator layers points to a limitation of MCNP to accurately calculate the scattering process of the neutrons in the moderator material. One possibility would be molecular vibrational and rotational excitation modes in the moderator material. Whereas this problem would be hardly observable in detectors with thin moderators (e.g. Ref. [28]), it would become more severe for thicker moderators. Interestingly, similar conclusions were drawn when comparing MCNP calculations with neutron-flux measurements performed with thick neutron detectors [29,30]. In order to compensate for these model deficiencies we scaled the calculated efficiencies for each ring independently to better match the experimental data (see scaled efficiency in Table 4). The new scaled efficiency-curve (solid line in Fig. 6, left) can thus be used to extrapolate the efficiency to energies below 200 keV.

It is worth noting that the relevant neutron energy range for β–delayed neutron emission in r-process nuclei is a few hundred keV. As an example, for the r-process nuclei around $A \sim 100-130$, spectroscopic studies of β–delayed neutron emitters [31–33] showed that $\hat{E}_n$ is typically much lower than $Q_\beta - S_n$. Neutron energies in the laboratory frame E_n were found to be 199 keV for ^{87}Br, 450 keV for ^{98}Rb, and 579 keV for ^{137}I. This result was further supported by the measured average neutron energies of fission fragments from ^{235}U ($\langle E_n \rangle = 575$ keV) and ^{239}Pu ($\langle E_n \rangle = 525$ keV), where, in addition, very few neutrons were found at $E_n \gtrsim 800$ keV [31,34]. According to these authors, the reason for the "compressed" E_n spectra is the preferred population of the lowest excited states in the final nuclei [33]. Our experimental efficiency calibration therefore covers the most critical energy range, and the condition of an energy independent efficiency for β–delayed neutrons is well fulfilled. As an example, ε_n shown in Fig. 6 (left) shows a relative variation of about ±5% for energies below 800 keV. This variation will contribute to the final uncertainty of the measured P_n. This uncertainty can be reduced if the neutron energies E_n can be constrained from experiment or theory.

3.3. Background

One limitation for the measurement of P_n, particularly for very exotic nuclei, is the neutron background rate (B_n). Its estimation requires to distinguish two different origins. First, there is the "intrinsic" background associated with the electronics of the NERO detector and its sensitivity to the neutrons present in the environment (mainly cosmic rays). Second, during the course of an experiment, there are beam-induced neutrons produced by nuclear reactions unrelated to the β–delayed neutron emission of interest. During experiments, neutron background rates measured with NERO in self-trigger mode can vary within about 5–10 s^{-1} depending on whether or not the beam is on target. As will be discussed later, the impact of these background rates is dramatically reduced when the neutrons are measured in coincidence with β decays.

Analysis of the ring-counting ratios for background runs (self-trigger mode) and production runs (external trigger mode) support the idea of an external and a beam-induced background source. As shown in Fig. 7 (left), measurements performed with NERO in external trigger mode (i.e. from β decays in the BCS) with β–delayed neutron emitters showed that the neutron counting rates were higher for the innermost ring and systematically decreased for the outer rings, in agreement with the results shown in Fig. 6 (right). On the other hand, background runs with beam off showed the opposite trend, with high rates in the outer ring, gradually decreasing for the inner ones (Fig. 7, center). This result suggests that these runs were mainly affected by an external source of background neutrons, most probably related to cosmic rays. Finally, background runs with beam on target showed an intermediate situation that could be explained as arising from a combination of external and internal sources (Fig. 7, right). Energy spectra obtained for background runs with the ADCs show the wall-effect shape expected for neutrons (see lower spectra in Fig. 3). Electronic and γ–ray contributions are largely below the discriminator thresholds.

4. Measurement of P_n

The NERO detector, together with the BCS, has been employed in numerous r-process motivated experiments performed at NSCL [5,6,35]. The exotic nuclei of interest are implanted in a 40 × 40-pixel DSSD in the BCS. β–delays are also detected in the DSSD and can be position-correlated to previously implanted

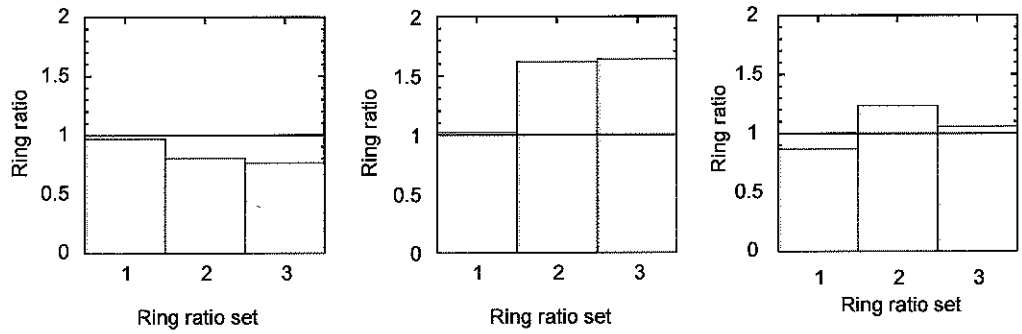

Fig. 7. Ratio of neutrons detected with different NERO rings for three different runs: production with β–delayed neutron emitters (left), background with beam off (center), and background with beam on (right). Histogram bin numbers 1, 2 and 3 correspond to ring ratios R_2/R_1, R_3/R_2, and R_3/R_1, where R_{1-3} are the innermost, intermediate and external rings. Statistical errors are negligible.

ions during a maximum correlation rime t_c. P_n values were determined using the number of neutrons $N_{\beta n}$ detected in coincidence with an implantation-correlated β–delay event, according to the equation:

$$P_n = \frac{N_{\beta n} - B_{\beta n} - N_{\beta\beta n}}{\varepsilon_n N_\beta}, \tag{3}$$

where $B_{\beta n}$ is the number of background coincidences between β- like events (including real β decays and background from the BCS) and neutrons, and N_β is the number of detected parent β decays. $N_{\beta\beta n}$ is the number of detected β–delayed neutrons from the daughter nuclei and needs to be subtracted from $N_{\beta n}$. For the nuclear species analyzed in Refs. [5,6,35]. β- neutron coincidences associated with descendant nuclei other than the β–delay daughter were negligible. In this case, using the Batemann equations [36], it is possible to write explicitly the value of $N_{\beta\beta n}$ as

$$N_{\beta\beta n} = (1 - P_n)C, \tag{4}$$

where C is a constant given by

$$C = \frac{\lambda_2 P_{nn} N_\beta \varepsilon_n}{\lambda_2 - \lambda_1}\left[1 - e^{-\lambda_1 t_c} - \frac{\lambda_1}{\lambda_2}(1 - e^{-\lambda_2 t_c})\right]. \tag{5}$$

In this equation, P_{nn} is the neutron-emission probability of the daughter nucleus, and λ_1 and λ_2 are the decay constants of the mother and daughter nuclei, respectively. Inserting Eqs. (4) and (5) into Eq. (3), and rearranging terms:

$$P_n = \frac{N_{\beta n} - B_{\beta n} - C}{\varepsilon_n N_\beta - C}. \tag{6}$$

The value of N_β for a given nucleus is calculated as the product of the total number of implantations in the DSSD, and the β–detection efficiency.

The NERO background rate given in Section 3.3 is the "free" neutron background rate without any coincidence requirements. In practice, however, P_n values are determined from neutrons measured in coincidence with β decays. The number of background β–neutron coincidences for a given nucleus can be written as $B_{\beta n} = B_n(\beta) + B_n(B_\beta)$; where $B_n(\beta)$ is the number of "free" background neutrons in random coincidence with parent β decays, and $B_n(B_\beta)$ is the number of "free" background neutrons in random coincidence with background β-like events in the BCS.

$B_n(B_\beta)$ as a function of time and detector pixel can be reliably estimated from the β–neutron coincidence rates outside of the correlation window t_c of any ion implantations. $B_n(B_\beta)$ for a specific parent nuclide can then be calculated by summing the specific backgrounds at the time and location of each individual ion implantation event. The high granularity of the DSSD detector greatly reduces this background.

$B_n(\beta)$ can be calculated as the product of the number of parent β decays detected N_β and the probability for at least one "free" background neutron to be detected in random coincidence with each parent β decay, i.e.:

$$B_n(\beta) = N_\beta \sum_{k=1}^{\infty} \frac{(R_b\tau)^k}{k!} e^{-R_b\tau} = N_\beta(1 - e^{-R_b\tau}), \tag{7}$$

where τ is the TDC time window defined in Section 3.1, and R_b is the "free" neutron background rate. For a typical value $R_b \simeq 10\,s^{-1}$, about 0.2% of the detected parent β decays are in random coincidence with a background neutron, setting the order of magnitude of the lowest P_n values that can be measured with NERO under these conditions.

The P_n values and their errors obtained in various NSCL experiments can be found in Refs. [5,6]. The P_n values measured in these experiments agree well with perviously measured well established data.

5. Summary and conclusions

The neutron detector NERO has been built at NSCL enabling the measurement of β–delayed neutron emission probabilities of r-process nuclei with fast rare isotope beams. The specific design was motivated by the requirement of achieving a high, energy-independent neutron detection efficiency up to ≈ 1 MeV, and accommodating a large pixelated β–counting system, necessary to perform measurements with fragmentation beams. MCNP simulations were carried out during the design phase to find the optimum configuration.

Studies of the detector efficiency at various neutron energies were performed with a ^{252}Cf source, and with neutrons from a number of resonant and non-resonant reactions at ISNAP. MCNP calculations reproduce reasonably well the energy dependence of the detector efficiency. On the other hand, the MCNP calculations slightly overestimate the absolute efficiency of the second and third rings, when the neutrons traverse a larger volume of polyethylene. An overall scaling of the calculated efficiency to the measured data can be used to extrapolate the detector efficiency to smaller and larger neutron energies. The small energy dependence (of about 5%), for neutron energies below 800 keV, represents the main contribution from the efficiency correction to the total uncertainty of P_n.

NERO is currently used with the BCS at NSCL, but can be used with other β–decay stations at other rare isotope facilities. It will also be used to fully exploit the much higher production rates expected in new generation facilities like FRIB at NSCL, FAIR at GSI and RIBF at RIKEN.

Acknowledgments

This work was supported in part by the Joint Institute for Nuclear Astrophysics (JINA) under NSF Grant PHY-02-16783 and the National Superconducting Cyclotron Laboratory (NSCL) under NSF Grant PHY-01-10253.

References

[1] K.-L. Kratz, J.-P. Bitouzet, F.-K. Thielemann, P. Möller, B. Pfeiffer, Astrophys. J. 403 (1993) 216.
[2] E.M. Burbidge, G.R. Burbidge, W.A. Fowler, F. Hoyle, Rev. Mod. Phys. 29 (1957) 547.
[3] A.G.W. Cameron, Publ. Astron. Soc. Pac. 69 (1957) 201.
[4] F. Farouqi, K.-L. Kratz, B. Pfeiffer, T. Rauscher, F.-K. Thielemann, AIP Conf. Proc. 819 (2006) 419.
[5] F. Montes, A. Estrade, P.T. Hosmer, S.N. Liddick, P.F. Mantica, A.C. Morton, W.F. Mueller, M. Ouellette, E. Pellegrini, P. Santi, H. Schatz, A. Stolz, B.E. Tomlin, O. Arndt, K.-L. Kratz, B. Pfeiffer, P. Reeder, W.B. Walters, A. Aprahamian, A. Wöhr, Phys. Rev. C 73 (2006) 035801.
[6] J. Pereira, S. Hennrich, A. Aprahamian, O. Arndt, A. Becerril, T. Elliot, A. Estrade, D. Galaviz, R. Kessler, K.-L. Kratz, G. Lorusso, P.F. Mantica, M. Matos, P. Möller, F. Montes, B. Pfeiffer, H. Schatz, F. Schertz, L. Schnorrenberger, E. Smith, A. Stolz, M. Quinn, W.B. Walters, A. Wöhr, Phys. Rev. C 79 (2009) 035806.
[7] G. Grosshög, in: D.N. Poenaru, W. Greiner (Eds.), Experimental Techniques in Nuclear Physics, Walter de Gruyter, 1997, p. 235 (Chapter 7).
[8] G. Rudstam, K. Aleklett, L. Sihver, At. Data Nucl. Data Tables 53 (1993) 1.
[9] .B. Pfeiffer, K.-L. Kratz, P. Möller, Prog. Nucl. Energy 41 (2002) 39.
[10] T. Mehren, B. Pfeiffer, S. Schoedder, K.-L. Kratz, M. Huhta, P. Dendooven, A. Honkanen, G. Lhersonneau, M. Oinonen, J.-M. Parmonen, H. Penttilä, A. Popov, V. Rubchenya, J. Äystö, Phys. Rev. Lett. 77 (1996) 458.
[11] Computer code MCNP 5.0, ORNL (RCICC), Oak Ridge, TN, 2003.
[12] J.S. Hendricks, S.C. Frankle, J.D. Court, ENDF/B-VI data for MCNP, LANL Report LA-12891, Los Alamos, 1994.
[13] J. Elson, private communication; <http://pico-systems.com>.
[14] O.I. Batenkov, A.B. Blinov, M.V. Blinov, S.N. Smirnov, Atomic Energy 64 (2005) 489.
[15] J.K. Bair, F.X. Haas, Phys. Rev. C 7 (1973) 1356.
[16] E. Ramström, T. Wiedling, Nucl. Phys. A 272 (1976) 259.
[17] C.R. Brune, I. Licot, R.W. Kavanagh, Phys. Rev. C 48 (1993) 3119.
[18] E. Lund, P. Hoff, K. Aleklett, O. Glomset, G. Rudstam, Z. Phys. A 294 (1980) 233.
[19] T.R. Wang, R.B. Vogelaar, R.W. Kavanagh, Phys. Rev. C 43 (1991) 883.
[20] W.A. Fowler, C.C. Lauritsen, T. Lauritsen, Rev. Mod. Phys. 20 (1948) 236.
[21] J.F. Ziegler, J.P. Biersack, M.D. Ziegler, The Stopping and Ranges of Ions in Matter, Lulu Press, Morrisville, NC, 2008.
[22] J.L. Zyskind, C.A. Barnes, J.M. Davidson, W.A. Fowler, R.E. Marrs, M.H. Shapiro, Nucl. Phys. A 343 (1980) 295.
[23] P. Yalçin, Y. Kurucu, Appl. Radiat. Isotopes 62 (2005) 63.
[24] R.G. Helmer, C. van der Leun, Nucl. Instr. and Meth. A 450 (2000) 35.
[25] C. Iliadis, Nuclear Physics of Stars, Wiley-VCH, Weinheim, 2007 (Appendix D.2).
[26] J.P. Schiffer, A.A. Kraus, J.R. Risser, Phys. Rev. 105 (1957) 1811.
[27] W. Brüchle, Radiochim. Acta 91 (2003) 71.
[28] Y. Danon, R.C. Block, R.E. Slovacek, Nucl. Instr. and Meth. A 352 (1995) 596.
[29] ESARDA NDA Working Group, ESARDA Bulletin 33, November 2003, p. 26.
[30] B. Wolle, R. Bätzner, T. Baloui, G. Gonda, H. Klein, B. Wiegel, J. Wittstock, Rev. Sci. Instrum. 70 (1999) 1194.
[31] K.-L. Kratz, in: Proceedings of the Consultants' Meeting on Delayed Neutron Properties, IAEA, Vienna, 1979, p. 103.
[32] K.-L. Kratz, W. Rudolph, H. Ohm, H. Franz, M. Zendel, G. Hermann, S.G. Prussin, F.M. Nuh, A.A. Shihab-Eldin, D.R. Slaughter, W. Halverson, H.V. Klapdor, Nucl. Phys. A 317 (1979) 335.
[33] K.-L. Kratz, A. Schröder, H. Ohm, M. Zendel, H. Gabelmann, W. Ziegert, P. Peuser, G. Jung, B. Pfeiffer, K.D. Wünsch, H. Wollnik, C. Ristori, J. Crançon, Z. Phys. A 306 (1982) 239.
[34] T.R. England, E.D. Arthur, M.C. Brady, R.J. LaBauve, LA-11151-MS, 1998.
[35] P.T. Hosmer, H. Schatz, A. Aprahamian, O. Arndt, R.R.C. Clement, A. Estrade, K.-L. Kratz, S.N. Liddick, P.F. Mantica, W.F. Mueller, F. Montes, A.C. Morton, M. Ouellette, E. Pellegrini, B. Pfeiffer, P. Reeder, P. Santi, M. Steiner, A. Stolz, B.E. Tomlin, W.B. Walters, A. Wöhr, Phys. Rev. Lett. 94 (2005) 112501.
[36] J. Cetnar, Ann. Nucl. Energy 33 (2006) 640.
[37] J.I. Prisciandaro, A.C. Morton, P.F. Mantica, Nucl. Instr. and Meth. A 505 (2003) 140.

PHYSICAL REVIEW VOLUME 72, NUMBER 8 OCTOBER 15, 1947

A Neutron Detector Having Uniform Sensitivity from 10 Kev to 3 Mev

A. O. HANSON* AND J. L. MCKIBBEN
Los Alamos Scientific Laboratory, Santa Fe, New Mexico
(Received July 10, 1947)

A neutron detector having approximately uniform sensitivity from 10-kev neutron energy to 3-Mev energy is described. The arrangement, known as a long counter, consists of a paraffin cylinder about 10″ outer diameter ×12″ long surrounding a long boron trifluoride proportional counter. Sensitivity curves are given for two of the best arrangements. The response is flat over the above range to about 10 percent.

A NEUTRON detector which has a uniform efficiency for neutrons of widely different energies has many advantages for certain types of measurements. A large water bath containing slow-neutron detectors in some form fulfills this requirement and has been very useful in determining the number of neutrons emitted by various neutron sources.[1] The examination of the number of slow neutrons as a function of the distance from the source in such a water bath gives additional information regarding the energy of the neutrons.[2] There are many experiments, however, where the use of a large water bath is either awkward or gives erroneous results because of the effect of the degraded neutrons reflected from the bath into the experimental setup.

In order to achieve a high efficiency in a detector of reasonable size an attempt was made to find a suitable arrangement of paraffin surrounding a boron detector. The analogy with the water bath experiment suggested that a long boron counter embedded in a block of paraffin would have a counting rate which would not depend much on the energy of the neutrons. The first detector constructed consisted of a boron-lined ionization chamber 20 cm long surrounded by a cylinder of paraffin 20 cm long and 17 cm in diameter, this was used with its axis pointed toward the neutron source. Preliminary tests on the sensitivity of this counter showed that the sensitivity was very nearly the same for neutron energies of from 0.4 Mev to 2 Mev; these tests served to encourage the development of counters along the same lines. This type of detector will be referred to as a long counter.

The theoretical treatment of the sensitivity of this type of counter is quite complicated and has not been worked out. There are, however, certain qualitative arguments which may help in understanding the behavior of these counters and which may serve to suggest further improvements.

Examine first an arrangement in which a long thermal-neutron detector is embedded in a large (semi-infinite) slab of paraffin and in which neutrons of various energies are incident upon this slab in the direction parallel to the axis of the detector. The neutrons entering the paraffin will be slowed down primarily by the hydrogen atoms to thermal energies and some of these neutrons will be captured by the central thermal-neutron detector and will be recorded as counts in some manner. If the neutrons have a very high energy, the mean free path of these neutrons is initially large and therefore will be slowed down an appreciable distance from the front face of the slab. After a number of collisions, the mean free path will be reduced to such an extent that these neutrons have a very small chance of escaping out of the front face of the slab. This is not the case, however, for neutrons having energies of the order of 100 kev or less, since in this case the mean free path of the neutrons does not change appreciably as the neutrons approach thermal energies.[3] These neutrons would therefore have a much larger probability of escaping out of the surface of the semi-infinite slab as compared to the high energy neutrons. This effect is partially compensated for by the fact that the less energetic neutrons would need to make fewer collisions before becoming thermal-

* Now at the University of Illinois, Urbana, Illinois.

[1] E. Amaldi, L. R. Hafstad, and M. A. Tuve, Phys. Rev. 51, 896 (1937).

[2] R. D. O'Neal, Phys. Rev. 70, 1 (1946).

[3] C. L. Bailey, W. E. Bennett, T. Bergstralh, R. G. Nuckolls, H. T. Richards, and J. H. Williams, Phys. Rev. 70, 583 (1946); D. H. Frisch, *ibid.*, 589 (1946).

ized, but the effect would be such that the detection efficiency for high energy neutrons would be several times greater than that for very low energy neutrons.

If the sensitivity for low energy neutrons is to be approximately the same as that for neutrons of high energy, some modification of this idealized arrangement must be made. The success of the first long counter must be ascribed to a fortunate choice of the dimensions of the paraffin block such that the increased probability of escape of high energy neutrons from the sides of the block compensated in some degree for the escape of low energy neutrons from the front face. The effect of the size of the paraffin cylinder has been investigated roughly and is indicated in a later section of this report. The size of the central cavity made by the detector is perhaps important although no systematic investigation of its effect was made. It will be shown, however, that the introduction of additional holes in the front face affected the low energy sensitivity of one of the counters appreciably.

DESCRIPTION OF COUNTERS

Two counters were used quite extensively and will be described here in detail. The first consisted of a central BF_3 proportional counter 1 inch in diameter, which had an effective length of 8 inches. This tube was surrounded by paraffin cylinders 12 inches long and 6, 8, and 12 inches in diameter. The counter with the 8 inch paraffin cylinder is shown in Fig. 1. The proportional counter protrudes slightly from the front face of the paraffin block but is protected from direct thermal neutrons by means of a cadmium shield. The proportional counter is supported by means of ceresin wax in the center of an aluminum tube which also serves as an electrical shield. The body of the counter was a $\frac{1}{32}$-inch wall brass tube and was soldered to Kovar glass seals. The central electrode consisted of a 10-mil Kovar wire. The $\frac{1}{4}$-inch intermediate electrode was used as a guard ring and was connected to ground. The counter was filled with enriched BF_3 (80 percent B^{10}) to a pressure of 25 cm Hg. With -2700 volts on the outer shell the proportional counter gives a gas amplification of about 10. The signal was further amplified by means of a model 100 linear amplifier[4] with a R-C time constant of 5 microseconds and the pulse was counted by means of a model 200 discriminator and scale-of-64 circuit.[5] Except in the cases where impure BF_3 was used, because of leaks in the tube or filling system, the bias curves (counting rate against minimum pulse height recorded) were such that a change in the bias voltage by a factor of two in either direction would not change the counting rate by more than 5 percent. The counting rate was not affected by the gamma radiation from an unshielded 500-mg radium source used at a distance of 40 cm from the counter.

The other counter, which will be referred to as the shielded long counter, is shown in Fig. 2. The principal modification is that an additional paraffin and boron shield is used so as to make it less sensitive to neutrons which have been scattered about the room. The proportional counter is similar except that it was 10.5 inches long,

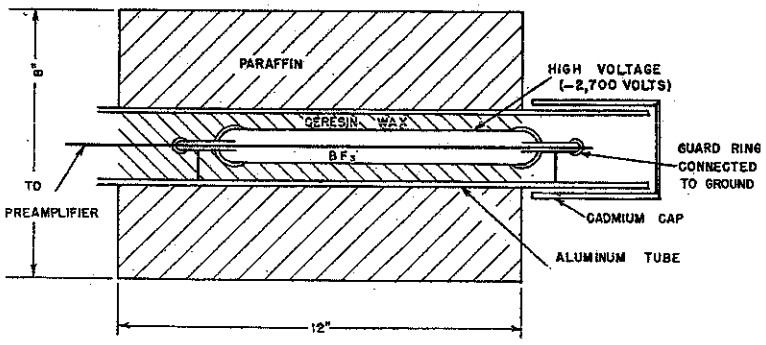

FIG. 1. 8-inch OD long counter.

[4] Designed by M. Sands.
[5] Designed by W. Higinbotham.

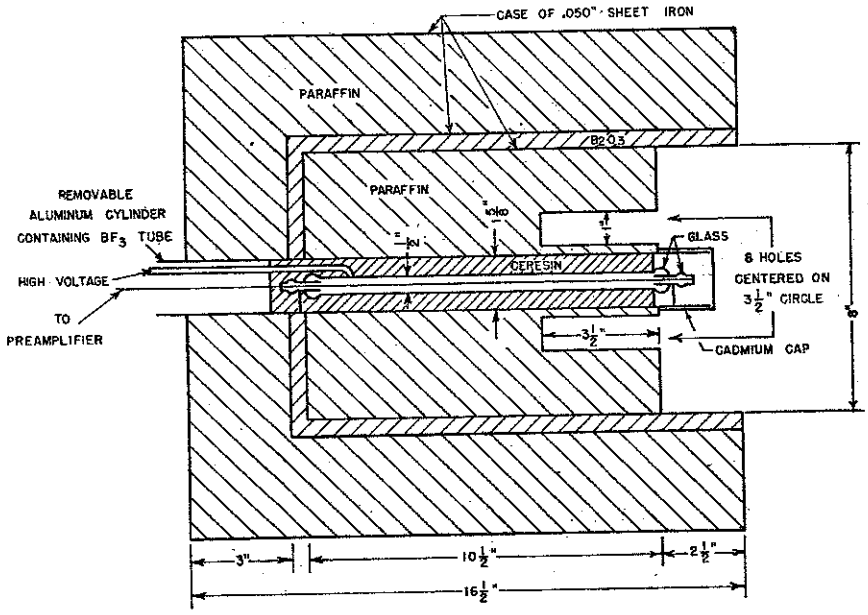

FIG. 2. Shielded long counter.

½ inch in diameter, and was filled with BF_3 to a pressure of 40 cm. For most of the measurements made with these counters it was convenient to use a matched pair of the counters in the arrangement shown in Fig. 3. In addition to increasing the sensitivity of the over-all system, such an arrangement minimizes errors due to exact positioning of sources.

SENSITIVITY CURVES

The data on the sensitivity of the counters to neutrons of various energies were obtained by three methods, namely:

(1) By comparing the counting rates in the counters due to various radioactive neutron sources whose total neutron yield had been compared by some other method such as the water bath technique. Photo neutron sources used were Sb-Be and Y-Be. Alpha neutron sources used were Po-BF_3[6] and Ra-Be. The energies of these sources were taken to be 0.023, 0.16, 2.2 and 5 Mev, respectively. While the energy of the photo neutron sources should be well defined, the alpha neutron sources give a spectrum and the values given represent only average energies. The assignment of an average energy to the neutrons from Ra-Be is especially dubious since the energy spectrum of these neutrons extends out to about 14 Mev. The fraction of neutrons below 0.1 Mev, however, is estimated to be less than 10 percent.[7]

(2) The degradation of the energy of the neutrons from a given source by surrounding the source with spheres of graphite and heavy water. A graphite sphere, 24 cm in diameter, was used which had the effect of reducing the

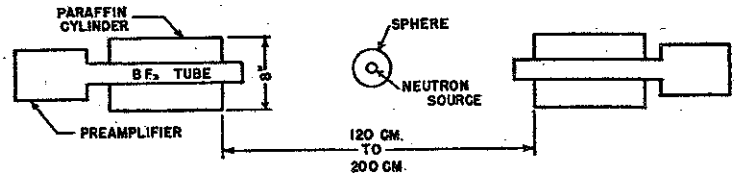

FIG. 3. Experimental arrangement with a pair of 8-inch OD long counters.

[6] H. T. Richards, LADC—288.
[7] A. A. Yalow, R. S. Yalow and M. Goldhaber, Phys. Rev. 69, 253A, 1946.

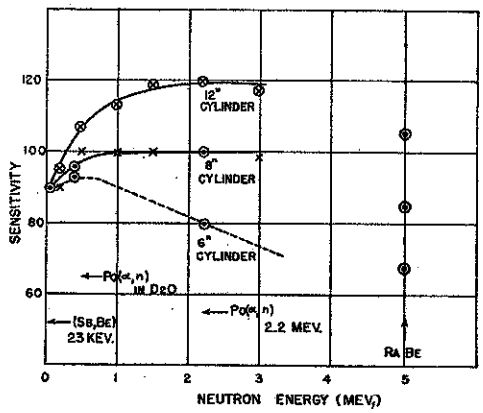

FIG. 4. Sensitivity of 8-inch OD and 12-inch OD long counters. The X's and circled X's represent points obtained with Li^7 (p, n) and D (d, n) neutron sources. Although the curves are not continued beyond 3 Mev the general trends of the curves above this energy are indicated by the points obtained with the Ra-Be source.

average energy of the neutrons by a factor of about 2. A heavy-water sphere, 20 cm in diameter, served to reduce the average energy of the neutrons by a factor of 4 or more. Since neither graphite nor heavy water absorbs neutrons appreciably, the number of neutrons emerging from the sphere would be the same as that emitted from the source. A change in the counting rate with the sphere around the source was therefore taken as a measure of the change in the sensitivity of the counter to the modified spectrum of neutrons. The use of D_2O was, of course, limited by the fact that any source having sufficiently high energy gamma rays would give rise to photo-neutrons from the deuterium. In the case of yttrium it was found that the number of photo-neutrons from deuterium caused by the high energy ray (~2.8 Mev) was only 3 percent of that due to the Be and hence could be accurately taken into account.

(3) The use of homogeneous neutrons of known energy from the Li (p, n) and D (d, n) reactions. In these experiments the flux of neutrons into the counters was determined by counting the fissions occurring in a standardized sample of uranium 235. The energies of these neutrons are accurately known, and the flux measurement are considered to be reliable so that these points should be quite significant.

The summary of the data on the first counter with 6-, 8- and 12-inch cylinders are shown in Fig. 4. Since very few data were obtained with the 6-inch cylinder, the curve is sketched in only to indicate the general trend of the sensitivity curve as the size of the paraffin cylinder is reduced. It is seen that the 8-inch cylinder gives the best approximation to a uniform sensitivity over the region shown. Other tests with neutrons absorbable by cadmium indicated that the sensitivity of the counter to thermal neutrons was about 70 on the scale used in Fig. 4. The sensitivity of this counter would be somewhat affected by the arrangement in which it is used. For most of the tests described here the counters were used as a matched pair in the arrangement shown in Fig. 3 so as to reduce errors caused by the location of the sources. This pair of counters was used in the center of a room approximately 15 by 20 feet at a height of about 50 inches above the floor. In spite of precautions to keep all other material as far from the counters as possible about 15 percent of the counting rate in the counters was due to scattered neutrons when a Ra-Be source was placed at a distance of 1 meter from the front face of the counters. The absolute sensitivity of this counter was such that it would give about 1 count for every 10^5 neutrons emitted from a source placed at a distance of 1 meter from the front face.

The shielded counter is less sensitive to scattered neutrons by a factor of about 3 and hence largely eliminates this objectionable feature of the 8-inch long counter. The sensitivity of this counter to high energy neutrons is considerably

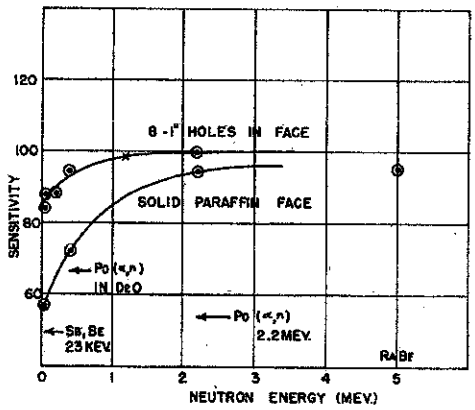

FIG. 5. Sensitivity of shielded long counters.

increased due to the larger mass of paraffin in the shield, and the sensitivity to low energy neutrons is therefore relatively low. The use of holes in the front face, however, increases the sensitivity to low energy neutrons to a sufficient extent so that the response curve of the counter is about as good as that of the previous counter. The effect of these holes is clearly indicated in the sensitivity curves shown in Fig. 5. It seems probable that the sensitivity of this counter would remain fairly constant up to energies of about 5 Mev, but there has been no work done to indicate the trend of the sensitivity curve in this range of energies.[8] No doubt further improvement in the response curve for both high energy neutrons and low energy neutrons can be accomplished by using more suitable paraffin arrangements.

The detectors described here have been found useful in many problems requiring a high and approximately uniform sensitivity to neutrons of various energies. Some of the applications have been the determination of the yield and angular distribution of neutrons from various (p, n) and (d, n) sources as a function of energy, the preliminary measurement of neutron yield from various radioactive sources, and the determination of the number of delayed neutrons accompanying fission.

This paper is based on work performed under Contract No. W-7405-Eng-36 with the Manhattan Project at the Los Alamos Scientific Laboratory of the University of California. The information contained herein will appear in Division V of the Manhattan Project Technical Series as part of the contribution of the Los Alamos Laboratory.

[8] Preliminary measurements with 16.5-Mev neutrons indicate that the sensitivity of the shielded counter for these neutrons is approximately 40 on the scale used in Fig. 5 (R. F. Taschek, private communication).

Available online at www.sciencedirect.com
SCIENCE DIRECT®
ELSEVIER
Nuclear Instruments and Methods in Physics Research A 505 (2003) 466–469
NUCLEAR INSTRUMENTS & METHODS IN PHYSICS RESEARCH Section A
www.elsevier.com/locate/nima

FIGARO: detecting nuclear materials using high-energy gamma-rays

B.J. Micklich[a,*], D.L. Smith[a], T.N. Massey[b], C.L. Fink[a], D. Ingram[b]

[a] *Technology Development Division, Argonne National Laboratory, Argonne, IL 60439, USA*
[b] *Edwards Accelerator Laboratory, Department of Physics and Astronomy, Ohio University, Athens, OH 45701, USA*

Abstract

The potential diversion of nuclear materials is a major international concern. Fissile (e.g., U, Pu) and other nuclear materials (e.g., D, Be) can be detected using 6–7 MeV gamma-rays produced in the $^{19}F(p,\alpha\gamma)\,^{16}O$ reaction. These gamma-rays can induce neutron emission via photoneutron and photofission processes in nuclear materials. However, they are not energetic enough to generate significant numbers of neutrons from common benign materials. Neutrons are counted using an array of BF_3 tubes in a polyethylene moderator. A strong increase in neutron count rates is seen when irradiating depleted uranium, Be, D_2O, and ^6Li, with little or no increase for other materials (e.g., H_2O, SS, Cu, Al, C, ^7Li). Experiments using both photon and neutron shielding show that the technique is resistant to countermeasures. We have reduced the neutron background from proton beam reactions (thus increasing the system's sensitivity) and have tested a high-current gas cell which should be capable of operating at proton beam currents of up to 100 μA.

PACS: 25.20; 28.20; 89.20.Dd

Keywords: Nuclear materials detection; Low-energy proton accelerator; Gamma-rays; Photofission

1. Introduction

The potential diversion of nuclear materials is a major international concern, and the development of effective methods for deterrence of nuclear smuggling is a prime objective of national security programs. Fissile (e.g., U, Pu) and other nuclear materials (e.g., D, Be) can be detected using 6–7 MeV gamma-rays produced in the $^{19}F(p,\alpha\gamma)\,^{16}O$ reaction using a technique we call FIGARO (Fissile Interrogation using Gamma Rays from Oxygen). The FIGARO concept is illustrated in schematic form in Fig. 1. This gamma source reaction was in fact the one used in the first demonstration of photofisson [1], and our utilization of it is described in earlier work [2,3]. These gamma-rays are energetic enough to induce neutron emission via photoneutron and photofission processes in nuclear materials. However, they are not energetic enough to generate significant numbers of neutrons from common benign materials.

The FIGARO technique is very efficient in its use of the photon probing radiation and the neutrons produced, reducing the amount of dose imparted. Nearly all of the photons generated are

*Corresponding author. Tel.: +1-630-252-4849; fax: +1-630-252-5287.
E-mail address: bjmicklich@anl.gov (B.J. Micklich).

0168-9002/03/$ - see front matter
doi:10.1016/S0168-9002(03)01122-7

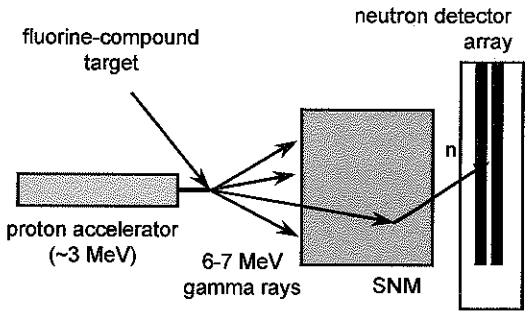

Fig. 1. Conceptual diagram of the FIGARO concept.

Table 1
(γ,n) thresholds for selected elements (only isotopes with thresholds above 7.2 MeV are listed)

Element	Isotope	Abundance (%)	γ,n threshold (MeV)
Lithium	^{7}Li	92.5	7.250
Carbon	^{12}C	98.90	18.722
Nitrogen	^{14}N	99.63	10.553
	^{15}N	0.37	10.833
Oxygen	^{16}O	99.76	15.664
	^{18}O	0.20	8.044
Aluminum	^{27}Al	100	13.058
Silicon	^{28}Si	92.23	17.180
	^{29}Si	4.67	8.474
	^{30}Si	3.10	10.609
Iron	^{54}Fe	5.845	13.378
	^{56}Fe	91.754	11.197
	^{57}Fe	2.119	7.646
	^{58}Fe	0.282	10.044
Copper	^{63}Cu	69.17	10.853
	^{65}Cu	30.83	9.9102

capable of inducing neutron emission from the target materials. In contrast, for an electron linear accelerator operating at 9 MV, typically only about 5% of the X-rays have energies greater than 6 MeV. The electron linac also produces about 2% of its photons above 7.5 MeV, the energy at which (γ,n) neutrons can be emitted by common benign materials (see Table 1), this being the average nuclear binding energy. Thus, in practice electron linacs must operate in a pulsed mode to reject (γ,n) neutrons from benign materials, and they detect fissile/fissionable materials using delayed neutrons from fission. These represent less than 1% of the total neutrons emitted. FIGARO, however, can use all emitted neutrons as part of the signal since there are very few neutrons emitted from benign materials, thus increasing the sensitivity and reducing the false alarm rate. The restriction to pulsed operation of an electron linac also precludes its use for detecting non-fissionable nuclear materials such as D, ^{6}Li, and Be.

2. Experimental program

The experiments were performed using the 4.5 MV Tandem Van de Graaff accelerator at the Ohio University Edwards Accelerator Laboratory. We measured both the high-energy photon yields and neutron production using several types of fluorine targets for proton energies between 1.5 and 4.25 MeV [4,5]. The gamma production targets included solid targets of crystalline CaF_2 and MgF_2 and gas targets of SF_6 with foil windows of tungsten, nickel, or aluminum. Neutron measurements were made for both the bare source and for selected materials in a controlled geometry. Neutrons were counted using an array of BF_3 tubes in a polyethylene moderator. Recent research on FIGARO has focused on three areas: (1) demonstration that the system gives positive indications only for nuclear materials (specificity), (2) reduction of neutron background, and (3) demonstration of a high-current gas target.

3. Material specificity

A large number of materials have been examined in a standard experimental arrangement to demonstrate that FIGARO produces signals from nuclear materials and not from common benign materials. Several elements that would be expected to produce (γ,n) neutrons, but would not be expected to be found in normal commercial or personal items, were included, such as Zr, Hf, and Mo. Fig. 2 shows that a strong increase in neutron count rates is seen when irradiating depleted uranium, Be, and D_2O, with little or no increase for benign materials (e.g., Al, H_2O, SS, graphite).

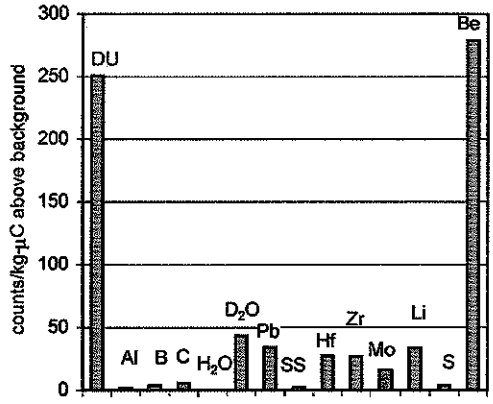

Fig. 2. Normalized neutron count rates for selected nuclear and common materials.

Table 2
(p,n) thresholds for selected elements (only isotopes with thresholds under 3.5 MeV are listed)

Element	Isotope	Abundance (%)	p,n threshold (MeV)
Lithium	^{7}Li	92.41	1.880
Carbon	^{13}C	1.11	3.236
Oxygen	^{18}O	0.20	2.574
Iron	^{57}Fe	2.119	1.647
	^{58}Fe	0.282	3.144
Cobalt	^{59}Co	100	1.887
Nickel	^{61}Ni	1.140	3.070
	^{64}Ni	0.926	2.496
Copper	^{65}Cu	30.83	2.167
Gold	^{197}Au	100	1.389

Experiments have been performed to assess the resistance of the FIGARO technique to various shielding countermeasures, such as medium- to high-Z gamma shielding to reduce gamma-induced reactions, hydrogenous neutron shielding to prevent neutrons from reaching the detector, or some combination of the two. Both copper and lead gamma shields were investigated, along with neutron shields of polyethylene, borated polyethylene (BPE), lucite, and borax. These experiments show that the FIGARO technique is resistant to countermeasures [3]. Sufficient count rates for nuclear material detection could still be achieved using commercially available high-current (10–100 μA) accelerators.

4. Reduction of neutron background

Possible sources of beam-on neutron background are (p,n) and (γ,n) reactions with materials in the beamline and target area. This background can be largely reduced by careful selection of materials. For example, components which intercept the proton beam should have a (p,n) threshold higher than the proton beam energy used. This makes nickel unsuitable as a gas cell window because of its relatively low (p,n) threshold (see Table 2), verified by high neutron production for proton energies greater than 2.75 MeV. Other common materials such as oxygen, iron, and copper also have lower (p,n) thresholds, while carbon is less of a problem if the proton energy is restricted to under 3.25 MeV. Since carbon cannot be completely excluded from any system, we generally operate at $E_p \approx 3$ MeV to reduce neutron production. Likewise, the use of elements with (γ,n) thresholds under 7.5 MeV should be avoided.

Attention to such details significantly reduced the neutron background from that seen in our initial efforts. However, despite our best efforts, a small residual background remained [3]. We performed systematic measurements in which localized neutron shielding was placed sequentially along the beamline to identify the source of the remaining background. In this way, our residual background was traced to the entrance region of the gas cell, specifically in the aluminum aperture plate. It was discovered that there were small amounts (about 0.125%) of copper impurity in what was assumed to be a pure aluminum aperture plate. Measurements of neutron production in a pure copper plate indicated that this amount of copper would cause the neutron background seen. Additionally, when the aperture plate was covered with pure Al foil sufficiently thick to stop all incident protons, the neutron background was further reduced. A new aperture plate fabricated from pure aluminum is expected to solve this problem. Such efforts are important because reductions in the neutron background directly increase the system's sensitivity.

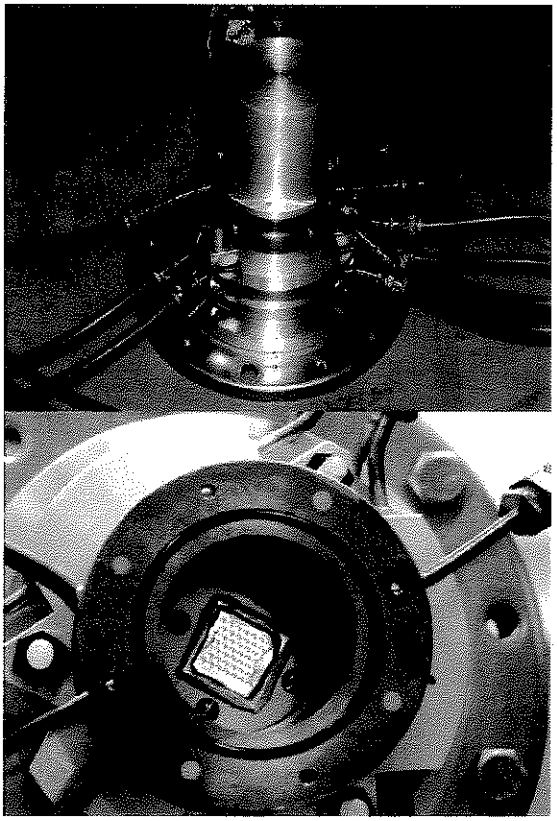

Fig. 3. Photographs of new high-current gas cell with gridded aperture plate.

5. High-current gas cell

A high-current gas cell (Fig. 3) has been designed with an Al foil window and a gridded aperture plate having a proton beam transmission of approximately 50%. The cell has undergone stable operation for proton beam currents of up to 8 μA, and should be capable of operating at currents of up to 100 μA.

6. Summary

Our research on the FIGARO technique has shown that it provides a robust method for detection of nuclear materials while minimizing false positives. Minimization of neutron background increases system sensitivity, thus helping in FIGARO's resistance to countermeasures.

Acknowledgements

This work was supported by the US Department of Energy. Argonne National Laboratory is operated by the University of Chicago for the US Department of Energy under contract W-31-109-ENG-38.

References

[1] R.O. Haxby, W.E. Shoupp, W.E. Stephens, W.H. Wells, Phys. Rev. 59 (1941) 57.
[2] D.L. Smith, F. Maekawa, Y. Ikeda, Fusion Eng. Des. 47 (2000) 403.
[3] B.J. Micklich, D.L. Smith, T.N. Massey, D. Ingram, A. Fessler, Proceedings of the 16th Conference on Appl. Accel. Res. Ind., AIP 576, Denton, TX, 1–5 November 2000.
[4] A. Fessler, T.N. Massey, B.J. Micklich, D.L. Smith, Nucl. Instr. Meth. A 450 (2000) 353.
[5] B.J. Micklich, D.L. Smith, T.N. Massey, C.L. Fink, D. Ingram, Nucl. Instr. Meth. A (2003), these proceedings.

DWG. NO. RS-PI-0813-101 REV.

REVISION	REVISED BY	DATE	DESCRIPTION	APP'V'D

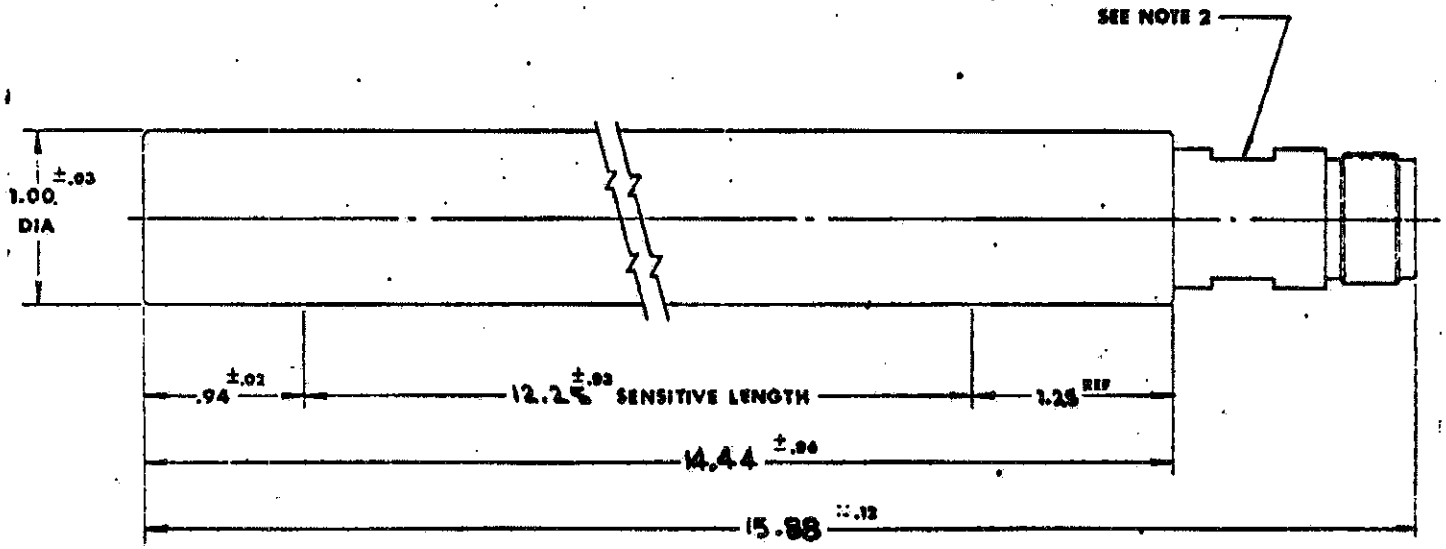

ITEM	PART/ASS'Y NO.	DESCRIPTION	QTY.

2- H.V. CONNECTOR MATES WITH ANY SERIES H.V. PLUG SUCH AS 59UG/59

1- REMOVE BURRS, BREAK EDGES WHEN APPLICABLE.

NOTES:

UNLESS OTHERWISE SPECIFIED, DIMENSIONS ARE IN INCHES AND DIMENSIONAL LIMITS AS FOLLOWS:

SURFACE FINISH 63		.XX DECIMAL	±.01
FRACTIONAL	±1/64	.XXX	±.005
ANGULAR	±0° 30'	.XXXX	±.0050

REUTER-STOKES CLEVELAND, OHIO 44128

TITLE: PROPORTIONAL COUNTER BF-3

MAT'L.: ALUM. CONSTRUCTION

DRAWN BY	DATE	CHECKED BY	DATE	APPROVED BY	DATE	SCALE	DWG. NO.	REV.
GM	6/24/77	Glengard	8-18-77	C.D. Jr.	8/19/77	1:1	RS-PI-0813-101	

SIZE A

40 21

3D view of FIGARO in MCNP6 from Z-Mesh Simulation

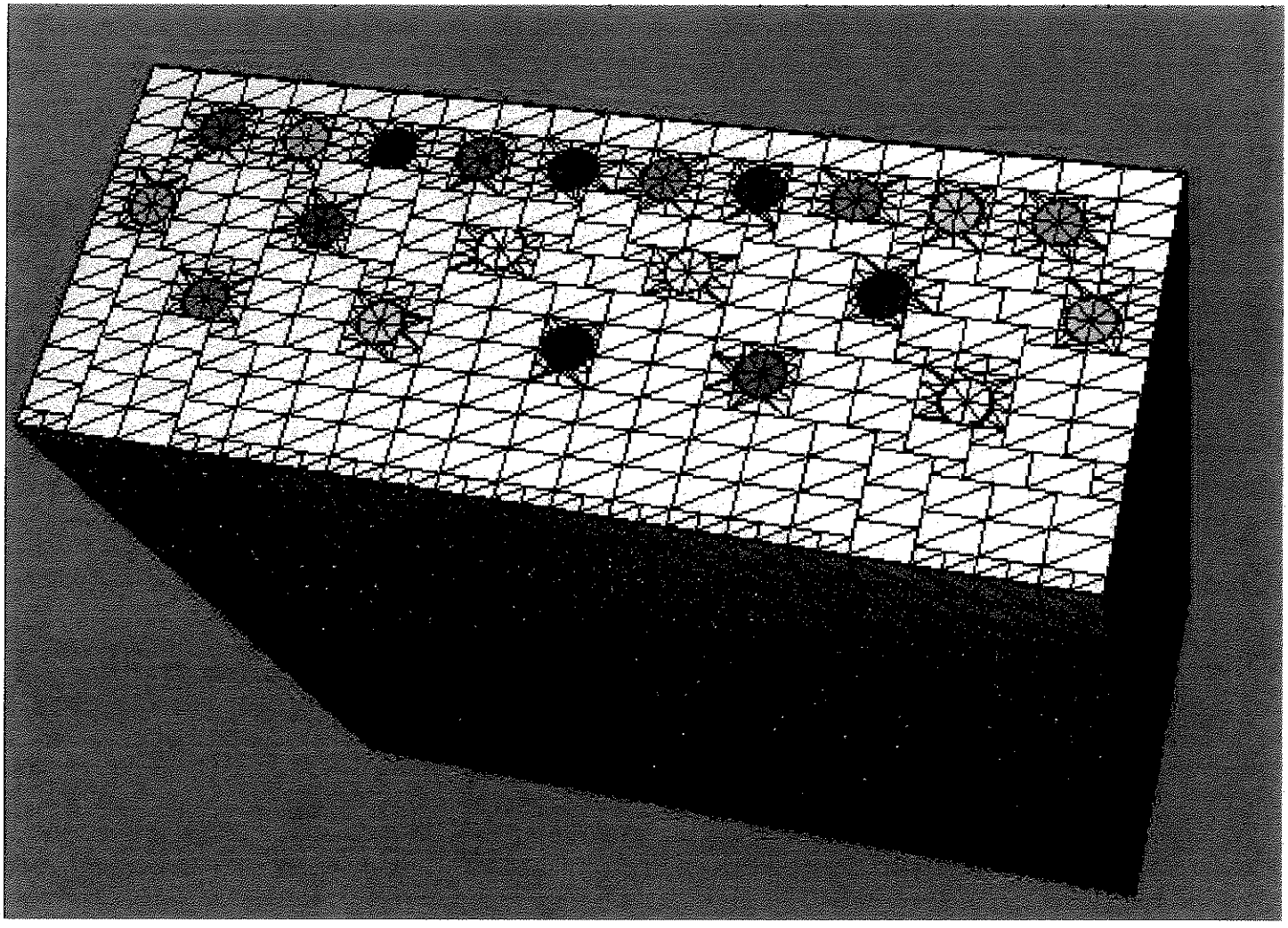

21 1"-diameter BF_3 proportional counters (0.7 atm)
embedded within a ~8.5" x 24" x 24" polyethylene block

2D views of FIGARO in MCNP6 from Z. Meisel simulation

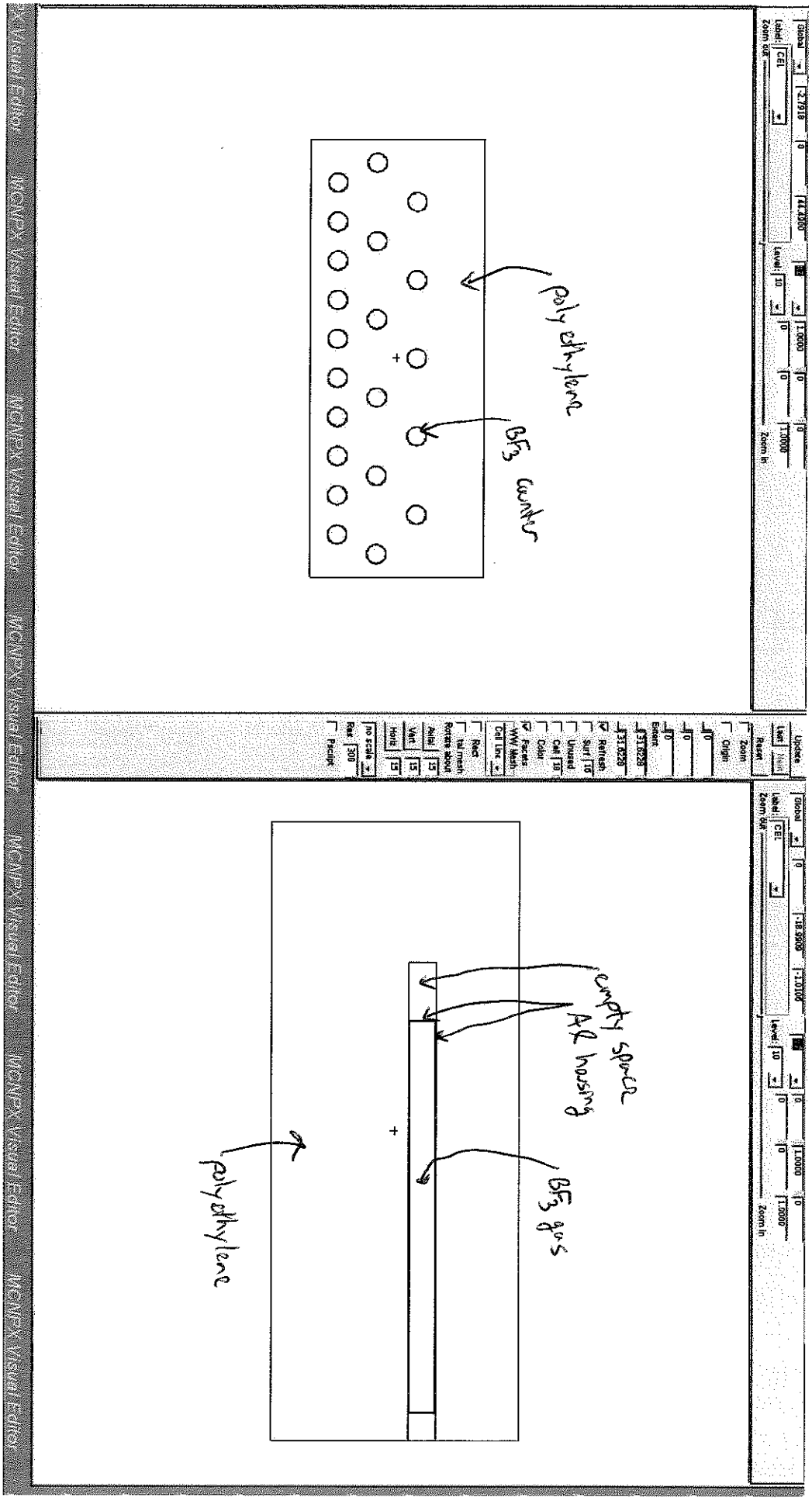

Trajectories for 20 neutron trajectories from ^{252}Cf in MCNP6 from Z. Meisel simulation

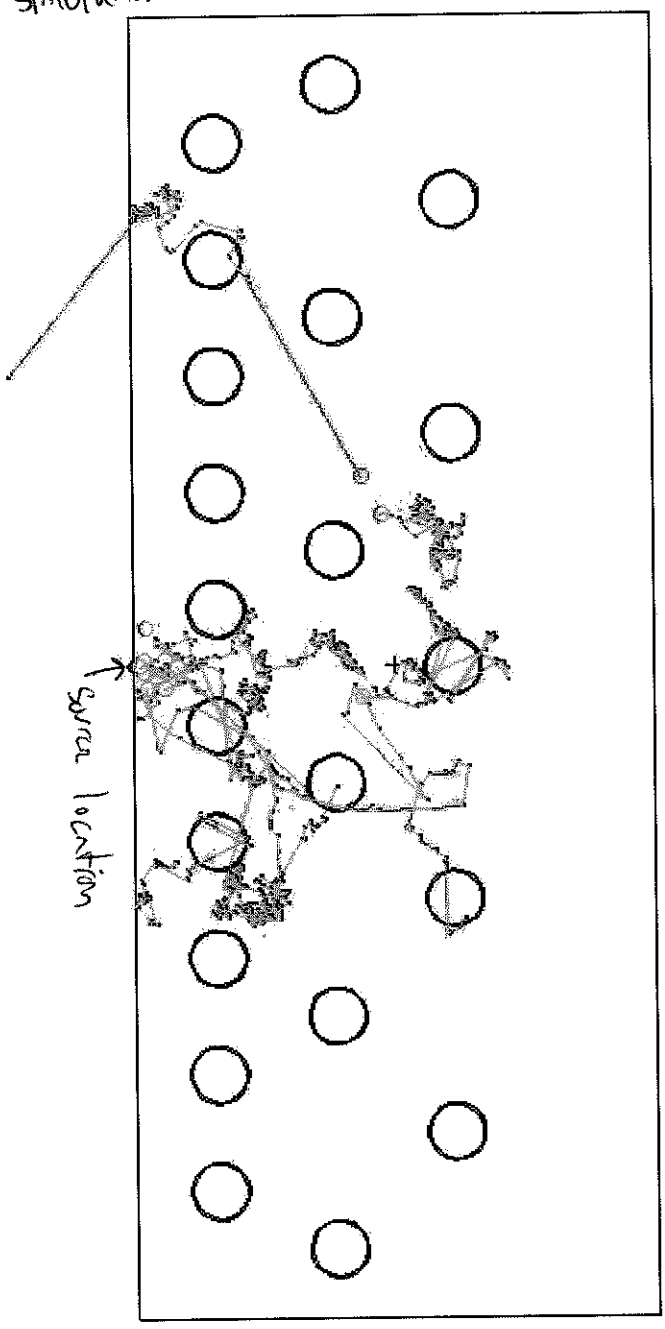

Letter from Tom Massey, April 2010

Hi,

The source is initially 50 microcuries of 252Cf.
0r 1.85 MBq on 15 Jan 2010. Source # G5-857 for Eckert and Ziegler isotope Products.

We have been following the decay and the fission rate. There have been some drops in fission rate which are greater than the decay rate. Our best understanding was that this was due to sputtering losses in the source. We have setup to have the bias just above the alphas and count all of the fission.

I can purge the Cf chamber and bring the pressure back to the nominal value with a few hours work.

The 252Cf fission source is currently in a fission chamber where the fissions rate can be determined. This source can be removed for the fission chamber if desired. The source is roughly the size of a quarter. Its current activity is 10 microcuries. The neutron yield in as given by the most recent ENDF is:

NEUTRONS PER SPONTANEOUS FISSION : NUBAR

TOTAL = 3.7676 +- 0.0047 (REF. 1)
DELAYED = 0.0086 +- 0.0010 (REF. 2)
PROMPT = 3.7590 +- 0.0048

1. E.J. AXTON, BCNM REPORT GE/PH/01/86 (JUNE 1986)
2. T.R. ENGLAND, PRIV. COMMUNICATION (1990)

The self fission branch is evaluated as 3.086 +/- 0.008 %

The total neutrons expected is (3.7676)(0.0386)(10)(10E-6)*3.7E10 = 54,000 n/second.

The neutron spectrum of 252Cf is well known and may make an additional check on your MCNP calculations.

Cf-252 Technical data

The Cf-252 used to prepare your order was taken from Eckert & Ziegler Isotope Products Laboratories Lot #4995502 and it had the following composition as of 22 Dec 09.

Nuclide	Mass %	Activity %
Cf-249	9.641	0.142
Cf-250	30.082	11.766
Cf-251	14.602	0.0832
Cf-252	45.674	88.010

The Cm-248 decay product was last separated on 3Apr 01

Isotopic composition provided by Oak Ridge National Laboratory

If you have any questions, please contact Eckert & Ziegler Isotope Products Technical Service: 661-309-1010

Cf-252 calculation

Initial activity	Assay Date	Current Date	Delta T	Half-life	Current activ	Fission bran	Neutrons/fiss	Neutrons/sec	neutrons/microcurie
49.9	1/10/2006	04/05/16	10.232	2.64	3.3992355	0.0386	3.676	17,846	5250.0632

International Journal of Applied Radiation and Isotopes, 1969, Vol. 20, pp. 453–461. Pergamon Press. Printed in Northern Ireland

Californium-252 Neutron Sources for Medical Applications*

A. R. BOULOGNE and A. G. EVANS
Savannah River Laboratory, E. I. du Pont de Nemours and Company, Aiken, South Carolina 29801

(*Received* 30 *December* 1968)

Californium-252 neutron sources are being prepared to investigate the value of this radionuclide in diagnosing and treating diseases. A gram of ^{252}Cf emits $2{\cdot}34 \times 10^{12}$ neutrons per sec through spontaneous fission.

A source resembling a cell-loaded radium needle was developed for neutron therapy. Four micrograms of ^{252}Cf were electrodeposited on a platinum–iridium wire, 0·51 mm in dia. and 20 mm in length, and the wire was doubly encapsulated. Since therapy needles are normally implanted in the body, very conservative design criteria were established to prevent leakage of radioactive material.

A more intense source, containing 100 μg of ^{252}Cf was prepared for neutron radiography experiments. This source is pelletized ^{252}Cf oxide in a platinum metal matrix doubly encapsulated in stainless steel. The active source volume was approximately 6 mm^3.

Methods are being developed to prepare very intense californium sources that could be used eventually for neutron radiography and for diagnosis by activation analysis.

DES SOURCES NEUTRONIQUES DE CALIFORNIUM-252 POUR LES APPLICATIONS MÉDICALES

On est en train de préparer des sources neutroniques de californium-252 afin de juger la valeur de ce radionucléide pour la diagnostique et le traitement des maladies. Un gramme de ^{252}Cf émet $2{,}34 \times 10^{12}$ neutrons par seconde par fission spontanée.

On a mis à point une source semblable à une aiguille de radium chargée dans une cellule. Quatre microgrammes de ^{252}Cf furent électrodéposés sur un fil de platinum-iridium ayant un diamètre de 0,51 millimètre et une longueur de 20 millimètres, et le fil fut deux fois encapsulé. Vu que d'habitude les aiguilles thérapiques sont implantées dans le corps, on a établi des critériums de dessin très conservatifs afin d'éviter l'écoulement de matériel radioactif.

On a préparé une source plus puissante, contenant 100 microgrammes de ^{252}Cf, pour des expériences dans la radiographie des neutrons. Cette source consiste en des boulettes d'oxyde de ^{252}Cf dans une matrice de platinum métallique deux fois encapsulée en acier inoxydable. Le volume actif de la source fut environ 6 millimètres cubes.

On est en train de développer des méthodes pour la préparation de très fortes sources de californium qui pourrait éventuellement servir à la radiographie de neutrons et à la diagnostique par analyse d'activation.

ИСТОЧНИКИ НЕЙТРОНОВ ^{252}КАЛИФОРНИЯ ДЛЯ ПРИМЕНЕНИЯ В МЕДИЦИНЕ

Источники нейтронов ^{252}калифорния изготовлялись для исследования ценности этого радиоизотопа в диагностике и лечении болезней. 1 гр ^{252}калифорния излучает $2{,}34 \times 10^{12}$ нейтронов в секунду самопроизвольным делением.

Для нейтронной терапии была изготовлена подобная источнику радиевая игла с элементом. Отложения от 4-× микрограммов ^{252}Cf собираются на платиново-иридиевой

* The information contained in this article was developed during the course of work under Contract AT(07-2)-1 with the U.S. Atomic Energy Commission.

проволоке диаметром в 0,51 мм и длиной в 20 мм; проволока помещается в двойную капсюлю. Так как иглы для терапии вставляются обычно в тело, то конструкция их должна была быть совершенно безопасной и защищенной от проникновения излучения радиоактивного материала.

Более сильный источник, содержащий 100 микрограммов ^{252}Cf был изготовлен для экспериментов по нейтронной радиографии. Этим источником является окись ^{252}Cf в гранулах в металлической платиновой матрице с двойной капсюлей из нержавеющей стали. Объем активного источника приблизительно 6 мм^3.

Разрабатываются методы изготовления очень сильных источников из калифорния, которые могли бы применяться для нейтронной радиографии и для диагноза посредством активационного анализа.

KALIFORNIUM-252-NEUTRONENQUELLEN FUR MEDIZINISCHE ANWENDUNGEN

Es wurden Kalifornium-252-Neutronenquellen hergestellt, um den Wert dieses Radionukliden bei der Diagnose und der Behandlung von Krankheiten zu untersuchen. Ein Gramm von ^{252}Cf gibt 2,34 $\times$ 10^{12} Neutronen je sec durch spontane Spaltung ab.

Eine Quelle ähnlich einer Radiumnadel mit Zellenladung wurde für die Neutronentherapie entwickelt. Vier Mikrogramm von ^{252}Cf wurden auf einem Platin-Iridium-Draht von 0,51 mm Durchmesser und 20 mm Länge galvanisch niedergeschlagen und der Draht wurde zweifach eingehülst. Da die Therapienadeln normalerweise im Körper verbleiben, wurden sehr konservative Kriteria aufgestellt, um einen Verlust von radioaktivem Material zu vermeiden.

Eine stärkere Quelle mit 100 μg von ^{252}Cf wurde zubereitet für Versuche mit Neutronenradiographie. Diese Quelle ist ein ^{252}Cf-Oxyd in der Form von Kügelchen in einer zweifach in rostfreiem Stahl eingehülsten Platinmatrize. Das aktive Quellenvolumen war etwa 6 mm^3.

Es werden zur Zeit Verfahren entwickelt, um sehr kräftige Kaliforniumquellen herzustellen. Sie könnten später für Neutronenradiographie und zur Diagnose durch Aktivierungsanalyse benutzt werden.

INTRODUCTION

The possibility of using neutrons for radiotherapy was recognized soon after their discovery[1]. Recently, better understanding of the physical and biological interactions of neutrons with tissue has lent impetus to research in this field[2].

Californium-252 sources are being developed to investigate the value of this radionuclide in diagnosing[3] and treating diseases.[4,5] The nuclide is encapsulated in needles and afterloading cells and tubes, which can be implanted in tissue, inserted into body cavities, or used as surface applicators. Californium-252 therapy sources resemble cell-loaded radium sources except that Cf_2O_3 is uniformly electrodeposited on the source rod or fixed in a platinum matrix (inside the cell) instead of being loosely mixed with an inert filler in the cell. These neutron sources can be handled in the same manner as other radiotherapy sources, and the problems of radiation protection are straightforward[6]. Unlike gamma sources, neutron sources must be stored in hydrogenous shields rather than high density materials such as lead.

More intense californium-252 sources can be prepared in a variety of geometries for use in neutron radiography and diagnosis by neutron activation analysis[7].

CHARACTERISTICS OF CALIFORNIUM-252

Californium-252 is a trivalent actinide with an effective half-life of 2·65 yr and emits 2·34 $\times$ 10^{12} neutrons per sec per g (4·4 $\times$ 10^9 neutrons per sec per c) by spontaneous fission.[8] The average neutron energy of the fission spectrum (Fig. 1) is 2·3 MeV. Gamma production rate is 1·3 $\times$ 10^{13} photons per sec per g, exclusive of internal conversion X-rays. Gamma dose rate is 1·4 $\times$ 10^2 R per hr per g at 1 m. The neutron dose rate is 2·4 $\times$ 10^3 rem per hr per g at 1 m. The gamma spectrum is shown in Fig. 2. Californium-252 emits 1·9 $\times$ 10^{13} alpha disintegrations per sec per g (6·11 MeV per disintegration).

Total heat output from the isotope is 39 W per g; $\sim$50 per cent of this is due to alpha decay. Pressure produced by helium from alpha decay and by fission gases in a therapy source containing 10 μg of ^{252}Cf (5·4 mc) approximates 9 psig at body temperature 37°C and 11 psig at

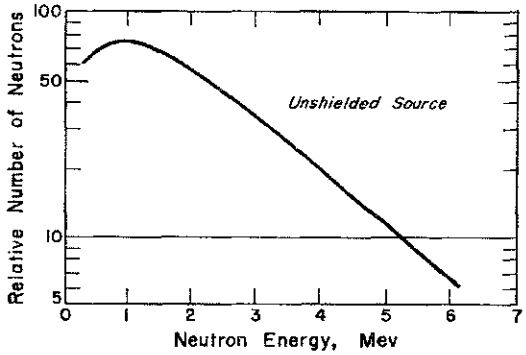

FIG. 1. Neutron energy spectrum of ^{252}Cf.

autoclave temperature 115°C (at infinite decay).

SOURCE PREPARATION PROCEDURES

Californium sources for medical therapy are prepared by electrodeposition of $^{252}Cf(OH)_3$, and sources for radiography are prepared by coprecipitation of $^{252}Cf(OH)_3$ with $Fe(OH)_3$. Both methods require hyperpure californium. Organic degradation products of ion exchange materials, ammonium alpha-hydroxyisobutyrate used to separate californium from other actinides and lanthanides, and inorganic salts from process equipment and glassware corrosion interfere seriously in the production of uniform, adherent californium sources in high yield.

Californium-252 purification

To purify californium, the tripositive elements are scavenged by ferric hydroxide, and then the actinides are extracted from 12M LiCl–0·1 M HCl to 0·61 M tri-isooctylamine in diethylbenzene by a laboratory-scale Tramex[9] process. Actinides are then stripped from the extractant with 8 M HCl and dried in platinum ware. Organic residues are wet ashed with a mixture of concentrated HNO_3 and H_2O_2.

Californium is separated from residual salts by sorption on a column of di-2-ethylhexyl phosphoric acid (HDEHP) on a diatomaceous earth support from 0·10 M HNO_3[10]. Californium is eluted from the HDEHP column with 4 M HNO_3, and the solids-free product is stored in HCl-leached fused quartz to avoid silicate contamination.

This procedure has been used successfully for more than a year to recover californium from spent electrolytes and from waste solutions from ferric hydroxide coprecipitation, and to purify it of organic and inorganic impurities after ion exchange separations. Californium obtained by this method produces consistent yields in the electrodeposition process of greater than 85 per cent on cylindrical cathodes with surface areas of 0·63 cm^2. Yields drop to 65 per cent when cathode surface area is reduced to 0·3 cm^2.

Electrodeposition

Electrodeposition is generally considered to be one of the best techniques to produce thin, uniformly distributed films of radio-elements on small, flat discs for the measurement of nuclear constants, for reactor or particle accelerator irradiation experiments, and for isotopic analysis by alpha particle or fission counting and alpha-energy measurements.[11,12] Excellent reviews and thorough studies of the electrodeposition of several individual actinides and lanthanides have been made to establish methods of producing disc sources for a variety of uses.[13–15]

Not many investigations have been reported, however, on the electrodeposition of californium[16]. None were found which attempted to produce thin, uniform, adherent films on cylindrical cathodes with surface areas of 0·3–0·6 cm^2.

At this Laboratory, californium is electrodeposited from aqueous solution in a simple cell (Fig. 3) with a specially prepared cathode. Since the cathode becomes the source, it must withstand considerable handling during the

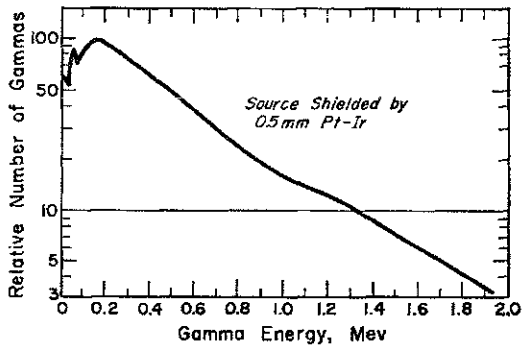

FIG. 2. Gamma energy spectrum of ^{252}Cf.

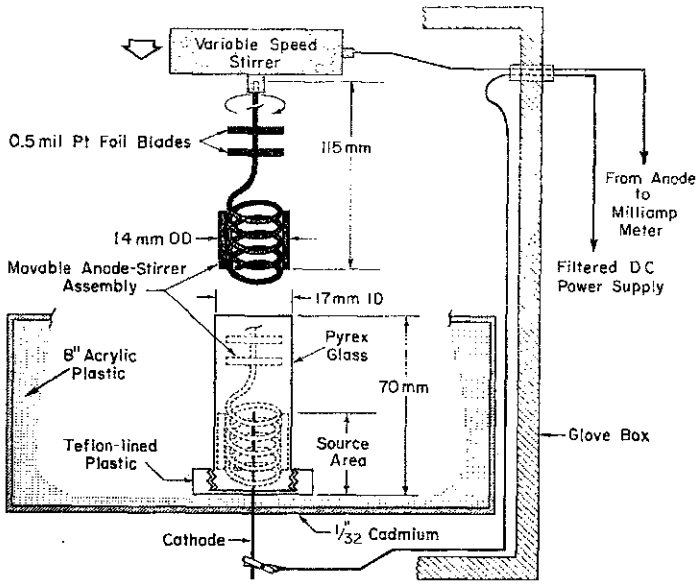

FIG. 3. Californium electrodeposition apparatus.

electrodeposition and still not exceed the very small dimensional tolerances required to fit inside the therapy source cell. After experimenting with various metals, an alloy of 90% platinum–10% iridium was chosen for the cathode because it is hard enough to assure a very straight source and is inert to acid corrosion and flaking. The portion of the Pt–Ir wire that serves as the cathode is sandblasted to increase the surface area and to provide a more adherent deposit.

Californium is electrodeposited by electrolytic base formation from an aqueous solution that is about 0·01 M ammonium nitrate and 0·10 M nitric acid. Hydrogen ions are removed from the cathode region causing precipitation of $Cf(OH)_3$.

$$6H_2O + 6\bar{e} \rightarrow 3H_2 + 6OH^-$$
$$2Cf^{3+} + 6OH^- \rightarrow 2Cf(OH)_3$$
$$\overline{2Cf^{3+} + 6H_2O + 6\bar{e} \rightarrow 2Cf(OH)_3 + 3H_2}$$

Nitric acid is reduced by hydrogen ions at the cathode.

$$H^+ + NO_3^- + H_2O + 2\bar{e} \rightarrow HNO_2 + 2OH^-$$
$$HNO_2 + 4H_2O + 6\bar{e} \rightarrow NH_3 + 6OH^-$$

Although hydrogen ions are formed at the anode by the destruction of water

$$2H_2O \rightarrow 4H^+ + O_2 + 4\bar{e}$$

the net hydrogen depletion as the electrolysis proceeds gradually reduces the acidity of the electrolyte from pH less than 1 to pH 5–6. About 1 min prior to discontinuing the current, the electrolyte is made basic (pH 8–9) so that the $Cf(OH)_3$ deposit is not immediately dissolved from the cathode when the current stops.

Procedural notes and discussion

General (Fig. 3). Medical sources containing up to 5 μg of ^{252}Cf are prepared in exhausted enclosures (glove boxes) to contain radioactive contamination. The electrolysis cells are enclosed in 8-in. cubes of an acrylic plastic covered with 1/32-in.- thick cadmium. These enclosures, as well as portable cadmium-covered plastic blocks, are used inside the glove box as neutron shields. Sources containing more than 5 μg of ^{252}Cf must be prepared in a shielded facility equipped for remote manipulation.

Electrodes. The helical anode is 16 gage Brown and Sharpe (B & S) pure platinum wire. The coil is constructed so that the anode-to-cathode distance is 5 mm across the entire length of the cathode (source) area. A variable speed electric

stirrer, capable of turning from a few rev/min to about 60 rev/min turns the anode during deposition. A typical cathode is made of 90% Pt–10% Ir alloy, is 0·51 mm in dia. (24 B & S gage wire), 80 mm in length, and has a cathode surface (source area) sandblasted to a length of 20 mm. However, a 90% Pt–10% Ir wire of any desired B & S gage can be used. The anode and cathode are degreased in acetone or trichloroethylene vapors, rinsed in 1 M HNO_3, and flamed to red heat (800°C) prior to use.

After the cathode is inserted through the cell base "Teflon"* liner and positioned so that the desired source area is exposed to electrolyte, the assembled cell is filled with distilled water and tested for leaks around the cathode seal and cell threads.

Electrolyte. Although californium can be electrodeposited from a chloride medium with good yields, a dilute nitrate system, about 0·01 M NH_4NO_3 and 0·10 M HNO_3, produced more consistent, higher yields and more uniform sources. Addition of uranium carrier decreased deposition time and increased yields[12]. Molecular plating[17] from an organic electrolyte (isopropanol) at voltages up to 200 V did not offer any advantages over deposition from aqueous media. Films formed by molecular plating from an organic electrolyte were generally neither adherent nor uniform.

Time and current density. The electrolyte is strongly acid (about pH 1) at the start of deposition. Over a period of 2½–3 hr at current densities of 280 mA per cm² (5–8 V d.c.), the electrolyte gradually approaches neutrality (pH 5–6). Current density and time vary with the amount of californium to be deposited. The following conditions consistently produce the most uniform, adherent sources in a reasonable period of time.

Cathode surface area (cm²)	Current density, (mA/cm²)	Time (hr:min)
0·3	370	1:00
	465	2:00
0·6	280	1:00
	560	1:30

* "Teflon"—Trademark of Du Pont.

It is difficult to electrodeposit more than 5 μg of ^{252}Cf on a cylindrical cathode of 0·6 cm² during a single deposition. If it is necessary to make a more intense source, the cathode from the initial deposition is flamed (to convert the hydroxide to the oxide), and is used again as the cathode in a second deposition with freshly prepared electrolyte and hyperpure $^{252}Cf(NO_3)_3$.

After the deposition is complete, the electrolyte is made alkaline (pH 8–9) by the addition of concentrated NH_4OH and the current is discontinued. Spent electrolyte is pipetted to a recovery flask and the cell carefully disassembled.

Encapsulation. The californium-bearing cathode is heated slowly and carefully to red heat inside the glove box using the oxygen–butane flame of a microtorch. This converts the $Cf(OH)_3$ to Cf_2O_3 and reduces the platinum black to platinum metal. The deposit is also more adherent perhaps because the heat annealed the sandblasted surface of the Pt–Ir cathode.

Wet and dry smear tests were conducted with cathodes containing nanogram quantities of ^{252}Cf. Acetone and saline solution (0·025 per cent by weight) were used in the wet tests. About 5 per cent of the $^{252}Cf_2O_3$ was removed by the initial smear—wet or dry—but after that, less than 0·01 per cent was transferable.

The californium-bearing end of the cathode is inserted into a Pt–Ir cell. After the inert section of the cathode wire is cut off, a Pt–Ir plug is inserted and sealed in place with silver braze alloy (flow point 855°C). Integrity of the source cell is verified by the procedure discussed in "Safety Tests". The sealed cell is then enclosed either in a therapy needle (Fig. 4), an afterloading cell (Fig. 5), or afterloading tube (Fig. 6).

Coprecipitation

Experimental point sources of californium-252 for neutron radiography are prepared by coprecipitation of $^{252}Cf(OH)_3$ with $Fe(OH)_3$.

Hyperpure ^{252}Cf is carried on a minimum of 0·5 mg of Fe^{3+} as a hydroxide precipitate. After centrifugation and removal of the supernate, the precipitate is transferred to a cone (Fig. 7) of 1·5-mil-thick platinum which has been hammer-welded to a thin (24 B & S gage) Pt–Ir wire to facilitate remote handling in a shielded facility. After dehydrating the precipitate under an infrared lamp, and heating to 200°C in a

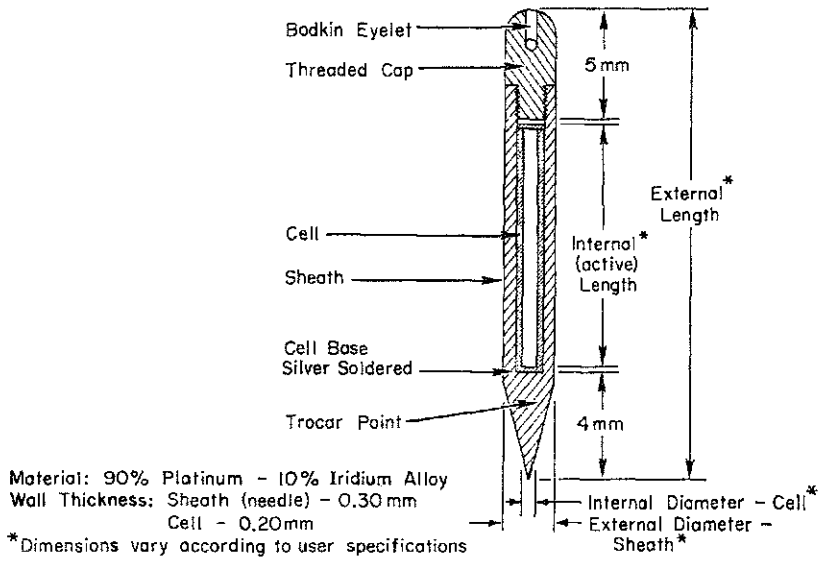

FIG. 4. Cell-loaded needle.

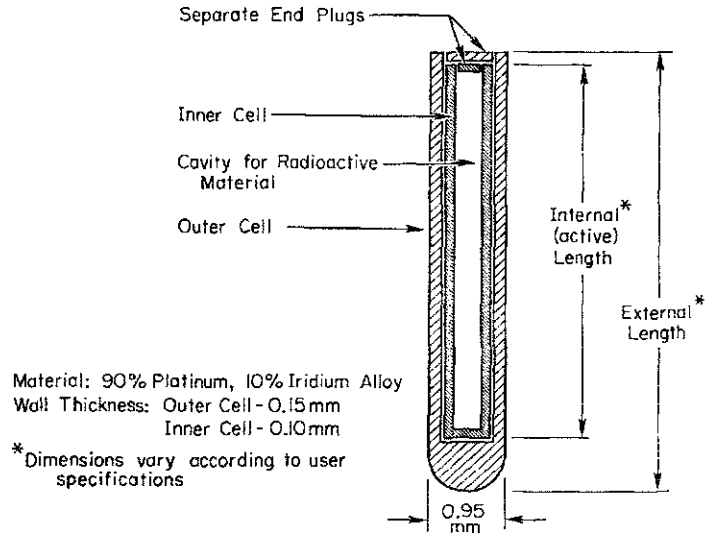

FIG. 5. Afterloading cell.

furnace, the cone is folded into a thin tube and placed in a pelletizer (Fig. 7) by drawing the Pt–Ir wire to which the folded cone is attached through the pelletizer base. The source pellet is then formed by inserting the ram and applying pressure. The source is removed from the pelletizer and slowly heated to red heat (800°C) in a furnace to convert remaining hydrous oxide to Fe_2O_3 and Cf_2O_3. At approximately 75 per cent of theoretical density, the active volume of the source is about 6 mm^3 after pelletizing and heating.

The source pellet, with its wire still attached, is inserted into a primary capsule (Fig. 8) which

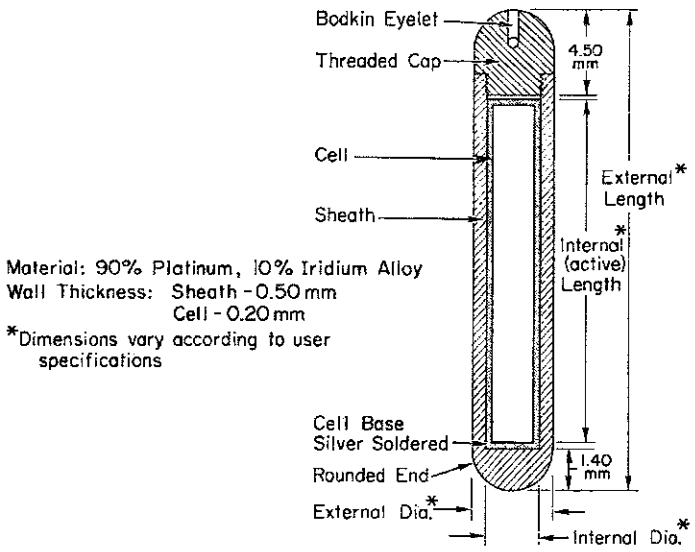

FIG. 6. Afterloading tube.

is sealed with silver braze alloy (flow point 855°C). This primary capsule is enclosed in an outer capsule (Fig. 9) which is sealed by welding. Outer capsules are designed to user specifications.

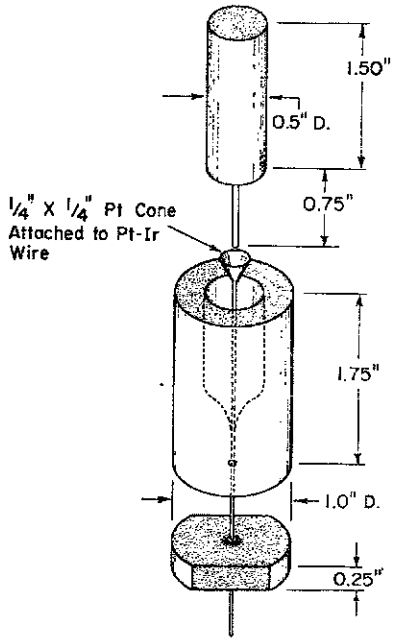

FIG. 7. Pelletizer.

Calibration

A manganese-bath method is used to determine the rate of neutron emission from the sources. The source is placed at the center of a cylindrical plastic tank (42 in. in dia. and 39 in. tall) that contains 900 l. of 0·45 M $MnSO_4$. After a timed irradiation to activate manganese atoms to ^{56}Mn, the tank is stirred thoroughly and a sample of the $MnSO_4$ solution is assayed with a counter calibrated for ^{56}Mn. Corrections are made for the leakage of neutrons from the tank and the capture of neutrons by hydrogen, oxygen, and sulfur atoms in the solution. Calibration of this system was validated with a californium-252 source previously calibrated at the National Bureau of Standards. The precision of the determination of the neutron

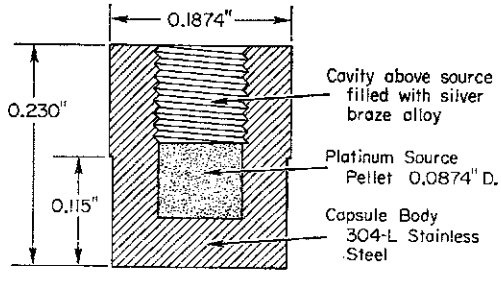

FIG. 8. ^{252}Cf source inner capsule.

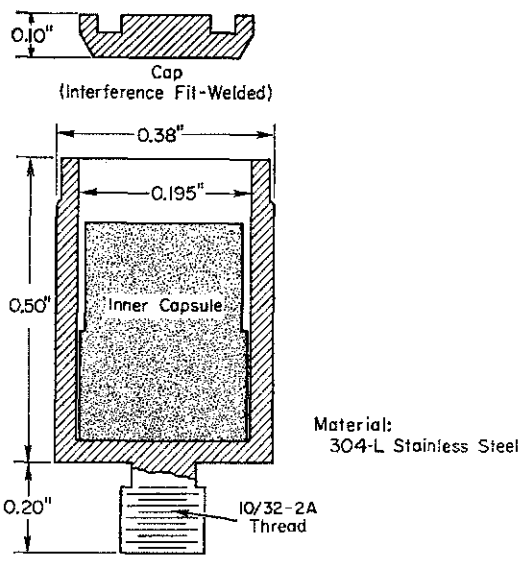

FIG. 9. ^{252}Cf source outer capsule.

emission rate is estimated to be approximately 5 per cent.

SAFETY TESTS

Californium-252 sources are designed and tested during and after construction to eliminate the possibility of leakage and to minimize the consequences of capsule rupture.

Therapy sources

Leak, dimensional, corrosion, mechanical, and metallographic tests are used to verify the soundness of encapsulation techniques.

In addition, a similar group of tests showed that therapy source components were not affected by exposure to fast and thermalized neutrons from nuclear reactors equivalent to a 5-yr exposure from 10 μg of ^{252}Cf.

Encapsulated dummy source cells and sheaths were pressurized separately in 30-psi helium for 30 min. Leak tests on individual pieces in a helium leak detector whose lower detection limit is $2{\cdot}4 \times 10^{-9}$ cm^3 of helium per sec indicated no leaks. (Leak tests are performed in this manner on each source when it is made.)

Seal integrity of a therapy source made in July, 1966 was tested in May, 1968 by smear and helium leak tests. Neither smearable contamination nor measurable helium leaks were detected.

The sealed source cells and sheaths were weighed to the nearest 0·1 mg. Length and diameter were measured to the nearest one-thousandth of an inch. There were no measurable changes in weight or dimensions as a result of exposure to fast and thermalized neutrons.

Each type of source component was exposed to water and to cold and warm saline solution (0·025 per cent sodium chloride by weight) for periods up to five months to test for leakage, changes in weight, or evidence of corrosion. Specimens were thoroughly examined at 50X magnification for evidence of deterioration of seals or corrosion but none was observed.

Sets of sealed dummy sources were divided into two groups. One group was irradiated and examined further by leak, mechanical, and metallographic tests. The other group was not irradiated and was examined by the same mechanical and metallographic tests.

The first group was exposed to $8{\cdot}8 \times 10^{13}$ nvt (neutron fluence) at the Health Physics Research Reactor, an unshielded assembly at Oak Ridge National Laboratory, to simulate the fast neutron exposure from the ^{252}Cf inside the cell of a therapy source. The same group of sources was exposed again to a thermalized neutron spectrum in a reactor at the Savannah River Laboratory, since the sources will be in a moderating medium most of the time, i.e. in tissue or a storage shield which will thermalize the neutrons produced by spontaneous fission of the ^{252}Cf. The neutron fluence in the second irradiation was $9{\cdot}72 \times 10^{14}$ nvt.

The irradiated group was again pressurized and leak tested. No leaks were found.

The mechanical property tests most commonly used to evaluate the quality of ductile metal products include hardness tests, bending tests, and visual metallography[19]. Irradiated and nonirradiated sources were examined with these three tests.

Diamond-point hardness, elastic deformation (yield strength), and plastic deformation (ultimate strength) tests showed no detectable changes after the needles were irradiated.

Specimens were prepared for visual metallography by mounting, cutting, grinding, polishing, and etching procedures. They were then photographed and examined in the metallograph. Sections of the sheath cap, wall, and

point, and cell wall and cell cap silver braze alloy joint were examined. There were no differences between irradiated and nonirradiated specimens.

Radiography source

Pressure created in the inner capsule by helium from alpha decay and fission gas buildup in a 100-μg ^{252}Cf source will be 4·8 atm (70·7 psig) at 30°C (at infinite decay).

Stress calculations assumed the capsules were single, hollow, thick-walled cylinders with well-bonded seals. Metallurgical examination of test specimens verified these assumptions. Maximum calculated safe pressures were 8525 psi for the inner capsule and 7653 psi for the outer capsule, both limited by allowable circumferential stress.

A dummy source was dropped onto a steel plate from heights of 30 and 66 feet. No significant damage occurred to the dummy source as a result of these tests.

FUTURE PLANS

Methods are being developed to prepare very intense californium sources that could be used eventually for neutron radiography and for diagnosis by neutron activation analysis.

REFERENCES

1. Stone R. S. *Am. J. Roentgenol.* **59,** 771 (1948).
2. Andrews J. R. *Am. J. Roentgenol.* **93,** 190 (1965).
3. Reinig W. C. and Evans A. G. Cf-252: A New Neutron Source for Activation Analysis. Presented at the International Symposium on Activation Analysis, Gaithersburg, Md., Oct. 1968 and to be published in the Proceedings.
4. Schlea C. S. and Stoddard D. H. *Nature, Lond.* **206,** 1058 (1965).
5. Wright C. N., Boulogne A. R., Reinig W. C. and Evans A. G. *Radiology* **89,** 337 (1967).
6. Wright C. N. *Hlth Phys.* **15**(5), 466 (1968).
7. Reinig W. C. *Nucl. Applic.* **5**(1) 24 (1968).
8. Stoddard D. H. USAEC Report DP-986 (1965).
9. Leuze R. E., Baybarz R. D. and Weaver B. *Nucl. Sci. Engng* **17,** 252 (1963).
10. Moore F. L. and Jurriaanse A. *Anal. Chem.* **39** (7), 733 (1967).
11. Ko R. *Nucleonics* **15,** 72 (1957).
12. Donnan M. Y. and Dukes A. K. *Anal. Chem.* **36,** 392 (1964).
13. Sanders S. M. Jr. and Leidt S. C. *Hlth Phys.* **6,** 189 (1961).
14. Barnett G. A., Crosby J. and Ferrett D. J. AERE-R-5097, 149 (1965).
15. Kim S. M., Noakes J. E., Akers L. K. and Miller W. W. USAEC Report ORINS-48 (1965).
16. Low-Beer Anne deg. and Story Troy L. Jr. USAEC Report DP-831, 58 (1962).
17. Parker W., Bildstein H., Getoff N., Fischer-Colbrie H. and Regal H. *Nucl. Instrum. Meth.* **26,** 61 (1964).
18. Faraci J. P. USAEC Report DP-1145 (1968).
19. Metals Handbook 1, *Properties and Selection of Metals,* 8th Ed., American Society for Metals.

Radiation Protection Dosimetry (2014), Vol. 161, No. 1–4, pp. 171–175
Advance Access publication 15 December 2013
doi:10.1093/rpd/nct327

MEASUREMENT OF THE ^{250}CF COMPONENT IN A ^{252}CF NEUTRON SOURCE AT KRISS

Jungho Kim*, Hyeonseo Park and Kil-Oung Choi
Korea Research Institute of Standards and Science, Daejeon 305-340, Republic of Korea

*Corresponding author: jungho@kriss.re.kr

Neutron emission rate measurements have been carried out at the Korea Research Institute of Standards and Science using a manganese sulphate bath system for ^{252}Cf and ^{241}Am-Be sources since 2004. The relative measurement method was chosen in 2012, and the neutron emission rates agreed with those by the absolute measurement method within uncertainties. The neutron emission rate of an old ^{252}Cf source has been measured three times: in 2004, 2009 and 2012. The ^{250}Cf component was fitted to a double-exponential function of ^{252}Cf+^{250}Cf, and the ratio of the ^{250}Cf component to the ^{252}Cf component was estimated to be 7.8 % in 2004 and 46.8 % in 2012. Underestimation of the neutron emission rates of old ^{252}Cf sources can be corrected if the neutron emission rate of the ^{250}Cf component is taken into account.

INTRODUCTION

^{252}Cf is an ISO-recommended neutron source for the calibration of neutron instruments including neutron dosemeters. ^{252}Cf is an efficient neutron source and is widely used in the neutron research field. It is a constituent of a D_2O-moderated ^{252}Cf source, which is also an ISO-recommended neutron source. When a ^{252}Cf source is produced, other californium isotopes ^{249}Cf, ^{250}Cf, ^{251}Cf, ^{253}Cf and ^{254}Cf are created during the production of ^{252}Cf. If the isotopes of small composition or short half-lives are neglected, only ^{250}Cf in a ^{252}Cf source is taken into account to produce neutrons. The half-life of ^{250}Cf is 13.08 y, and its isotopic ratio at the time of Cf production is typically 8.33[1,2]. It should be noted that the ^{250}Cf component in a ^{252}Cf source can affect the decay correction of the emission rate of a ^{252}Cf source because of its long half-life compared with that of ^{252}Cf (2.645 y). Another element that may affect the emission rate of a ^{252}Cf source is ^{248}Cm created from the eventual alpha-decay of ^{252}Cf. However, the half-life of ^{248}Cm is 3.48×10^5 y and is not a principal component of a ^{252}Cf source.

The effects of ^{250}Cf and ^{248}Cm in ^{252}Cf neutron sources were studied at the National Physical Laboratory (NPL). In the NPL report, the neutron emission rates of four ^{252}Cf sources were investigated, and it was found that the neutron emission rate of a 25-y-old source could be underestimated by 10 % based on the emission rate calibration done 5 y ago[1]. This means that calibration laboratories with old ^{252}Cf sources should take into account of the presence of ^{250}Cf.

The authors have ^{252}Cf and ^{241}Am-Be sources at the Korea Research Institute of Standards and Science (KRISS) and have carried out neutron emission rate measurements using a manganese sulphate bath system since 2004. The KRISS ^{252}Cf source, ^{252}Cf-II, is believed to have been manufactured in 1989 (the first calibration record is from 1989), and it has been calibrated three times since then (in 2004, 2009 and 2012) using the KRISS manganese sulphate bath system. From the neutron emission rates, the authors could study the ^{250}Cf component of the ^{252}Cf-II source. In this paper, the authors present the KRISS manganese sulphate bath system, the status of the neutron emission rate measurements and the results of the ^{250}Cf component in the ^{252}Cf-II source.

MATERIALS AND METHODS

KRISS manganese sulphate bath system

A manganese sulphate bath system was introduced at KRISS in 1988 (Figure 1). The spherical bath has an inner diameter of 125 cm and is filled with an aqueous solution of pure $MnSO_4$. The parameters of the KRISS manganese sulphate bath system are summarised in Table 1[3]. The $MnSO_4$ solution is stirred and circulated during the measurement at a flow rate of $\sim$10 l min^{-1}. The authors installed an NaI(*Tl*) detector at the central hole on the surface of the Marinelli beaker for measuring gammas.

Relative measurement of the neutron emission rate

The neutron emission rate (B) by the absolute measurement method can be expressed as follows:

$$B=\frac{A_{sat}}{\varepsilon_{Mn}}=\frac{1}{\varepsilon_{Mn}}\frac{N_{sat}}{\varepsilon_c}=\frac{1}{\varepsilon_{Mn}\varepsilon_c}\frac{N(t)}{(1-\exp(-\lambda T))}, \quad (1)$$

where A_{sat} is the saturated activity of ^{56}Mn, N_{sat} is the saturated gamma counting rate, $N(t)$ is the gamma counting rate at source-removal time t, ε_{Mn} is the neutron capture probability by ^{55}Mn, λ is the decay constant (7.46636×10^{-5} s^{-1}) of ^{56}Mn and T is the neutron irradiation time. The neutron capture

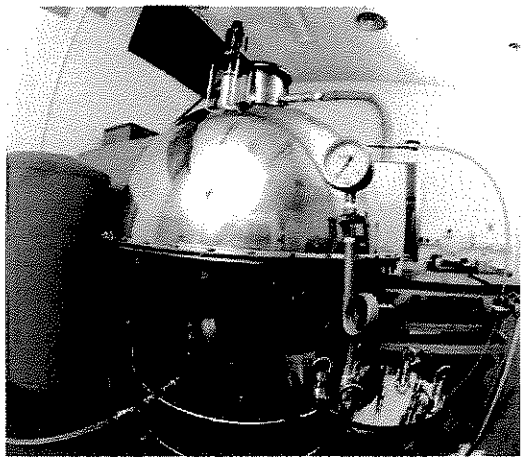

Figure 1. KRISS manganese sulphate bath system.

Table 1. Parameters of the KRISS manganese sulphate bath system.

Parameter	Value
Wall thickness	3 mm
Inner diameter	125 cm
$MnSO_4$ volume	~1022 l
Mass concentration	0.046798 (0.16 %)
Density (20°C)	1.0459 g cm^{-3} (0.0091 %)
H/Mn ratio	341.44 (0.16 %)
Flow rate	~10 l min^{-1}
Marinelli beaker size	~10 l
Gamma detector	NaI(*Tl*) φ3.81 × 3.81 cm

probability ε_{Mn}depends on the neutron source and its capsule type, and it was evaluated by a MCNP calculation. The gamma counting efficiency (ε_c) of an NaI(*Tl*) detector is evaluated with a reference ^{56}Mn solution. The authors produced the ^{56}Mn solution by irradiating thermal neutrons onto ^{55}Mn flake at Hi-flux Advanced Neutron Application Reactor research reactor in Korea. The specific activity of the solution was determined by the $4\pi\beta\gamma$ coincidence counting method[4].

The absolute method usually requires reactor-produced thermal neutrons to produce the ^{56}Mn solution. Because ^{56}Mn has a short half-life (2.57878 h), ε_c is not easy to measure. If a reference ^{56}Mn solution is unavailable, a reference neutron source with a well-known emission rate can be used instead of the ^{56}Mn solution. Firstly, the authors measure the gamma counting rate N_0 of the reference neutron source. Secondly, the authors measure the gamma counting rate $N_{0,r}$ of the unknown neutron source. N_0 and $N_{0,r}$ are the gamma counting rates at the time the source

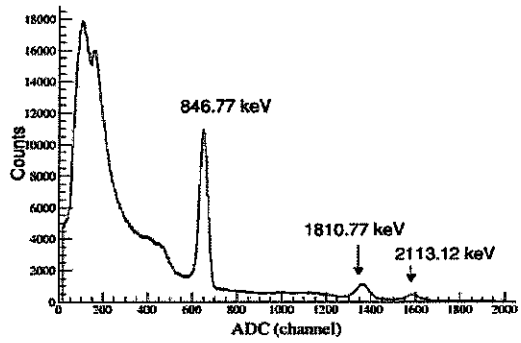

Figure 2. The pulse-height spectrum of ^{56}Mn gammas measured by the NaI(*Tl*).

was removed from the bath. Then, the neutron emission rate can be expressed as follows:

$$B = \frac{\varepsilon_{Mn,r}}{\varepsilon_{Mn}} \frac{N_0}{N_{0,r}} \frac{1-\exp(-\lambda T_r)}{1-\exp(-\lambda T)} B_r, \quad (2)$$

where the subscript r denotes the reference source. The authors measured the neutron emission efficiencies with the absolute method in 2004 and in 2008. The relative method was chosen in 2012.

RESULTS AND DISCUSSION

Gamma measurements

The neutron source was placed at the centre of the $MnSO_4$ sulphate bath for ~24 h and then removed from the bath. The measurement of the gammas from ^{56}Mn continued for ~5 d after the removal of the source. Figure 2 shows a typical pulse-height spectrum of ^{56}Mn measured by the NaI(*Tl*). The three primary gammas of 846.77, 1810.77 and 2113.12 keV are clearly seen. The typical threshold was set to be 30 keV. The fluctuation of the NaI(*Tl*) gain was monitored by the shifts of the three peaks, and the threshold was adjusted to the gain shift. Data were accumulated every 600 s.

Figure 3 shows the number of counts of ^{56}Mn gammas with time. The gamma counts increase after insertion of a neutron source and decrease after removal of the source. The number of counts from time t_1 to time t_2 in the decay phase of the measurement will be as follows:

$$C = \int_{t_1}^{t_2} [N_0 \exp(-\lambda t) + N_B] dt, \quad (3)$$

where N_0 is the neutron-induced gamma count rate at the source-removal time and N_B is the background count rate. The saturated gamma counting rate N_{sat} is $N_0(1-\exp(-\lambda T))$. In the growth phase of the

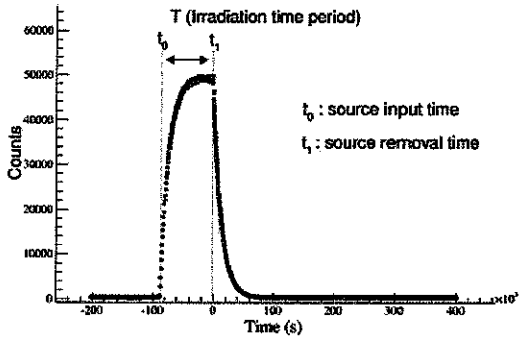

Figure 3. Number of gamma counts with time.

measurement, the number of counts from time t_1 to time t_2 can be written as $\int_{t_1}^{t_2} [N_{sat}(1 - \exp(-\lambda t) + N_B)dt\ N_0$ and N_B can be determined by fitting the data in the growth phase or in the decay phase. The authors fitted the data in the decay phase of the measurement to Eq. (3).

Neutron emission rates

The results of the neutron emission rates since 2004 are listed in Table 2. The ^{241}Am-Be-I source was chosen as a reference source for the relative measurement in 2012. If the neutron emission rates are compared with the absolute measurement and the relative measurement for the ^{252}Cf-I source and the ^{241}Am-Be-II source, the changes of the emission rates are 0.62 and 0.10 %, which are within the uncertainties. However, the emission rate of the ^{252}Cf-II source in 2012 (2009) was +26.6 % (+12.5 %) larger than the emission rate evaluated with the decay curve of ^{252}Cf from the time of the 2004 calibration. As mentioned in the section Introduction, the larger neutron emission rate is related to the ^{250}Cf component in a ^{252}Cf source. There is another nuclide in a ^{252}Cf source. The ^{248}Cm component is created from the alpha-decay of ^{252}Cf. If the ^{248}Cm component in a ^{252}Cf source (~0.1 % for ^{252}Cf source of >15 y[1]) is neglected, the emission rate from the reference date can be written as a double-exponential function,

$$R = R_{252} \exp(-\lambda_{252} t) + R_{250} \exp(-\lambda_{250} t) \qquad (4)$$

where t is the time from the reference date (in 2004), R_{252} is the neutron emission rates from the ^{252}Cf component at time t=0, R_{250} is the neutron emission rates from the ^{250}Cf component and λ_{250} and λ_{252} are the decay constants for ^{250}Cf and ^{252}Cf, respectively. If the ^{248}Cm component is considered, the ^{248}Cm component $R_{248}[1 - \exp(-\lambda_{252} t)]$ can be added to Eq. (4) where time t=0 corresponds to the production date of the source. However, it is hard to evaluate the

Table 2. Neutron emission rates of the KRISS neutron sources.

Neutron source (capsule type)	Emission rates with the absolute measurement (s^{-1})		Emission rates with the relative measurement (s^{-1})			
	1 April 2004	1 September 2009	Emission rate	Decay calculation (D)	1-D/M (%)	Date
^{252}Cf-I (M11)	2.051×10^8 (0.60 %)	5.019×10^7 (0.63 %)	2.097×10^7 (1.0 %)	2.097×10^7	+0.62	8 January 2013
^{252}Cf-II (X.224)	1.950×10^6 (0.62 %)	5.386×10^5 (0.62 %)	2.828×10^5 (1.1 %)	2.374×10^5	+16	17 October 2012
^{241}Am-Be-I (X.14)	1.229×10^7 (0.61 %)	1.227×10^7 (0.63 %)				
^{241}Am-Be-II (X.2)	2.325×10^5 (0.76 %)	2.344×10^5 (0.98 %)	2.334×10^5 (1.0 %)	2.332×10^5	+0.10	1 November 2012
^{252}Cf-III (M11)			2.360×10^7 (1.0 %)			9 November 2012
^{241}Am-Be-III (BP4013)			1.260×10^7 (1.0 %)			11 December 2012

contribution of the ^{248}Cm component by fitting only three data points, so the ^{248}Cm component was not included in this analysis.

The neutron emission rate of the ^{252}Cf-II source on 30 March 1989 was 9.84×10^{7} s^{-1} (calibration certificate on 30 March 1989 by J. L. SHEPHERD & Associates, Inc.). The authors did not use the emission rate in 1989, because it was not measured by them, and no uncertainty was given on the certificate. Figure 4 shows a fit made to the measurements with Eq. (4). The dotted line is the decay curve over time with only the decay constant of ^{252}Cf. The fitting parameters for the ^{252}Cf-II source give $1.803\times10^{6}\pm2.285\times10^{4}$ s^{-1} for R_{252} and $1.414\times10^{5}\pm6.605\times10^{3}$ s^{-1} for R_{250}. The emission rates from the ^{252}Cf component and the ^{250}Cf component on the measurement dates are summarised in Table 3. The ratio of the ^{250}Cf component to the ^{252}Cf component is 7.8 % in 2004 and reached 46.8 % in 2012. The ratio on the date of the first emission measurement can be estimated as 0.34 % and the neutron emission rate as 9.231×10^{7} s^{-1}, which were obtained from the fit to the 2004–2012 measurements. The estimated neutron emission rate was 6.2 % smaller than that on the certificate in 1989. The ^{250}Cf component cannot be compared with the ^{252}Cf component, because no data were given on the certificate in 1989. The ^{250}Cf component in the ^{252}Cf-II source has an effect on calibrations. If the emission rate of the source is extrapolated forwards in time from the last calibration (17 October 2012) with only the decay constant of ^{252}Cf, extrapolation could lead to underestimations of 0.3, 0.8, 1.4, 1.9, 3.1, 4.2, 5.4 and 6.5% for 30, 60, 90, 120, 180, 240, 300 and 360 d, respectively. The abovementioned underestimation of the neutron emission rate is not ignorable and gives rise to incorrect calibration factors when calibrations are performed with the ^{252}Cf-II source. Therefore, old ^{252}Cf sources need to be calibrated frequently with a manganese sulphate bath system or checked for their neutron fluence rate with a standard neutron fluence monitor such as a long counter. Then, the ^{250}Cf component and the ^{252}Cf

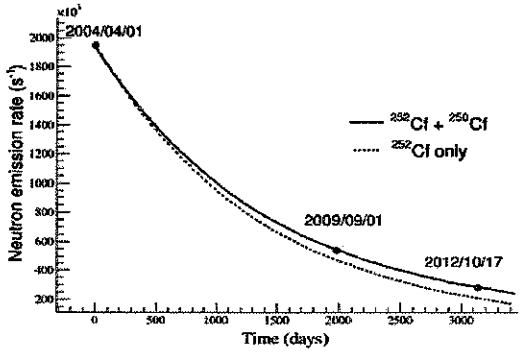

Figure 4. Curve fitted to the emission rate measurements of the ^{252}Cf-II source. The dotted line is the decay curve of ^{252}Cf.

Table 3. Emission rates from the ^{252}Cf component and the ^{250}Cf components in the ^{252}Cf-II source.

Isotope	1 April 2004		1 September 2009		17 October 2012	
	Emission rate (s^{-1})	Fraction (%)	Emission rate (s^{-1})	Fraction (%)	Emission rate (s^{-1})	Fraction (%)
^{252}Cf	1.803×10^{6}	92.7	4.358×10^{5}	80.4	1.921×10^{5}	68.1
^{250}Cf	1.414×10^{5}	7.3	1.061×10^{5}	19.6	8.988×10^{4}	31.9
^{250}Cf/^{252}Cf	0.078	0.243	0.468			
Total	1.944×10^{6}	5.419×10^{5}	2.820×10^{5}			
Measurement	1.950×10^{6} (0.62 %)	5.386×10^{5} (0.62 %)	2.828×10^{5} (1.1 %)			

component in ^{252}Cf sources can be evaluated by fitting the neutron emission rates to a double-exponential function.

CONCLUSIONS

^{252}Cf is an ISO-recommended neutron source, which is widely used for the calibration of neutron instruments. When a ^{252}Cf source is produced, the contribution of the ^{250}Cf component to the neutron emission rate of a ^{252}Cf source is negligible but the effect of the ^{250}Cf component becomes important with time. Neutron emission rate measurements have been carried out at KRISS with a manganese sulphate bath system for ^{252}Cf and ^{241}Am-Be sources with the relative measurement method in 2012. The neutron emission rate of an old ^{252}Cf source (^{252}Cf-II, >23 y) has been measured three times in 2004, 2009 and 2012. The ^{250}Cf component was fitted to a double-exponential function of ^{252}Cf+^{250}Cf. The ratio of the ^{250}Cf component to the ^{252}Cf component was estimated to be 46.8 % in 2012 whereas it was 7.8 % in 2004. This implies that the frequent recalibration is required to evaluate the neutron emission rate of old ^{252}Cf sources. Finally, the neutron emission rates should be fitted to a double-exponential function of ^{252}Cf+^{250}Cf using the previous neutron emission rates.

FUNDING

This work was supported by the Korea Research Institute of Standards and Science under the project 'Development of measurement standards for medical radiation', [13011026]; and the National Research Foundation of Korea (NRF) grant funded by the Korea government (MEST) [NRF-2010-0026095].

REFERENCES

1. Roberts, N. J. and Jones, L. N. *Investigation of the implication of ^{250}Cf and ^{248}Cm in ^{252}Cf neutron sources.* NPL Report DQL RN005, November (2004).
2. Roberts, N. J. and Jones, L. N. *The content of ^{250}Cf and ^{248}Cm in ^{252}Cf neutron sources and the effect on the neutron emission rate.* Radiat. Prot. Dosim. **126**(1–4), 83–88 (2007).
3. Park, H., Choi, K.-O., Lee, J.-M., Lee, K. B., Hahn, M. S. and Kralik, M. *Absolute measurement of the neutron emission rate with a manganese sulphate bath system.* J. Korean Phys. Soc. **47**(4), 603–609 (2005).
4. Park, T. S., Lee, J. M. and Hwang, H. Y. Appl. Radiat. Isot. **56**, 275–280 (2002).